



University of  
Stavanger

Faculty of Science and Technology

## MASTER'S THESIS

Study program/ Specialization: Offshore Technology/Marine – and Subsea	Spring semester, 2014  Open / <del>Restricted access</del>
Writer: Simen Thorgersen	..... (Writer's signature)
Faculty supervisor: Eiliv Fougner Janssen	
Thesis title: Comparison study of deepwater installation methods	
Credits (ECTS): 30	
Key words: <ul style="list-style-type: none"><li>- Deepwater</li><li>- Fiber rope</li><li>- Steel wire</li><li>- Operable sea-states</li><li>- Vessel availability</li></ul>	Pages: 74 + VIII  + enclosure: 16  Stavanger, 14/06/2014 Day/Month/Year

## Abstract

The combination of deeper offshore field developments and larger, more complex subsea structures results in new requirements and challenges for installation vessels and related deployment systems. The conventional vertical deployment system, utilizing steel wire as lifting line, is struggling to meet the industries requirement of installing heavy subsea structures in water depths exceeding 2000m.

The objective of this thesis is to find a viable solution to the challenges met during deepwater installation of subsea structures, and to possibly reduce the problem of vessel availability faced in the industry today.

This thesis considers new installation methods and assesses their applicability for deepwater installation through a state of the art review. A comparison study between a fiber rope deployment system and a conventional steel wire deployment system is conducted. The study cover all main challenges met during deepwater installation, and consider the installation of two different subsea structures.

Due to the low self-weight of fiber rope, the fiber rope deployment system is seen as applicable for deepwater installation with smaller vessels. The system is equipped with active heave compensators and constant tension function, making it applicable for overboarding and splash zone lifting. A feasibility study of deepwater installation with a smaller vessel, rigged with an A-frame and a fiber rope deployment system is conducted.

Dynamic analysis of splash zone lifting and lowering to seabed operations is performed with the modeling and analysis program ORCAFLEX. A laboratory exercise is performed to verify the ORCAFLEX model.

The fiber rope deployment system is found to be a viable substitute for the conventional steel wire system for deepwater purposes. The system solves the problem related to self-weight of steel wire and has a better weather limiting criteria for lowering to seabed operations. Positioning of the lifted object on the seabed is however found to be more challenging when utilizing fiber rope as lifting line.

The A-frame vessel rigged with a fiber rope deployment system is found to be applicable for deepwater installation of subsea structures weighing  $\leq 70Te$ . The installation can be performed for a wide range of sea-states in deepwater regions, and problems related to vessel availability can possibly be reduced.

## **Acknowledgement**

First and foremost, I would like to thank my faculty supervisor, Eiliv Fougner Janssen, for his support and encouragement during my work with this thesis. Without his help, this thesis would not have been the same.

I would also like to show my gratitude towards Irene Tveiten at Cortland Selantic AS - Bergen, for providing me with the fiber rope necessary to conduct my laboratory exercise. In addition, I would like to thank Yaaseen Amith Ahmad, for providing me with the technical measurement equipment required for the laboratory exercise.

To my fellow students in room D-207, thank you for making this semester a great experience with daily moments of humor and laughter. I would especially like to show my gratitude towards Samuel Simeon Honorat and Linn Underbakke, for their assistance during my laboratory exercise.

Last but not least, I would like to thank my girlfriend, Anne Karin Lindahl Hauge, for always being there for me and supporting me through the rough days.

# Contents

- Abstract ..... I
- Acknowledgement..... II
- List of Figures..... V
- List of Tables..... VII
- Abbreviations ..... VIII
- Definitions ..... VIII
- 1 Introduction..... 1
  - 1.1 Summary..... 1
  - 1.2 Objective & scope..... 2
  - 1.3 Methodology ..... 2
  - 1.4 Limitations ..... 3
- 2 Background study..... 4
  - 2.1 Subsea lifting ..... 4
  - 2.2 Deepwater installation challenges ..... 7
  - 2.3 Subsea structures ..... 8
  - 2.4 State of the art review..... 9
  - 2.5 Fiber rope deployment system ..... 18
- 3 Fiber rope vs. steel wire - comparison study ..... 22
  - 3.1 Payload capacity ..... 22
  - 3.2 Horizontal offset due to current..... 25
  - 3.3 Dynamic analysis ..... 30
  - 3.4 Laboratory exercise - verification of the ORCAFLEX model ..... 50
- 4 Feasibility study - deepwater installation with smaller vessels ..... 59
  - 4.1 A-frame vessel ..... 59
  - 4.2 Dynamic analysis ..... 59
  - 4.3 Operational criteria ..... 64
  - 4.4 Results - dynamic analysis..... 65
  - 4.5 Operable sea-states..... 68
  - 4.6 Vessel operability ..... 68
  - 4.7 Summary - feasibility study ..... 70
- 5 Discussion..... 70
- 6 Conclusion ..... 72
- 7 Further work..... 72

References..... 73  
APPENDIX ..... 75

## List of Figures

FIGURE 2.1: FORCES ON SEAFASTENING .....	4
FIGURE 2.2: REQUIRED CLEARANCES, LIFTING OFF FROM DECK AND MANEUVERING OBJECT CLEAR OF TRANSPORTATION VESSEL .....	5
FIGURE 2.3: SPLASH ZONE LIFTING, RECREATED FROM REF [2].....	6
FIGURE 2.4: LANDING ON SEABED .....	7
FIGURE 2.5: DIFFERENCE IN LOAD CONTROL AND POSITIONING, SHALLOW WATER VS. DEEPWATER .....	8
FIGURE 2.6: PENDULOUS INSTALLATION, REF [5], FIG. 1 .....	9
FIGURE 2.7: PENCIL BUOY INSTALLATION.....	11
FIGURE 2.8: SUBSEA DEPLOYMENT SYSTEM. REF [9] .....	12
FIGURE 2.9: FIBER ROPE DEPLOYMENT SYSTEM, 125Te SWL, REF [12], FIGURE 2 .....	15
FIGURE 2.10: 46Te SWL, FIBER ROPE DEPLOYMENT SYSTEM MOBILIZED ON TOISA PERSEUS, REF [11], FIGUE.10 .	21
FIGURE 3.1: PAYLOAD CAPACITY AS A FUNCTION OF WATER DEPTH.....	24
FIGURE 3.2: PAYLOAD CAPACITY OF DIFFERENT SIZED STEEL WIRE AS A FUNCTION OF WATER DEPTH.....	24
FIGURE 3.3: HORIZONTAL OFFSET DUE TO CURRENT, THEORETICAL MODEL, DNV-RP-H103, FIGURE 5-1.....	26
FIGURE 3.4: VESSEL MODEL, ORCAFLEX.....	31
FIGURE 3.5: DETERMINING INITIAL POSITION OF THE 6D BUOY, ORCAFLEX.....	32
FIGURE 3.6: ORCAFLEX MODEL, SUBSEA TREE .....	33
FIGURE 3.7: ORCAFLEX MODEL, MANIFOLD .....	33
FIGURE 3.8: WAVE DIRECTION VS. VESSEL HEADING .....	34
FIGURE 3.9: HYDRODYNAMIC ADDED MASS .....	37
FIGURE 3.10: NATURAL PERIOD OF LIFTING SYSTEM, SUBSEA TREE INSTALLATION .....	40
FIGURE 3.11: NATURAL PERIOD OF LIFTING SYSTEM, MANIFOLD INSTALLATION .....	40
FIGURE 3.12: VERTICAL CRANE TIP MOTION TRANSFER FUNCTION.....	41
FIGURE 3.13: DYNAMIC FORCE, SUBSEA TREE INSTALLATION, STEEL WIRE.....	45
FIGURE 3.14: DYNAMIC FORCE, SUBSEA TREE INSTALLATION, FIBER ROPE.....	46
FIGURE 3.15: DYNAMIC FORCE, MANIFOLD INSTALLATION, STEEL WIRE.....	46
FIGURE 3.16: DYNAMIC FORCE, MANIFOLD INSTALLATION, FIBER ROPE .....	47
FIGURE 3.17: MOTION OF LIFTED OBJECT, SUBSEA TREE, STEEL WIRE .....	48
FIGURE 3.18: MOTION OF LIFTED OBJECT, SUBSEA TREE, FIBER ROPE.....	48
FIGURE 3.19: MOTION OF LIFTED OBJECT, MANIFOLD, STEEL WIRE .....	49
FIGURE 3.20: MOTION OF LIFTED OBJECT, MANIFOLD, FIBER ROPE.....	49
FIGURE 3.21: EXPERIMENTAL SETUP, SIDE VIEW .....	51
FIGURE 3.22: EXPERIMENTAL SETUP, TOP VIEW .....	51
FIGURE 3.23: DETERMINATION OF ROPE LENGTH .....	52
FIGURE 3.24: REAL-TIME GRAPH, CATMAN EASY .....	52
FIGURE 3.25: ANALOG FISH WEIGHT .....	53
FIGURE 3.26: FIBER ROPE SECURED IN A LOOP.....	53
FIGURE 3.27: WEIGHT TRANSDUCER CONNECTION .....	53
FIGURE 3.28: PRE - LOADING THE FIBER ROPE .....	54
FIGURE 3.29: CAMERA VIEW .....	54
FIGURE 3.30: FIBER ROPE INITIAL POSITION.....	55
FIGURE 3.31: FIBER ROPE MAXIMUM POSITION AND ROPE ELONGATION .....	55
FIGURE 4.1: AIRY WAVE .....	62
FIGURE 4.2: CRANE TIP MOTION TRANSFER FUNCTION, SUBSEA TREE .....	63



## List of Tables

TABLE 2.1: WEIGHT AND DIMENSION OF VARIOUS SUBSEA STRUCTURES, REF [4], TABLE 1 .....	8
TABLE 2.2: SWOT ANALYSIS, PENDULOUS INSTALLATION METHOD.....	16
TABLE 2.3: SWOT ANALYSIS, PENCIL BUOY METHOD.....	17
TABLE 2.4: SWOT ANALYSIS, UTILIZATION OF A SUBSEA DEPLOYMENT SYSTEM .....	17
TABLE 2.5: SWOT ANALYSIS, UTILIZATION OF A FIBER ROPE DEPLOYMENT SYSTEM.....	18
TABLE 3.1: SUBMERGED WEIGHT OF LIFTING LINES [KG/M] .....	23
TABLE 3.2: “LOSS” OF INCREASED WIRE CAPACITY.....	25
TABLE 3.3: SUBMERGED WEIGHT OF SUBSEA STRUCTURES [kN] .....	28
TABLE 3.4: SUBMERGED WEIGHT OF LIFTING LINES [N/M].....	28
TABLE 3.5: INPUT PARAMETERS, HORIZONTAL OFFSET CALCULATION, SUBSEA TREE.....	29
TABLE 3.6: INPUT PARAMETERS, HORIZONTAL OFFSET CALCULATION, MANIFOLD.....	29
TABLE 3.7: HORIZONTAL OFFSET DUE TO CURRENT.....	29
TABLE 3.8: LINE CONNECTION, SUBSEA TREE INSTALLATION .....	32
TABLE 3.9: LINE CONNECTION, MANIFOLD INSTALLATION .....	32
TABLE 3.10: INPUT PARAMETERS, LIFTING LINE, ORCAFLEX ANALYSIS.....	38
TABLE 3.11: INPUT PARAMETERS, SUBSEA STRUCTURE, ORCAFLEX ANALYSIS.....	39
TABLE 3.12: LENGTH OF LIFTING LINE CAUSING RESONANT MOTION .....	42
TABLE 3.13: MAXIMUM ALLOWABLE DYNAMIC FORCE IN LIFTING LINE, OPERATIONAL CRITERION 1, SUBSEA TREE INSTALLATION.....	43
TABLE 3.14: MAXIMUM ALLOWABLE DYNAMIC FORCE IN LIFTING LINE, OPERATIONAL CRITERION 1, MANIFOLD INSTALLATION.....	43
TABLE 3.15: MAXIMUM ALLOWABLE DYNAMIC FORCE IN LIFTING LINE, OPERATIONAL CRITERION 2 .....	44
TABLE 3.16: SEATATES COVERED IN THE DYNAMIC ANALYSIS .....	44
TABLE 3.17: RESULTS LABORATORY EXERCISE .....	56
TABLE 3.18: MAX ELONGATION MEASURED VS. ORCAFLEX/CALCULATED ROPE ELONGATION .....	58
TABLE 3.19: ROPE STIFFNESS, MEASURED VS. THEORETICAL.....	58
TABLE 4.1: HYDRODYNAMIC ADDED MASS AT DIFFERENT SUBMERGENCE LEVELS, SUBSEA TREE .....	61
TABLE 4.2: HYDRODYNAMIC ADDED MASS AT DIFFERENT SUBMERGENCE LEVELS, MANIFOLD .....	61
TABLE 4.3: SLAM COEFFICIENT & SLAM AREA .....	62
TABLE 4.4: CRITICAL LENGTHS OF LIFTING LINE, A-FRAME VESSEL INSTALLATION.....	63
TABLE 4.5: SUBSEA TREE, OPERATIONAL CRITERION 1, SPLASH ZONE LIFTING .....	64
TABLE 4.6: SUBSEA TREE, OPERATIONAL CRITERION 2, SPLASH ZONE LIFTING .....	64
TABLE 4.7: MANIFOLD, OPERATIONAL CRITERION 1, SPLASH ZONE LIFTING .....	64
TABLE 4.8: MANIFOLD, OPERATIONAL CRITERION 2, SPLASH ZONE LIFTING .....	65
TABLE 4.9: OPERATIONAL CRITERIA, RESONANT MOTION .....	65
TABLE 4.10: SUBSEA TREE INSTALLATION, DYNAMIC FORCE IN LIFTING LINE [Te], SPLASH ZONE .....	66
TABLE 4.11: MANIFOLD INSTALLATION, DYNAMIC FORCE IN LIFTING LINE [Te], SPLASH ZONE.....	67
TABLE 4.12: SUBSEA TREE INSTALLATION, DYNAMIC FORCE IN LIFTING LINE [Te], RESONANCE .....	67
TABLE 4.13: MANIFOLD INSTALLATION, DYNAMIC FORCE IN LIFTING LINE [Te], RESONANCE .....	67
TABLE 4.14: MANIFOLD, OPERABLE SEA-STATES .....	68
TABLE 4.15: SUBSEA TREE INSTALLATION, OPERABLE SEA-STATES GULF OF MEXICO .....	69
TABLE 4.16: SUBSEA TREE INSTALLATION, OPERABLE SEA-STATES OFFSHORE ANGOLA .....	69



## Abbreviations

- BOB<sup>®</sup>: Braid optimized for bending
- CTCU<sup>™</sup>: Cable traction control unit
- DCV: Deepwater construction vessel
- DP: Dynamic Positioning
- FRDS: Fiber rope deployment system
- HLV: Heavy lift vessel
- JIP: Joint industry project
- MBL: Minimum breaking load
- PLEM: Pipeline end manifold
- PLET: Pipeline end termination
- RAO: Response amplitude operator
- RMS: Rope management system
- ROV: Remotely operated vehicle
- SDA: Subsea distribution assembly
- SDS: Subsea deployment system
- SDV: Submersible deployment vessel
- SUTA: Subsea umbilical termination assembly
- SWL: Safe working load
- SWOT: strength, weakness, opportunity and threat
- 6DOF: Six degrees of freedom

## Definitions

Deepwater: Water depths > 2000m

$\rho_{sw}$ : 1025kg/m<sup>3</sup>

$\rho_{steel}$ : 7900 kg/ m<sup>3</sup>

# 1 Introduction

## 1.1 Summary

Deepwater field developments rely on complex subsea equipment, in order to enable production from subsea wells and deliver the produced hydrocarbons to a floating production unit or an onshore processing plant.

The combination of deeper offshore field developments and larger, more complex subsea structures results in new requirements and challenges for installation vessels and related deployment systems. The conventional deployment systems, utilizing steel wire as deployment line, are struggling to meet the requirement of installing subsea structures at water depths exceeding 2000m. The reason for this is the high self-weight of steel wire, which significantly reduces the available payload capacity of the wire at large depths.

This thesis covers a state of the art review where new installation methods, challenging the conventional steel wire deployment system, are studied. The methods are compared, and the method seen as the most applicable for solving deepwater installation issues is taken further for a comparison study with a conventional system.

The installation method chosen for the comparison study is the usage of a fiber rope deployment system, developed by the company ODIM. The utilization of fiber rope as lifting line solves the problems related to self-weight of steel wire, however the mechanical behavior of fiber ropes are fairly different.

The two systems are compared with respect to:

- Payload capacity at large water depths
- Positioning and control
- Operable sea-states
- Landing on seabed

The fiber rope deployment system has so far been used from subsea equipment support vessels/multi-purpose diving support vessels. A conventional deck crane is used for overboarding and splash zone lifting, while the fiber rope deployment system is used for lowering to seabed operations. This has proven to be a viable solution for solving the problems related to self-weight of steel wire. The availability of these large installation vessels is scarce and the day-rate is high.

The weight and power requirement of a fiber rope deployment system is significantly lower than for a steel wire system. The fiber rope deployment system is therefore seen as applicable for deepwater installation with smaller vessels. The fiber rope deployment system has active heave compensation and constant tension systems, making it applicable for overboarding and splash zone lifting. This thesis therefore covers a feasibility study of utilizing a fiber rope deployment system on a smaller vessel, rigged with an A-frame, to perform splash zone lifting and lowering to seabed operations.

## 1.2 Objective & scope

The objective of this thesis is to find a viable solution to the challenges met during deepwater installation of subsea structures. The thesis also assess a possibly to reduce the problem of vessel availability faced in the industry today. New installation methods, challenging the conventional steel wire deployment system, are arising in the market. Their applicability for deepwater installation will be considered. The fiber rope deployment system is considered to be the most suitable for deepwater purposes, and will be compared to a conventional steel wire deployment system. The comparison study will cover all major challenges met during deepwater installation operations. The comparison study is performed to obtain an overview of the methods applicability to substitute the conventional system for deepwater purposes. The possibility to perform deepwater installation of subsea structures with smaller vessels, when utilizing the fiber rope deployment system, will also be assessed.

## 1.3 Methodology

In order to find a viable solution to the challenges met during deepwater installation and to possibly reduce the problem of vessel availability, the following steps are covered in this thesis:

### **1. State of the art review**

New installation methods and their applicability for deepwater installation are assessed. A SWOT (Strength, Weakness, Opportunity and Threat) analysis of each installation method is performed. The method considered to be the most applicable for deepwater purposes is taken further for a comparison study with a steel wire deployment system.

### **2. Comparison Study**

The installation method chosen for the comparison study is a fiber rope deployment system. The comparison study covers the installation of two different subsea structures, in order to account for difference in dynamic behavior of different shaped structures. The two structures to be considered are a subsea tree weighing 70Te with dimensions 6x6x7m, and a manifold weighing 115Te with dimensions 9x7x5m. The fiber rope deployment system is compared to the conventional steel wire system by:

- Spreadsheet calculations are performed to assess the difference in payload capacity of the system at large water depths
- Spreadsheet calculations based on DNV-RP-H103 is performed to assess the difference in horizontal offset due to current. I.e. problems related to positioning and control of the lifted object
- Dynamic lifting analysis is performed with the modelling and simulation program ORCAFLEX, to assess differences in dynamic behavior of the two systems. I.e. difference in operable sea-states. The dynamic lifting analysis is performed for environmental loading conditions representable for the deepwater region Gulf of Mexico

The comparison study is performed to obtain an overview of the methods applicability to substitute the conventional steel wire system for deepwater purposes

### **3. Laboratory exercise**

The axial stiffness of the lifting line is crucial to the dynamic behavior of the lifting system. A laboratory exercise is performed to verify the ORCAFLEX model and input parameters. The elongation of a fiber rope, subjected to different static loads, is measured. Results are compared to the line elongation in an ORCAFLEX model and to theoretically calculated rope elongation.

### **4. Feasibility study**

A feasibility study for deepwater installation with smaller vessels, rigged with a fiber rope deployment system, is performed. The study is performed to assess the possibility of reducing the problems related to vessel availability. The study is performed by:

- Dynamic lifting analysis for splash zone lifting and lowering to seabed operations are performed with the modelling and analysis program ORCAFLEX

The analysis is based on installation with an A-frame vessel, and the analysis covers the installation of two different subsea structures. The results from the dynamic analysis are compared with annual scatter diagrams for two different deepwater regions to assess differences in vessel operability. The two subsea structures are identical to the structures used in the comparison study. The two deepwater regions chosen is the Gulf of Mexico and Offshore Angola.

## **1.4 Limitations**

This thesis is limited by the vessel RAO data used for the dynamic analysis of offshore lifting operations. RAO data for specific offshore installation vessels where unknown, and all analysis are based on RAO data provided for the standard vessel model in ORCAFLEX. The standard vessel in ORCAFLEX is based on an offshore tanker and may not be optimal for offshore installation work. The dynamic analysis is performed without accounting for the effect of active heave compensation, guide wires, and lifting slings.

Hydrodynamic drag and slam coefficients are set to the minimum recommended value in DNV-RP-H103, and are not found by specific computerized fluid dynamic analysis or laboratory testing.

## 2 Background study

### 2.1 Subsea lifting

A subsea lifting operation consists of several different phases that need to be considered during design of subsea structures and planning of installation work. Each of these phases is further discussed below.

#### 2.1.1 Seafastening

Seafastening is the principal of securing the structures to be transported and installed offshore to the vessel deck. The seafastening need to be able to withstand the forces introduced by the vessels motion during transit. The main forces acting on the seafastening are a result of vessel roll and pitch motion. The total force on seafastening due to either roll or pitch motion will be [1]:

The gravitational force caused by the roll/pitch angle + the force caused by the roll/pitch acceleration. Figure 2.1 below shows an illustration of the forces introduced by vessel roll motion. [1]

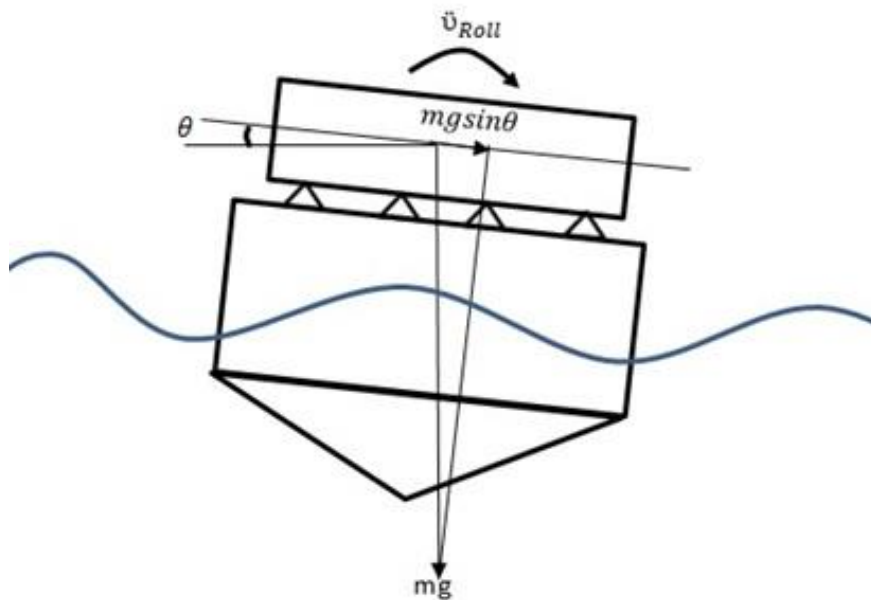


Figure 2.1: Forces on Seafastening

Where:

$$\ddot{\theta}_{Roll} = \text{Roll acceleration [m/s}^2\text{]}$$

$$m * g * \sin \theta = \text{Gravitational force caused by the roll angle [N]}$$

$$\theta = \text{Roll angle [deg]}$$

### 2.1.2 Lifting off from deck and maneuvering object clear of transportation vessel

During lift off from deck and maneuvering the object clear of the transportation vessel, the following aspects should be considered according to DNV-RP-H103, section 9.1.1.2.

1. Clearance between lifted object and crane boom.
2. Clearance between the underside of the lifted object and grillage/seafastening structure on the vessel.
3. Clearance between crane boom and any other object/structure.
4. Bottom clearance between crane vessel and seabed for lifting operations at small water depths.

The different clearances are presented in Figure 2.2 below.

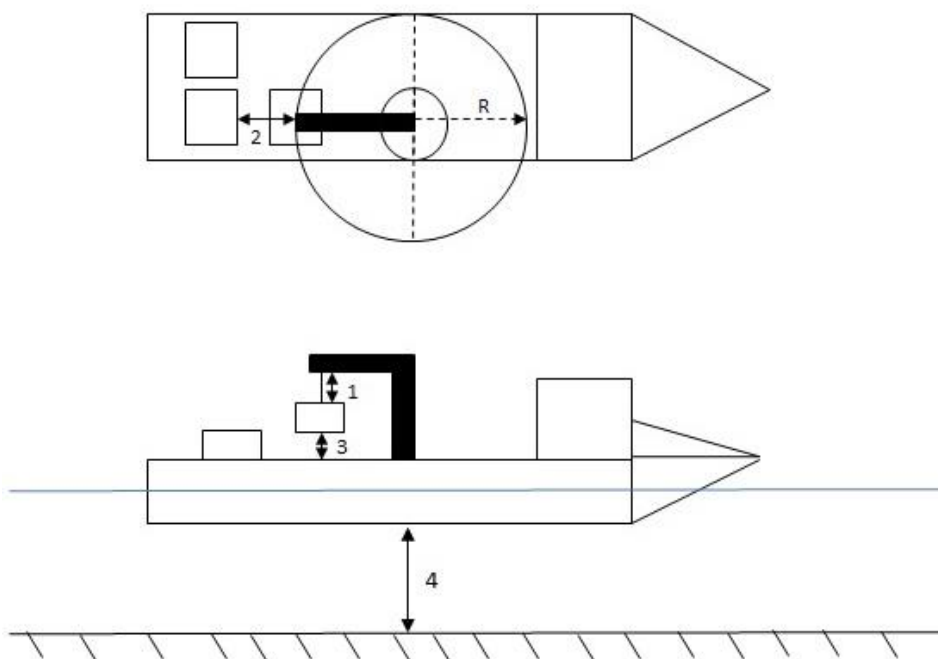


Figure 2.2: Required Clearances, Lifting off from Deck and Maneuvering Object Clear of Transportation Vessel

Where:

$R$  = Crane boom radius

1 - 4 = Clearances listed above

### 2.1.3 Lifting through splash zone

Lifting through splash zone is one of the most critical phases of a subsea lift, and is often the restricting factor related to weather criteria for the operation. During splash zone lifting, the operation has a transition from lifting in air to a subsea lift, which greatly affects the dynamics of the lifting operation. When entering the water, the lifted object will experience slamming wave forces which could damage the object. Further on, hydrodynamic added mass and drag damping forces will affect the systems dynamic response, which differ from when the object is slightly submerged until it is fully submerged. The oscillating sea surface can cause loss of buoyancy and lead to snap loads in

the lifting line, if the lowering speed and timing of the operation is not thoroughly planned. Figure 2.3 below presents two different stages of a splash zone lifting operation. [2]

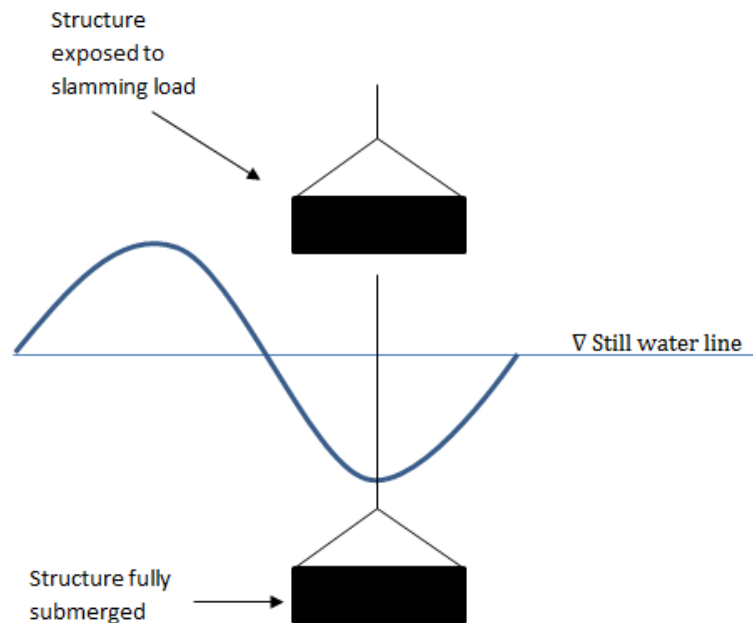


Figure 2.3: Splash Zone Lifting, Recreated from REF [2]

#### 2.1.4 Lowering to seabed

Lowering to seabed is one of the more stable phases of the subsea lift. The hydrodynamic added mass is constant and drag forces are constant for constant vessel motion. The determination of dynamic behavior is hence more predictable than for splash zone lifting. The dynamic behavior of the lifting system (lifted object, crane wire and crane) does however change with cable length. As the cable length is increased, the stiffness of the lifting system is decreased, and the natural period of the lifting system is increased. When performing subsea lifting operations in deepwater, the natural period of the lifting system can become equal to the natural period of the installation vessel. When the lifting system is in resonance with the installation vessel, large motion of the lifted object can occur, and possibly cause slack sling conditions and large dynamic forces in the lifting line. This could severely increase the risk of the lifting operation and possibly reduce the operable sea-states. [1]

#### 2.1.5 Landing on seabed

Landing on seabed is also seen as one of the more critical phases of a subsea lifting operation. Motion of the lifted object can cause slamming forces between the lifted object and the seabed/other structures, resulting in damage of the equipment. The lifting system will also change its response to the vessel oscillating motion, by going from a free end system to a fixed end system. This will increase the risk of slack sling conditions and large dynamic forces in the lifting line. The two stages of the landing on seabed operation are presented in Figure 2.4 below. [1]

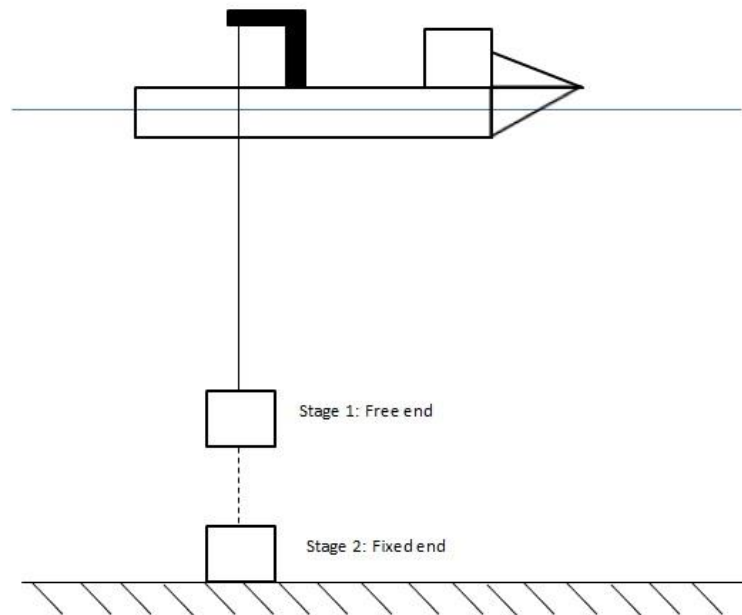


Figure 2.4: Landing on Seabed

## 2.2 Deepwater installation challenges

When performing installation of subsea structures in deepwater areas, new challenges arise as a result of the increased water depth. These challenges can generally be classified in the following respective areas [3]:

- Lifting and lowering technology
- Load control and positioning
- Metocean effects and weather window requirements

The challenges related to lifting and lowering technology is the weight of the structures to be installed, which combined with the dynamic response, can exceed the capacity of the lifting system. Conventionally steel wire deployment systems are used for installation work, but the applicability of steel wire systems are reduced as the water depth is increased. This is related to the large self-weight of steel wire, which reduces the available payload capacity of the wire at increasing water depths. When lowering heavy structures on long lifting lines, there is also a significant risk of resonant motion between the oscillating surface vessel and the lifting system. This can introduce large dynamic forces and result in failure of the lifting line. [3]

Challenges with load control and positioning will increase at greater water depths. Due to the long length of lifting line, relatively small currents can cause a very large offset between the installation vessel and the structure being landed on the seabed. Deepwater soil conditions also tend to be very soft, and bearing capacity failure of the seabed beneath the subsea structure may cause an unacceptable structure orientation. Also control of the deployment system hook will be more challenging. After releasing the subsea structure, the hook will become less controllable and could get entangled with the subsea structure. The difference in positioning of the subsea structure is presented in Figure 2.5 below. [3]



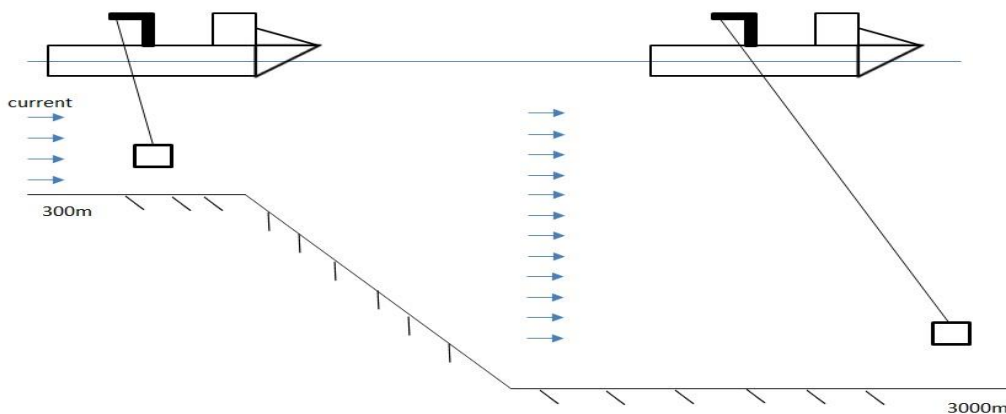


Figure 2.5: Difference in Load Control and Positioning, Shallow Water vs. Deepwater

Challenges with metocean effects and weather window requirements are related to the increased time required to perform the installation, when the water depth is increased. Duration of the lowering operation and recovery of the deployment line will increase, and the time needed for positioning and control will increase. The required duration of weather windows, in order to perform the operation, will hence be larger than for a similar operation in more shallow water. [3]

### 2.3 Subsea structures

Deepwater field developments rely on subsea structures to produce and deliver hydrocarbons to a floating production unit or an onshore processing plant. Subsea structures vary greatly in size, shape and weight. Table 2.1 below presents typical range of weight and dimension for a variety of subsea structures. Stated values are only an approximate indication. [4]

Table 2.1: Weight and Dimension of Various Subsea Structures, REF [4], Table 1

Subsea Structure	Weight [Te]	Dimension (L x B x H)( $\phi$ x H) [m]
Processing Modules	200 - 400	Up to (15x15x8)
Manifolds	50 - 400	(5x5x4) - (25x20x8)
PLEMs	50 - 400	(5x5x4) - (25x20x8)
Template	100 - 400	(10x10x6) - (30x20x7)
Riser Base	50 - 200	Up to (20x20x10)
PLETs	30 - 100	(5x4x3) - (10x8x6)
SDAs	50 - 100	(5x5x4) - (10x10x8)
SUTAs	5 - 50	Up to (5x5x6)
Pumping Modules	5 - 50	(1x1x1.5) - (5x5x6)
Vertical Jumpers	5 - 50	Up to (50x6)(LxH)
Horizontal Jumpers	5 - 50	Up to (50x15)(LxB)
Suction Pile	40 - 200	(4.5x15) - (10x30)
Drag Anchor	50 - 75	Up to (15x5)
Subsea Tree	10 - 70	Up to (5x5x6)
Mid-Water Arch	50 - 100	(10x6x4) - (20x9x5)

Due to the large variety of size, shape and weight of subsea structures, the applicable installation method/vessel will vary for different structures.

## 2.4 State of the art review

In order to assess new and innovative installation methods, capable of solving the issues related to deepwater installation, a state of the art review is conducted. The state of the art review covers the four newly developed installation methods listed below:

1. Pendulous installation method
2. Pencil buoy method
3. Utilization of a subsea deployment system
4. Utilization of a fiber rope deployment system

The methods are compared, and the method most applicable for deepwater installation is taken further for a comparison study with a conventional steel wire, vertical deployment system.

### 2.4.1 Pendulous installation method

The pendulous installation method is a non-conventional method for installing subsea structures in deepwater areas. The method was developed by the company Petrobras in order to install a 280Te manifold in 1900m water depth. The main drivers for developing this method was the low availability and high cost of specialized deepwater construction vessels (DCV) and heavy lift vessels (HLV), which could have led to high cost and possible deviation from schedule. The usage of synthetic fiber rope deployment systems was also assessed, but there was no field proven or prototypes of a fiber rope deployment system in the market that could fulfill the project requirements. [5]

The method can be performed with two standard offshore support vessels like e.g. diving support vessels, ROV support vessels or even DP class anchor handling tugs which are smaller vessels with a lower day rate and a higher availability than the DCV/HLV. One of the vessels have to be equipped with a conventional deck crane or A-frame, to allow for over boarding and splash zone lifting, while the other vessel has a fiber rope deployment winch.[5]

The deployment line will be pre-rigged with lifting slings, and buoyancy elements will be fitted to the rope to reduce the required lifting capacity. The method is capable of installing structures up to 300Te at 3000m water depth. [5]

The pendulous installation method is presented in Figure 2.6 below.

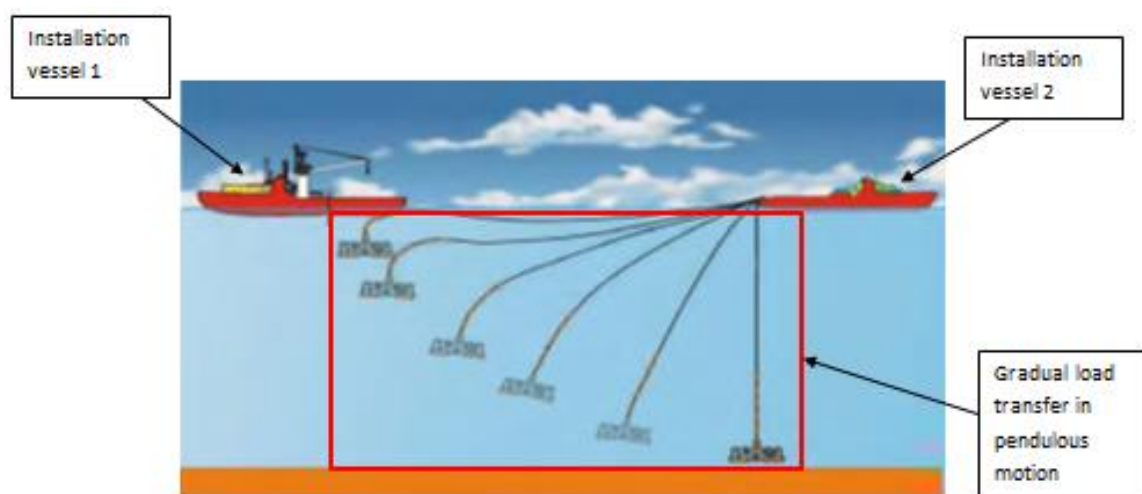


Figure 2.6: Pendulous Installation, REF [5], Fig. 1

Installation sequence [5]:

1. The structure is fastened and secured to the lifting line of the A-frame block on the first installation vessel.
2. Position the two vessels stern to stern and connect the fiber deployment rope, pre-rigged with buoyancy elements, from the second vessel to the lifting arrangement.
3. Connect a conventional steel launch wire on the first vessel to the lifting arrangement.
4. Slowly move the second vessel until the entire length of deployment line is paid out. Distance between the two vessels should be 90% of the length of deployment line.
5. The structure is overboarded, lifted through splash zone and lowered to a water depth of minimum 50m, while paying out the launch line of the first vessel.
6. Stop paying out the launch line and continue paying out the A-frame lifting line until 100% of the load is transferred from the lifting line to the deployment line.
7. Disconnect the A-frame lifting line.
8. Continue paying out the launch wire to cause a gradually load transfer from the launch wire of the first vessel to the deployment line of the second vessel. This results in the structure moving in a pendulous motion. Continue paying out the launch wire until the load is transferred to the deployment line of the second vessel.
9. Move the first vessel toward the second vessel in to slacken the launch line.
10. Release the launch wire from the lifting arrangement.
11. Recover the launch line and lower the structure to the seabed by the second vessel deployment line.

In addition to avoiding the usage of specialized installation vessels, for deployment of large structures in deepwater, the method also reduces many of the problems related to the usage of fiber ropes. Fiber ropes have a lower axial stiffness than the conventional steel wire, and the lifting arrangement can get into resonance with the installation vessel at lower water depths than when a conventional steel wire system is used. Since the lowering operation is performed in a pendulous motion, water depths leading to resonance can be avoided. Using a pre-laid deployment line which is longer than the critical water depth, will avoid possible resonant motion. [5]

Fiber ropes are sensitive to temperature variations, and often loose capacity at higher temperatures. Since the deployment line is pre-laid, one will reduce heat generation caused by rapid cyclic loading, experienced when utilizing an active heave compensation system during conventional vertical lowering operations. Fatigue failure due to repeated cyclic bending over sheaves, high susceptibility to abrasion and high compressive weight on the rope drum is also avoided. [5]

### 2.4.2 Pencil buoy method

The pencil buoy method is a subsurface transportation and installation method developed by the company Aker Marine Contractors. The pencil buoy method reduces the offshore installation sequence from a lifting and lowering operation to a pure lowering operation. This is done by wet towing the structure from an inshore load out site to the desired offshore location. [6]

The method is based on usage of standard equipment onboard ordinary offshore construction vessels, in combination with tailor-made special equipment. The method has the capacity to transport equipment weighing 150 – 370Te and the typical capacity during installation is 60 – 370Te. The special equipment is a slender pencil shaped buoy, a passive heave compensator and required rigging equipment. The pencil buoy is a steel structure with ring stiffeners, designed with several water tight compartments to fulfill the requirement of sustaining one-compartment damage. [6]

Installation sequence [7]:

1. The structure is transported from the construction yard to the load out site by a transportation barge to reduce the wet tow distance.
2. The structure is lifted from the transportation barge by a crane vessel, at a nearby inshore transfer site with sufficient water depth.
3. The load is transferred from the crane vessel to the installation vessel winch wire.
4. The pencil buoy is launched from the installation vessel, and the load is transferred from the installation vessel winch wire to the pencil buoy.
5. The structure is towed to the desired offshore location.
6. At arrival the load is transferred back to the installation vessel winch wire and the pencil buoy is recovered.
7. The structure is lowered to the seafloor and installed.

A sketch of the towing operation, recreated from REF [7], is presented in Figure 2.7 below.

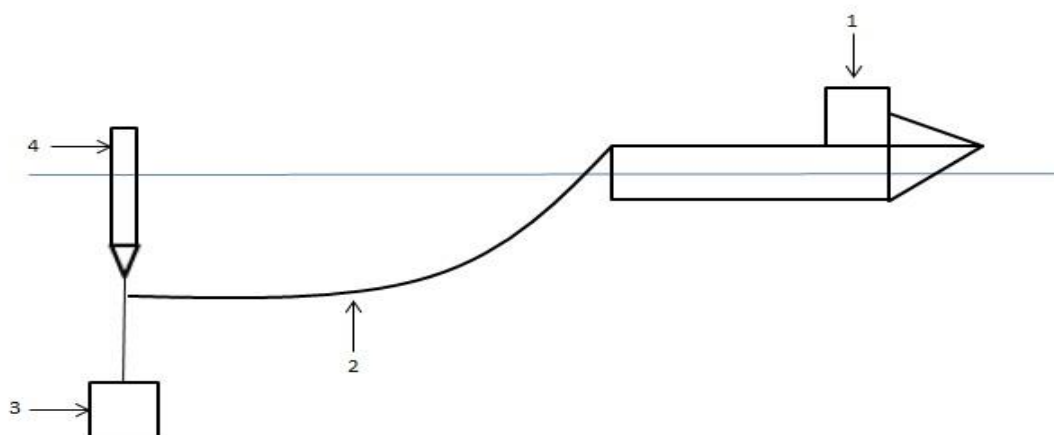


Figure 2.7: Pencil Buoy Installation

Where:

1. Installation vessel
2. Tow line
3. Lifted object
4. Pencil buoy

The towing operation can be designed for an unrestricted summer storm, while the lowering operation is a typical weather window operation. The lowering operation has weather criteria equal to or better than for typical heavy lift vessels. [6]

The main advantages of the pencil buoy method are the avoidance of offshore lifting. Lifting the structure through splash zone at an inshore sheltered area reduces the required crane capacity, it reduces the risk of pendulum motion of the structure in air, and it reduces the slamming wave loads on the structure. I.e. the risk picture is changed. The weather criteria for the operation are less strict, and the required duration of the offshore lifting operation is reduced. Smaller vessels can also be utilized, because a large deck space area for transportation is no longer required and the usage of large deck cranes is avoided. [6]

However the method only allow for installation of a single structure pr. offshore trip. The reduced transit speed makes the method inefficient for installation of several structures, or installation work at remote locations. The method also requires a crane vessel to transfer the structure from the transportation barge to the installation vessel.

#### 2.4.3 Utilization of a subsea deployment system

The subsea deployment system (SDS) is an installation method developed by the company Subsea Deployment Systems Ltd. The method is based on the usage of a submersible deployment vessel (SDV) to transport and install subsea equipment. The method allow for installation of subsea structures weighing from a hundred tons to several thousand tons, in water depths of 100-3000m, without the usage of a HLV. [8]

The SDS avoids offshore over boarding and splash zone lifting, by submerging the subsea structure at an inshore location before towing it offshore. This reduces the dynamic loading on the structure and vessel equipment (crane, wire, lifting slings), hence allowing for installation in rougher weather conditions than traditional methods. The subsea deployment system is presented in Figure 2.8 below. [8]

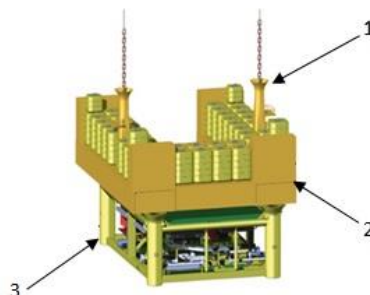


Figure 2.8: Subsea Deployment System. REF [9]

Where:

1. Cain Tower
2. Submersible deployment vessel
3. Subsea structure to be installed

The subsea deployment system is also less sensitive to weather conditions during landing on seabed operations. When installing subsea structures with conventional methods (vertical deployment), there is an instant change in tension in the hoist wire when the structure lands on the seabed. This can lead to slack sling conditions and large snap loads, damaging the lifting slings and hoist wire. The risk of the operation is hence increased, and the operable sea-states can be further limited. To reduce the risk of slack sling condition, it is usually desirable to fully release the load as soon as it has been landed. This reduces the possibility to relocate the structure if it has been landed off target. [8]

The SDS anchors the SDV and the structure to the seabed by the tow chain clump weight, and the tow vessel movement will not affect the SDV/structure. The structure is landed on seabed by lowering two control chains from the installation vessel into the chain towers fitted on the SDV. Since the control chains can move freely in the chain towers, the SDV and structure will not be affected by the movement of the installation vessel, and there is no risk of slack slings or snap loads. The structure can hence be repositioned after landing, without increasing the operational risk. [8]

The required weather window duration is also significantly reduced when using the SDS, compared to a conventional installation method. Since the SDV and structure are anchored close to the seabed, by the tow chain clump weight, the time needed for lowering the structure to seabed is fairly short. This reduces the weather window needed for the operation. The lowering operation can also be suspended at any time by raising the control chains from the chain towers, without any increased risk to structure or personnel. [8]

Installation sequence [10]:

1. The structure is loaded-out into the SDV. This can be done by numerous different methods depending on the available equipment and water depth.
2. If there is limited water depth at the load-out location, the SDV and structure will be towed in shallow draught surface tow, until a location with sufficient water depth is reached.
3. When the water depth is sufficient, the SDV is ballasted down by flooding the hulls
4. SDV in deep draught surface tow. Only the castles and control chain towers are breaking the surface.
5. At a suitable water depth, the tow vessel will pay-out the tow wire and the tow chain clump weight, causing the SDV to submerge. By adjusting the transit speed and length of the tow wire, the tow vessel can control the depth of the SDV.
6. When approaching the designated offshore location, the tow vessel will slow down and adjust the tow wire. The tow chain clump weight is kept above the seabed until it can be landed at an appropriate parking area. The SDV and the subsea structure will now be floating above the seabed, and be anchored by the tow chain clump weight.

7. The SDV will be positioned by two control chains suspended from the installation vessel. The chains will be lowered into the chain towers, and the height of the SDV will be adjusted by raising/lowering the control chains.
8. The structure will be landed on the seabed by fully lowering the control chains into the chain towers. The chains will be temporarily disconnected, and contribute to the on-bottom stability before ballasting.
9. Ballast weight is added to the ballast chain lockers by the installation vessel to balance the weight of the structure (avoid the SDV to float-off when the structure is released), and allow for disconnection.
10. After disconnecting the structure, the installation vessel will reconnect to the control chains and raise them until the SDV is neutrally buoyant. The SDV will be maneuvered away from any subsea assets, before the control chains are completely removed and the SDV can float above the seabed. The SDV is still anchored by the tow chain clump weight.

#### **2.4.4 Utilization of a fiber rope deployment system**

The fiber rope deployment system is a new deployment system, developed by the company ODIM. The fiber rope deployment system is similar to traditional vertical deployment, but utilizes fiber rope as deployment line for subsea lifting operations. The usage of traditional steel wire systems have become unpractical, and are struggling to meet the industries demand of installing heavy structures in water depths exceeding 2000m. The reason for this is the large self-weight of steel wire, which severely reduces the allowable payload capacity of the wire. Hence very large wires are needed to install subsea structures at great water depths. Larger wires require larger storage drums, higher winch power, and larger vessels. Fiber ropes have been seen as a solution to the self-weight problem related to steel wire, since fiber ropes are close to neutrally buoyant in water. However the mechanical behavior of fiber ropes is different from the behavior of steel wire, and traditional handling systems are not applicable to use in combination with fiber ropes. [11]

The challenges that needed to be solved regarding a fiber rope deployment system were [11]:

1. Recovery of an empty hook with a neutrally buoyant line would cause the rope to get spooled onto the storage drum at low tension. When deploying a heavy object the high tensioned rope can squeeze into softly spooled on layers.
2. Fiber ropes are sensitive to creep. In order to avoid excessive creep of fiber ropes it is recommended to store the rope at a tension below 10% of its minimum breaking load.
3. Due to the low axial stiffness of fiber ropes, the rope will experience significant elongation as tension is increased, which can cause slippage between the fiber rope and the traction winch drums.
4. Due to the reduced axial stiffness of fiber ropes compared to steel wire, resonant conditions can be experienced at lower water depths than traditionally.
5. Internal heat buildup, during cyclic bending over sheaves, can cause a reduction of the fiber ropes strength and modulus.

ODIM overcame these challenges with a new cable traction control unit (CTCU). The CTCU has a traction unit that secures constant tension of the rope on the storage drum, during deployment of

structures and recovery of an empty hook. This results in avoidance of creep and squeezing of rope into softly spooled layers. The CTCU also has a set of individually operated sheaves used to de-tension the rope. The individually operated sheaves assure slip control, by adjusting the speed of each sheave to compensate for rope elongation. The system has active heave compensation, which reduces the large motion and forces experienced when the lifting system is in resonance with the installation vessel. It is also equipped with a constant tension system. The fiber rope deployment system can operate at a higher winch pay – out rate than a steel wire system, hence reducing the required duration of an operable weather window. [11]

Installation sequence [11]:

1. The structure to be installed is transported to the desired offshore location by a typical installation vessel.
2. The structure is overboarded and lifted through the splash zone by a conventional deck crane and lowered to a convenient water depth (e.g. 1000m).
3. The load is transferred from the deck crane of the installation vessel to the fiber rope deployment system.
4. The structure is lowered and landed on seabed by the fiber rope deployment system, and the empty hook is recovered.

The largest fiber rope deployment system developed today has the capacity to install structures up to 125Te down to a water depth of 3000m, and has successfully solved the self-weight problems related to the conventional steel wire system. Fiber ropes also have the possibility of being repaired offshore by trained personnel. If a section of rope is worn, the rope section can be cut out, and a new piece of rope can be spliced in. The sheaves of the fiber rope deployment system are designed to handle splices. Figure 2.9 below presents a 125Te SWL fiber rope deployment system. [12]

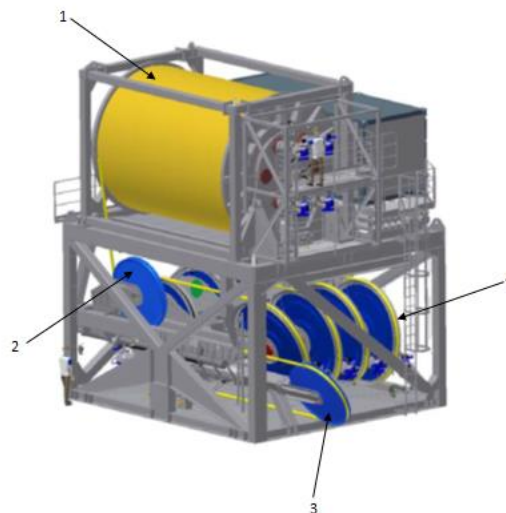


Figure 2.9: Fiber Rope Deployment System, 125Te SWL, REF [12], Figure 2



Where:

1. Storage drum
2. Spooling device
3. Inboard damping device
4. Cable traction control unit

The company Aker Oilfield Services has used a 125Te fiber rope deployment system in two fall configuration to successfully install subsea trees for Petrobras. Maintenance requirements had however been underestimated, and time and planning for maintenance had not been prioritized. The offshore crew working on the installation vessel should have had more extensive training related to the fiber rope system, and documentation for rope management need to be improved. Also the splicing technique used was not verified, and slippage of rope splices occurred over time [13]

#### 2.4.5 Summary - state of the art review

All of the newly developed installation methods discussed above represents solutions to the challenges and requirements faced during deepwater installation.

The pendulous installation method introduces a method to install heavy subsea structures at great water depths, without the requirement of using DCV or HLVs. The method also solves the problems related to resonant motion between the lifting system and the crane tip motion. The risk is considered to be higher for performing a pendulous installation compared to conventional vertical deployment. Even though the method avoids problems with resonance during deployment, two vessels need to be located close to each other, introducing the risk of ship collision and reducing the operable sea-states. A SWOT analysis of the pendulous installation method is presented in Table 2.2 below.

Table 2.2: SWOT Analysis, Pendulous Installation Method

<b>Strength</b>	<b>Weakness</b>
<ul style="list-style-type: none"><li>- System capacity</li><li>- Resonant motion during deepwater installation avoided.</li></ul>	<ul style="list-style-type: none"><li>- Require two installation vessels</li><li>- Complex installation sequence</li><li>- Long operational duration</li></ul>
<b>Opportunity</b>	<b>Threat</b>
<ul style="list-style-type: none"><li>- Deepwater installation during seasons comprised with good weather</li></ul>	<ul style="list-style-type: none"><li>- Risk of ship collision</li></ul>

The pencil buoy method avoids offshore splash zone lifting and will reduce the weather criterion related to a subsea lifting operation. The method allows for installation of heavy structures with limited usage of large crane vessels, and can hence be a solution to vessel availability problems. The largest disadvantage of the pencil buoy method is that it is only capable of installing a single subsea structure per offshore trip, making the method inefficient for field developments at remote locations. The applicability of the pencil buoy method, for deepwater lifting operations, is also limited. The method depends on a conventional deployment winch, for lowering of subsea structures to the seabed, and will face the same problems related to payload capacity as a conventional deployment system. A SWOT analysis of the pencil buoy method is presented in Table 2.3 below.

**Table 2.3: SWOT Analysis, Pencil Buoy Method**

Strength	Weakness
<ul style="list-style-type: none"> <li>- System capacity</li> <li>- Applicable for harsh weather conditions</li> </ul>	<ul style="list-style-type: none"> <li>- Inefficient</li> <li>- Relies on deployment winch applicable for deepwater installation</li> </ul>
Opportunity	Threat
<ul style="list-style-type: none"> <li>- Installation of large structures with small vessels</li> </ul>	<ul style="list-style-type: none"> <li>- Breakage of tow line</li> </ul>

The subsea deployment system, as the pencil buoy method, is based on wet towing subsea structures offshore. The method avoids offshore overboarding and splash zone lifting operations. I.e. The method has the same advantages related to reduction of weather criterions and limited usage of large crane vessels. The method utilizes a subsea deployment vessel, with designated buoyancy tanks, to control the submergence level of the subsea structure during tow. Because the subsea deployment vessel and the structure to be installed are slightly buoyant during the operation, the effective tension in the lifting line is greatly reduced. The landing on seabed operation is not affected by motion of the surface vessel, and weather criterions can be further reduced. The method is seen as highly applicable for deepwater deployment of subsea structures, with inefficiency being the largest disadvantage. A SWOT analysis of the subsea deployment system is presented in Table 2.4 below.

**Table 2.4: SWOT Analysis, Utilization of a Subsea Deployment System**

Strength	Weakness
<ul style="list-style-type: none"> <li>- System Capacity</li> <li>- Applicable for harsh weather conditions</li> <li>- Ease of positioning and control</li> </ul>	<ul style="list-style-type: none"> <li>- Inefficient</li> <li>- Technology still under development</li> </ul>
Opportunity	Threat
<ul style="list-style-type: none"> <li>- Can be used for deepwater installation with smaller vessels</li> </ul>	<ul style="list-style-type: none"> <li>- No operational experience</li> </ul>

The fiber rope deployment system is similar to conventional vertical deployment, but solves the problems related to self-weight of steel wire. The fiber rope is close to neutrally buoyant in water and will have approximately the same payload capacity at any water depth. The fiber rope deployment system also has a higher possible winch pay-out rate than a steel wire system. This results in a shorter duration of the lifting operation, and hence a shorter operational weather window is required. This gives the system an advantage for deepwater lifting operations. One of the disadvantages related to fiber ropes, are the shorter expected time to failure than conventional steel wire. However, offshore repair of fiber ropes is possible. The fiber rope deployment system relies on an installation vessel with a large deck crane for overboarding and splash zone lifting, and problems related to vessel availability is still a governing factor. A SWOT analysis of the fiber rope deployment system is presented in Table 2.5 below.

Table 2.5: SWOT Analysis, Utilization of a Fiber Rope Deployment System

Strength	Weakness
<ul style="list-style-type: none"> <li>- Neutrally buoyant lifting line</li> <li>- Active heave compensated system</li> <li>- Offshore repair of lifting line</li> <li>- Deployment rate</li> </ul>	<ul style="list-style-type: none"> <li>- Dependent on large installation vessel</li> <li>- Maintenance challenges</li> </ul>
Opportunity	Threat
<ul style="list-style-type: none"> <li>- Can be used on smaller installation vessel, rigged with A-frame, for deepwater installation</li> </ul>	<ul style="list-style-type: none"> <li>- Behavior of rope splices</li> </ul>

#### 2.4.6 Conclusion - state of the art review

Utilization of a fiber rope deployment system is considered to be the most applicable method for overcoming the challenges related to deepwater installation of subsea structures. The system will therefore be taken further for a comparison study with a conventional steel wire deployment system. The fiber rope deployment technology solves the problems related to self-weight of steel wire and reduces the duration of deepwater lifting operations. The technology is also field proven and only requires a single installation vessel. It is also seen as a possibility to use a fiber rope deployment system on smaller vessels, rigged with A-frames, which can be used for overboarding and splash zone lifting. Problems related to vessel availability, for deepwater lifting operations, can therefore possibly be reduced.

### 2.5 Fiber rope deployment system

Utilization of a fiber rope deployment system (FRDS) is considered to be the most applicable installation method for overcoming the challenges related to deepwater lifting operations. A more thorough introduction of the fiber rope deployment system is therefore presented.

#### 2.5.1 Deployment system and rope management process

The conventional vertical deployment systems for subsea installations use steel wire as lifting line. The self-weight of steel wire have become a problem in water depths exceeding 2000m. The self-weight of steel wire increases rapidly with depth, reducing the available payload capacity of the lifting line, and increasing the required pulling force of the handling system. Due to the self-weight of steel wire, an increase in wire size to obtain a higher safe working load, leads to a minor change in available payload capacity in deepwater. Very large steel wires are therefore needed to perform installation of heavy equipment at great water depths. Large wires require larger and more powerful handling systems, which again require larger installation vessels. [11]

A solution to the self-weight problems, related to usage of steel wire, is the utilization of high strength, low weight synthetic fiber ropes. The fiber ropes are close to naturally buoyant in water, and the available payload capacity is approximately the same at any water depth. Compared to steel wire, the required pull force of the handling system is significantly smaller, and smaller vessels can be used for heavy installations in deep waters. The weight of fiber ropes in air is also significantly lower than the weight of steel wires, which simplifies handling and logistics. The fiber ropes can also be repaired offshore by cutting out worn segments of rope and splicing in new sections. When segments of steel wire are worn, the only possibility to continue using the wire is to cut off the end of the wire,

reducing the total length and possible installation depth. However, the behavior of fiber rope is significantly different from steel wire, and traditional rope handling systems are not applicable for usage in combination with fiber ropes. [11]

### **2.5.2 Challenges**

Subsea installation means deployment of a heavy structure and recovery of the empty hook. Recovery of an empty hook with a naturally buoyant line will lead to spooling the rope onto a storage drum at very low tension. When deploying a heavy object, the high tensioned rope can be squeezed into softly spooled on layers. In order to avoid this problem, a fiber rope handling system requires a traction unit. To avoid excessive creep of the fiber rope on the storage drum, it is recommended to store the rope at a tension lower than 10% of MBL. To keep the rope tension under the recommended limit, the traction unit is also needed during deployment of heavy structures. [11]

Fiber ropes also have lower axial stiffness than steel wire, resulting in a significant elongation of the rope as tension is increased. The elongation of the rope can cause damaging slippage between the fiber rope and the traction winch drums, if a traditional traction winch is used. The low axial stiffness of the fiber rope system, in comparison with a steel wire system, also means that resonant conditions can be experienced at more shallow water depths. [11]

One of the most desirable features of the fiber rope is its reparability, but to utilize this the rope handling system needs to be able to handle the splices i.e. changes in rope diameter. [11]

During deployment of subsea structures, it is common to use active/passive heave compensators to limit the vertical motion of the lifted object. This means constant cyclic bending over sheaves that can lead to fatigue failure of the deployment line. This is also the case for steel wire but an additional problem with fiber ropes, for repeated cyclic bending, is the danger of internal heat buildup and the sensitivity to heat of the fibers. Typically the fiber ropes strength and modulus increase at sub ambient temperatures but decrease at higher temperatures. [11]

### **2.5.3 Cable traction control unit**

The cable traction control unit (CTCU) is developed by the company ODIM during the last 10 years for handling of sensitive cables. Through a JIP the company developed a system with a cable traction control unit, for deepwater installation using fiber ropes as lifting line. The first CTCU system was designed with a safe working load of 46Te. [11]

The CTCU system is characterized by a series of individually operated sheaves used to de-tension the rope. The sheaves have to be designed with a minimum D:d ratio of 30:1, to fulfill the requirement set by the rope manufacturer for fiber ropes experiencing cyclic bending over sheaves. The sheaves are designed with sheave grooves allowing splice handling, and the coating on each sheave is based on load and required frictional capacity of each sheave. The rope is stored at low tension on a storage drum, which provides constant back tension for the CTCU to assure frictional capacity. From the storage winch, the rope is fed through a spooling device and an inboard damping device, before entering the sheaves of the CTCU. The inboard damping device is used to smoothen the tension between the CTCU and the storage winch. When leaving the CTCU, the rope is guided over the outboard damping device, which provides constant tension and pull limit control, before entering the overboarding device. [11]

The CTCU system has active load distribution, which shares the load between the sheaves within the frictional capacity of the sheaves, and the pulling capacity of the drive system for each sheave. To avoid slip, a designated slip control is utilized, which control the speed of the sheaves to compensate for rope elongation and diameter variation over splices. The CTCU system also has anti spin control, which detects and reacts upon an emerging spinning situation. Spin is detected by comparing the speed of each sheave with measured rope speed, and spin is avoided by reducing the torque on a sheave getting into a spinning situation. The CTCU system also has rope pre-conditioning, which brings the rope down to its nominal diameter during first time spooling. [11]

#### **2.5.4 Rope management system**

Any kind of steel wire or fiber rope will suffer from fatigue when subjected to cyclic bending over sheaves. At time of development there were limited field data available to support rope wear calculations. Conservative calculations were applied for assessing the rope retirement criteria in order to avoid premature rope failure during operations. [11]

In order to further develop the rope wear calculation methods, and establish less conservative retirement criteria, a rope management system (RMS) was developed as an integral part of the winch control system. The rope management system uses real time signals of position and tension, at any part of the rope, and compares the data with geometrical data (sheave diameter and distance between sheaves). Based on this, the rope management system can count the number of bends experienced by any part of the rope, and weigh each bend according to a factor given by bend radius and rope tension at each bend point. The rope management system makes it possible for the operator to utilize the rope fatigue life for all parts of the rope, and manage the condition of the rope as the rope configuration changes upon cutting and splicing. [11]

In the RMS, the rope is split into segments of e.g. 0.33m, and rope data for each segment is recorded. The data is presented on the winch operator computer in real time, and has a built in alarm function for inspection and replacement of rope segments. All the data is stored and can be post processed to improve the fiber rope wear calculations. When a rope segment reaches its retirement criteria, or the operator wish to check the residual strength of a rope segment to assess its actual condition, the segment is cut out and sent to a laboratory for testing. Data from the RMS system for the specific rope segment can be retrieved and compared with the laboratory test. Rope wear calculation methods can hence be improved continuously. [11]

#### **2.5.5 Increased capacity system**

The successful 46Te FRDS system, initiated the development of an increased capacity system. The new system would be able to install equipment weighing up to 250Te down to a water depth of 3000m, based on a 125Te SWL FRDS working in a two-fall configuration. The fiber rope to be used in the system was an 88mm, braid optimized for bending rope, delivered by the company Cortland. The rope has a 12x12 strand construction which provides high strength, low elongation, long-term creep resistance, and good cyclic fatigue performance. The rope has a minimum break load of 567Te and a SWL of 125Te, applying a safety factor of 4.5. [12]

The 250Te FRDS was bought by Aker Oilfield Services, who would use it for deepwater installation of subsea Xmas trees under a five year contract with Petrobras. The system was mobilized on the DOF-owned vessel Skandi Santos. The 250Te FRDS was used as the main lift winch and the system was rigged to operate through the vessel moonpool, via a moonpool tower system. Due to the harsh

weather offshore Norway at the time of mobilization, the system was tested in a deep water fjord. The test comprised the lowering of a 100Te clump weight down to approximately 1000m water depth. The test proved that deepwater lifting operations, using 125Te FRDS in two fall configuration, can be successfully performed. [12]

### 2.5.6 Field experience

The 46Te SWL fiber rope deployment system was used by Subsea 7 in 2006, to install subsea hardware in water depths of 2000 – 2750m in the Gulf of Mexico. The system was mobilized on the Subsea 7 vessel Toisa Perseus, and installed to work over the side of the vessel. During installation the fiber rope deployment system was used in combination with either the deck crane or the A&R winch. The deck crane/A&R winch would deploy the hardware down to a suitable depth, say 1000m, and the load would be transferred to the FRDS for further lowering to seabed. The high speed capability of the system was found to provide a considerable time saving for deepwater operations. Figure 2.10 below presents the 46Te FRDS mobilized on Toisa Perseus. [11]



Figure 2.10: 46Te SWL, Fiber Rope Deployment System Mobilized on Toisa Perseus, REF [11], Figure.10

A total of 190 deployments and recoveries were successfully conducted, and the rope performed very well without any major issues. The first rope inspection was performed after 140 installations, on the rope segment having seen the highest number of weighted bends. No damaged fibers were recorded and the outer layer was found to be in good condition. [11]

The 250Te SWL fiber rope deployment system has been used by Aker Oilfield Services to perform over 80 installations in 9 months for Petrobras. The operational experiences so far were that constant tension is needed while connected subsea. Long periods with usage of active heave compensation also caused the rope to reach the inspection retirement level earlier than expected, and maintenance requirements were found to be underestimated. The splicing technique used was not verified and slippage of rope splices occurred over time. [13]

### 3 Fiber rope vs. steel wire - comparison study

In the comparison study, the installation of two different subsea structures down to a water depth of 2950m will be reviewed. The chosen structures are a subsea tree with dimensions 6x6x7m, weighing 70Te, and a manifold with dimensions 9x7x5m weighing 115Te. Structures are based on Table 2.1, section 2.3. Dimensions of the subsea tree considered in the comparison study, is somewhat larger than stated in Table 2.1, and considered to provide a conservative analysis of subsea tree installation. The study will review different aspects related to deepwater subsea lifting.

#### 3.1 Payload capacity

For comparison of payload capacity at great water depths, a water depth of 3000m is applied in this analysis. A fiber rope with a safe working load (SWL) of 125Te will be compared to a steel wire with the same SWL. Selection of SWL is based on the largest capacity FRDS for single line deployment.

The fiber rope to be used in the study is a 12x12 strand, braid optimized for bending (BOB) rope, developed by the company Cortland. The rope has a specially developed coating to maximize the ropes durability in bending situations. The rope size to be utilized in the study is a 3 5/8" rope with a nominal diameter of 88mm, as used for the FRDS on Skandi Santos. [13]

The rope has a minimum tensile strength (minimum break load) of 567Te, applying a safety factor of 4.5 results in a SWL of 125Te. The rope has a weight in air of approximately 693.1 kg/100m. [14]

The steel wire that will be compared to the fiber rope is a Non-rotating 35xK19S Compacted steel wire, delivered by the company Kiswire. The chosen wire size is 2 5/8" and has a MBL of 3834kN. Applying a safety factor of 3.1 (In accordance with REF [15]), results in a SWL of 126Te at surface. The steel wire can be used with a lower safety factor than the fiber rope, due to the extensive experience with usage of steel wire as deployment line. Weight of the wire in air is approximately 2259kg/100m. [16]

##### 3.1.1 Submerged weight of lifting line

To assess the reduced payload capacity of the wire and the fiber rope at increasing water depth, the submerged weight of the wire/fiber rope need to be found.

When an object is submerged it experiences a buoyancy force, which is equal to the weight of the water displaced by the submerged object. The buoyancy force act in the opposite direction of the gravity force, and the submerged weight of the object will be lower than the weight of the object in air. The buoyancy force can be found as:

$$F_B = \nabla g \rho_{SW} \text{ [N]}$$

Where:

$\nabla$  = Displaced volume of water [m<sup>3</sup>]

$g$  = Acceleration of gravity [m/s<sup>2</sup>]

$\rho_{SW}$  = density of seawater [m<sup>3</sup>]

$F_B$  = Buoyancy force [N]

And the submerged weight of the object can be found as:

$$m_{\text{sub}} = \frac{F_G - F_B}{g} \text{ [Kg]}$$

$$F_G = mg \text{ [N]}$$

Where

$F_G$  = gravity force [N]

$m$  = weight of object in air per unit length [kg/m]

$m_{\text{sub}}$  = submerged weight of object per unit length [kg/m]

The submerged weight of the steel wire and the fiber rope is presented in Table 3.1 below. The submerged weight of the fiber rope is given in REF [13], while the submerged weight of the steel wire is calculated based on the equation above.

**Table 3.1: Submerged Weight of Lifting Lines [kg/m]**

Lifting Line	Submerged Weight [kg/m]
2 5/8 " Steel Wire	19.92
88mm Fiber Rope	0.87

### 3.1.2 Reduced payload capacity

The payload capacity of any lifting line will be reduced as the payout length of the line is increased due to the self-weight of the lifting line. The reduced payload capacity of a lifting line can for a subsea lifting operation be found as:

$$\text{Payload capacity} = \text{SWL} - (m_{\text{sub}} * L) \text{ [kg]}$$

Where:

SWL = Safe working load of the lifting line [kg]

$m_{\text{sub}}$  = Submerged weight of the lifting line per unit length [kg/m]

$L$  = Length of lifting line [m]

The steel wire and the fiber rope have a safe working load (payload capacity) at surface of 126Te and 125Te respectively. However, due to the difference in submerged weight of the two lifting lines, the payload capacity will differ significantly as length of the lines, i.e. the water depth increase. The payload capacity as a function of water depth is presented in Figure 3.1 below, both for steel wire and fiber rope. Length of the lifting line is assumed to be equal to the water depth.



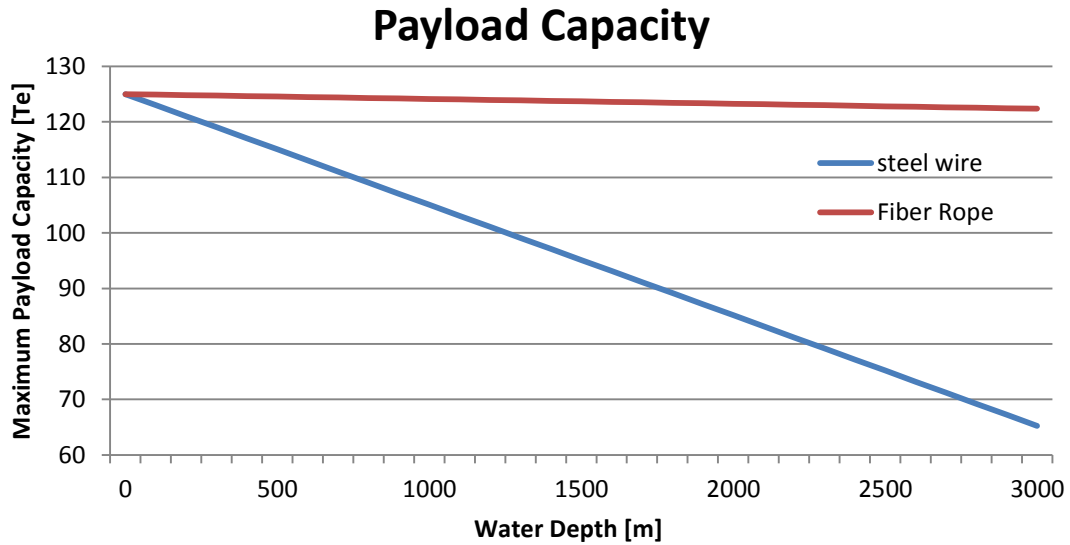


Figure 3.1: Payload Capacity as a Function of Water Depth

Figure 3.1 above displays the large difference in payload capacity for the two lifting lines as the water depth is increased. It is seen that the capacity of the fiber rope is slightly reduced from 125Te at surface, to 122.4Te at a water depth of 3000m. The capacity of steel wire is reduced from 125Te at surface, to 65.2Te at a water depth of 3000m. This highly inflicts the applicability of a steel wire system to perform installations in a large variety of water depths.

In order to have a steel wire with a payload capacity of 125Te at 3000m water depth, an increase in wire size is necessary. The capacity of different sized steel wires as a function of water depth is presented in Figure 3.2 below. Input data required for calculations is found in REF [16].

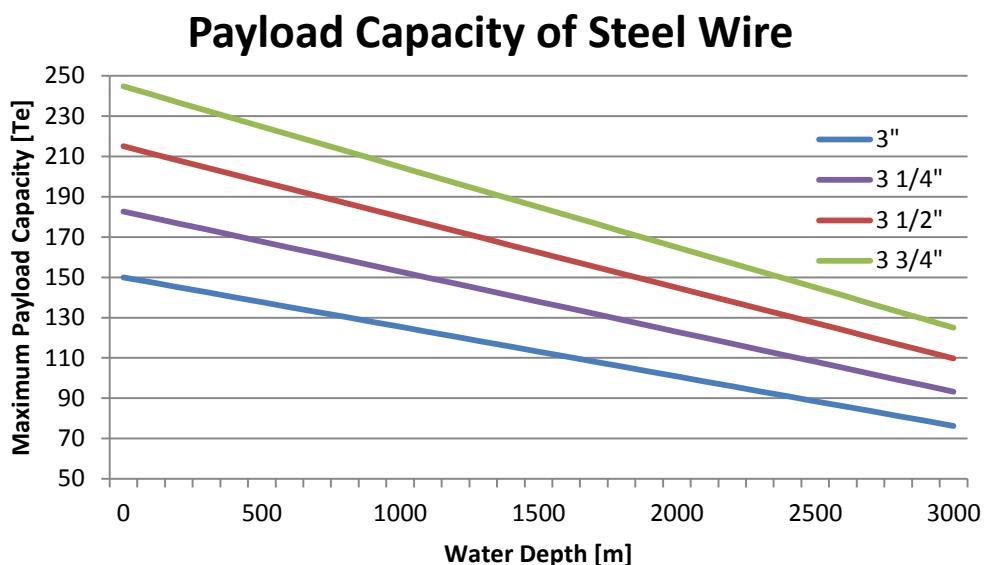


Figure 3.2: Payload Capacity of Different Sized Steel Wire as a Function of Water Depth

It is seen from Figure 3.2 above that a wire size of 3 3/4" is sufficient for obtaining a payload capacity of 125Te at 3000m water depth. A safety factor of 3.2 is applied to obtain the SWL of 125T, which is

approximately similar to the SWL of the fiber rope. From the figure it is also seen that the increase in payload capacity, gained when the wire size is increased, is reduced when operations are performed in deepwater. Table 3.2 below illustrates the “loss” of additional payload capacity at a water depth of 3000m.

**Table 3.2: “Loss” of Increased Wire Capacity**

Increase in wire size [inch] From – To	Increased Payload Capacity @Surface [Te]	Increased Payload Capacity @3000m [Te]
3 – 3 ¼	32.7	16.9
3 ¼ – 3 ½	32.3	16.6
3 ½ – 3 ¾	29.7	15.2

The “loss” of additional payload capacity is a result of the increased weight of the wire, when wire size is increased. In practice this means that steel wires used for heavy lifting at great water depths, rapidly becomes very large and impractical to handle. e.g. the increase in wire size from 2 5/8”, which had a payload capacity of 125Te at surface, to the 3 ¾” wire required to obtain a payload capacity of 125Te at 3000m, results in an increased wire weight in air from 2259kg/100m to 4524kg/100m.

**3.1.3 Summary – payload capacity**

From Figure 3.1 above it is seen that due to the low submerged weight of fiber rope, the capacity of the fiber rope deployment system will only be slightly reduced at a water depth of 3000m, making it applicable for deepwater purposes. The steel wire has a significant reduction in payload capacity, at a water depth of 3000m, and selection of wire size is crucial for deepwater operations. From Figure 3.2 and Table 3.2 above, it is seen that a rapid increase in wire size is necessary to obtain sufficient payload capacity at large water depths. This leads to challenges related to logistics, increased pull force of deployment winch, and the vessel deck load will increase. A larger wire size also require a larger drum winch to fulfill the D:d ratio required for bending steel wire.

**3.2 Horizontal offset due to current**

For any subsea lifting operation it is important to estimate the horizontal offset of the lifted object due to current during the operation. The horizontal offset is used to assess the payout length of deployment line required to reach the seafloor, and to manage positioning of the lifted object on the seafloor.

Figure 3.3 below illustrates the theoretical model for the horizontal offset due to current calculations:

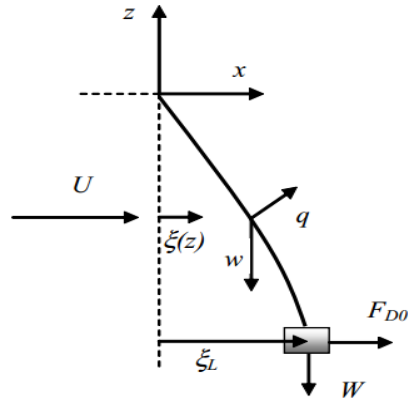


Figure 3.3: Horizontal Offset due to Current, Theoretical Model, DNV-RP-H103, Figure 5-1.

Where:

$q$  = Drag force on lifting line per unit length [N/m]

$F_{D0}$  = Drag force on lifted object [N]

$w$  = Submerged weight of lifting line [N/m]

$W$  = Submerged weight of lifted object [N]

$U$  = Current velocity [m/s]

$\xi(z)$  = Horizontal offset at an arbitrary water depth  $z$  [m]

$\xi_L$  = Horizontal offset of the lifted object [m]

According to DNV-RP-H103, section 5.2.2.2, the horizontal offset of a lifted object subjected to a uniform current can be found as:

$$\xi_L = L \left( \frac{q}{w} k - \lambda \right) \ln \left( \frac{k}{k+1} \right) + \frac{qL}{w} \text{ [m]}$$

Based on Figure 3.3 above, where:

$$k = \frac{W}{wL} \text{ [-]}$$

$$\lambda = \frac{F_{D0}}{wL} \text{ [-]}$$

$$q = \frac{1}{2} \rho_{sw} C_{Dn} D_c U^2 \text{ [N/m]}$$

$$F_{D0} = \frac{1}{2} \rho_w C_{Dx} A_x U^2 \text{ [N]}$$

$$W = F_G - F_B \text{ [N]}$$

$$F_G = M * g \text{ [N]}$$

$$F_B = \rho_{sw} * \nabla * g \text{ [N]}$$

$k$  = Ratio between the weight of the lifted object and weight of the lifting line [-]

$\lambda$  = Ratio between the drag on the lifted object and weight of the lifting line [-]

$C_{Dn}$  = Drag coefficient for normal flow past lifting line [-]

$C_{Dx}$  = Drag coefficient for flow past lifted object, x-direction [-]

$D_c$  = Lifting line diameter [m]

$A_x$  = Projected area of lifted object, x-direction [m<sup>2</sup>]

$F_G$  = Gravitational force [N]

$F_B$  = Buoyancy force [N]

$\nabla$  = Displaced volume of water [m<sup>3</sup>]

$g$  = Acceleration of gravity [m/s<sup>2</sup>]

$\rho_{SW}$  = density of seawater [kg/m<sup>3</sup>]

It is seen from Figure 3.3 above, that the horizontal offset due to current is dependent on both the submerged weight of the lifting line, and the drag force on the lifting line. The horizontal offset due to current will therefore differ when utilizing different lifting lines.

### 3.2.1 Case study

In order to compare the horizontal offset due to current, when using steel wire and fiber rope as deployment line, the installation of a subsea tree and a manifold will be considered. The subsea tree has dimensions 6x6x7m and weighs 70Te, while the manifold has dimensions 9x7x5m and weighs 115Te. The steel wire to be utilized is the 3 3/4" wire, found to have a payload capacity of 125Te down to a water depth of 3000m in section 3.1.2. The fiber rope to be utilized is the same 88mm 12x12 strand BOB rope, with a SWL of 125Te discussed in section 3.1.

In practice the current velocity will vary with depth and be represented by a velocity profile. This study does however focus on the difference in horizontal offset due to current, when utilizing different lifting lines. The current profile is therefore assumed to be constant for all water depths, with a current velocity set equal to 0.6m/s.

In order to calculate the horizontal offset due to current, for the two operational scenarios, the submerged weight of the lifted object need to be estimated. All compartments of the subsea structures are assumed to be filled with water during installation, and the displaced volume of water is assumed to be equal to the volume of steel for each structure. The displaced volume of water is hence found as:

$$\nabla = \frac{M}{\rho_{steel}} [m^3]$$

Where:

$$\rho_{steel} = \text{Density of steel [kg/m}^3\text{]}$$

$$M = \text{Weight of lifted object in air [kg]}$$

$$\nabla = \text{Displaced volume of water [m}^3\text{]}$$

And the submerged weight of the object can be found as:

$$W = F_G - F_B [\text{N}]$$

Where:

$$F_G = Mg [\text{N}]$$

$$F_B = \nabla g \rho_{SW} [\text{N}]$$

$$F_G = \text{Gravitational force [N]}$$

$$F_B = \text{Buoyancy force [N]}$$

$$g = \text{Acceleration of gravity [m/s}^2\text{]}$$

$$\rho_{SW} = \text{density of seawater [m}^3\text{]}$$

The submerged weight of the subsea tree and manifold is estimated based on the equations above, and results are presented in Table 3.3 below.

**Table 3.3: Submerged Weight of Subsea Structures [kN]**

Subsea Structure	Submerged Weight (W) [kN]
Subsea Tree	597.6
Manifold	982

The submerged weight of the fiber rope is already known from section 3.1.1. Submerged weight of the 3 3/4" steel wire is calculated as in section 3.1.1 and result are presented in Table 3.4 below.

**Table 3.4: Submerged Weight of Lifting Lines [N/m]**

Lifting Line	Submerged Weight (w) [N/m]
3 3/4" Steel Wire	391.2
88mm Fiber Rope	8.53

The other required input parameters are calculated and presented in Table 3.5 and Table 3.6 below, for installation of the subsea tree and the manifold located at a water depth of 3000m. Length of the lifting line is assumed to be equal to the water depth. The input parameters are calculated based on equations above.

Drag coefficient for flow past the steel wire is set in accordance with DNV-RP-H103, APPENDIX B, Table B-1. Drag coefficient for flow past the fiber rope is set in accordance with DNV-RP-E301, section B700.

**Table 3.5: Input Parameters, Horizontal Offset Calculation, Subsea Tree**

Subsea Tree	Steel Wire	Fiber Rope
Drag coefficient for normal flow past lifting line ( $C_{Dn}$ )	1.8	1.8
Drag coefficient for flow past lifted Object X– direction ( $C_{Dx}$ )	1.16	1.16
Ratio between the weight of the lifted object and weight of the lifting line (k)	0.509	23.35
Projected area of lifted object X-direction ( $A_x$ )	42m <sup>2</sup>	42m <sup>2</sup>
Current velocity ( $U_c$ )	0.6m/s	0.6m/s
Lifting line diameter ( $D_c$ )	0.0953m	0.088m
Drag force on lifting line per unit length (q)	39.65N/m	29.2N/m
Drag force on lifted object ( $F_{D0}$ )	8990N	8990N
Ratio between the drag force on the lifted object and weight of the lifting line ( $\lambda$ )	0.0077	0.351

**Table 3.6: Input Parameters, Horizontal Offset Calculation, Manifold**

Manifold	Steel Wire	Fiber Rope
Drag coefficient for normal flow past lifting line ( $C_{Dn}$ )	1.8	1.8
Drag coefficient for flow past lifted object X– direction ( $C_{Dx}$ )	1.163	1.163
Ratio between the weight of the lifted object and weight of the lifting line (k)	0.837	33.4
Projected area of lifted object X-direction ( $A_x$ )	63m <sup>2</sup>	63m <sup>2</sup>
Current velocity (U)	0.6m/s	0.6m/s
Lifting line diameter ( $D_c$ )	0.0953m	0.088m
Drag force on lifting line per Unit Length (q)	39.65N/m	29.2N/m
Drag Force on Lifted Object ( $F_{D0}$ )	13520N	13520N
Ratio between the drag force on the lifted object and weight of the lifting line ( $\lambda$ )	0.0115	0.656

### 3.2.2 Results - horizontal offset due to current

The horizontal offset due to current is calculated for each installation scenario at a water depth of 3000m, and results are presented in Table 3.7 below.

**Table 3.7: Horizontal Offset Due to Current**

Structure to be Installed	Horizontal Offset Steel Wire[m]	Horizontal Offset Fiber Rope[m]
Subsea Tree	161	258
Manifold	131.1	208.8

### 3.2.3 Summary - horizontal offset due to current

It is seen from Table 3.7 above that the horizontal offset due to current differ greatly for the two lifting lines. This is a result of the difference in submerged weight, which together with the submerged weight of the lifted object, causes the force counteracting the drag force on the lifted object and lifting line, REF Figure 3.3 above.

The increased horizontal offset due to current, when utilizing fiber rope as lifting line compared to steel wire, causes a larger challenge related to positioning of the lifted object on the seafloor. This can possibly increase the time required to position the lifted object, and hence increase the duration of the operation. This again reduces the advantage gained by having a higher deployment rate for

the fiber rope deployment system compared to a steel wire system. When the weight of the lifted object is increased, the difference between the two lifting lines is reduced. The reason for this is that the counteracting force caused by the submerged weight of the lifting line, represent a smaller factor of the total counteracting force.

### 3.3 Dynamic analysis

The dynamic effects experienced during offshore lifting operations are the limiting factor with respect to operable sea-states. The reaction between the lifting system, in this thesis considered to be the lifting line and lifted object, and the oscillating crane tip motion can introduce large dynamic forces in the lifting line. These dynamic forces can cause a load exceeding the safe working load of the lifting system, resulting in breakage of the lifting line and loss of the subsea structure.

Usually the dynamic forces experienced during splash zone lifting will be larger than those experienced during lowering to seabed. Splash zone lifting will hence cause the limiting weather criteria for the lifting operation. Resonant motion between the lifting system and the oscillating crane tip motion, can however cause large dynamic effects during lowering to seabed operations, and possibly result in even stricter weather criteria for the operation.

Due to the low axial stiffness of the fiber rope, resonant conditions will occur at more shallow water depths for a fiber rope deployment system than for a similar steel wire system. For installation work at shallow water depths, a steel wire system will hence be preferable to avoid the effect of resonant motion. Due to the large axial stiffness of the steel wire, resonant conditions will only occur at large water depths. Since the payload capacity of a steel wire system is reduced with water depth, large dynamic effects at large water depths will be more critical than for a fiber rope system.

The dynamic response of a lifting system depends on the shape and weight of the lifted object, and the axial stiffness of the lifting line. The dynamic effects experienced during any lifting operation will therefore vary for installation of different subsea structures, and for usage of different lifting lines.

#### 3.3.1 Case study

To assess the difference in dynamic behavior of a fiber rope deployment system and a steel wire system, a dynamic analysis will be performed using the modelling and analysis program ORCAFLEX. The analysis will cover the lowering operation of different subsea structures, from a water depth of 500m down to a water depth of 2950m. Splash zone lifting analysis is not covered since the fiber rope deployment system and the steel wire system, both perform splash zone lifting using a deck crane with steel wire as lifting line. There will hence not be any difference in dynamic behavior during splash zone lifting.

The dynamic analysis of the lowering to seabed operation will be performed for two different subsea structures, to account for different dynamic behavior of structures with different shapes. The chosen structures are a subsea tree with dimensions 6x6x7m with a weight in air of 70Te, and a manifold with dimensions 9x7x5m with a weight in air of 115Te. The analysis will be performed for environmental loading conditions representing the environment in the Gulf of Mexico. The Gulf of Mexico is chosen, because it is one of the areas in the world where deepwater fields are currently being developed.

### 3.3.2 ORCAFLEX model

The modelling and analysis program ORCAFLEX, gives options for modelling of vessels, different structures, and connection elements. Because no RAO data is known for any specific installation vessel, the standard vessel model in ORCAFLEX is used for the analysis. The line function is used to model the lifting line, and the 6D buoy function is used to model the two subsea structures.

#### 3.3.2.1 Installation vessel

The standard vessel model in ORCAFLEX is based on an offshore tanker, however the size and weight of the vessel is seen as representable as a typical installation vessel. Length of the vessel is 103m and the weight is 9017.95Te. The vessel is however narrow and will be more sensitive to roll motion than a typical installation vessel. A sketch of the vessel model is presented in Figure 3.4 below.

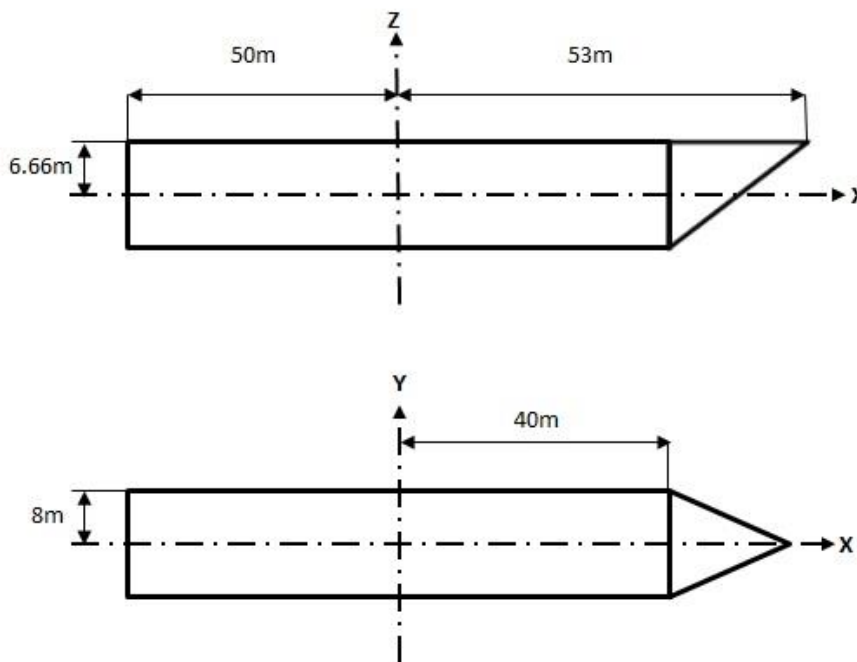


Figure 3.4: Vessel Model, ORCAFLEX

For purpose of the analysis, the vessel primary motion is set to “none”, and the vessel superimposed motion is set to “displacement RAOs + harmonic motion”. Included in static calculation is set to “calculated 6DOF” and included effects are set to “added mass and damping”. The vessel initial position in the global coordinate system is set to  $(x, y, z) = (0, 0, 0)$ . The vessel heading is set to  $22.5^\circ$  to introduce vessel roll motion. No other vessel settings are changed.

#### 3.3.2.2 Lifting line

The “Line” function in ORCAFLEX is used to model the fiber rope and steel wire as lifting lines instead of the “winch function”. The “Line” function works as a connection, with a given mass and stiffness between two structures, while the “winch” function works as a massless connection between two structures. The line function will hence account for different weight of the two lifting lines. The line is connected to the installation vessel to simulate lowering over side of the vessel, and connected at the top of the 6D buoy (subsea structure). Connection points are presented in Table 3.8 and Table 3.9 below.



Table 3.8: Line Connection, Subsea Tree Installation

Connection	Object Relative Position		
	X	Y	Z
Vessel	0	8	6.66
6D buoy	0	0	3.5

Table 3.9: Line Connection, Manifold Installation

Connection	Object Relative Position		
	X	Y	Z
Vessel	0	8	6.66
6D buoy	0	0	2.5

Under the option “line type” the properties of the line can be set to represent each of the two lifting lines. For the “geometry and mass” section, the outer diameter and mass per unit length of line is set. The inner diameter of line is set to zero. ORCAFLEX uses the outer/inner diameter and weight per unit length to calculate the submerged weight of the line, and hence calculate the effective tension in the line during simulation. Under the “structure” section, the axial stiffness of the line is set. No other line parameters are changed.

### 3.3.2.3 Subsea structure

For modelling of the two subsea structures, the “6D buoy” function is used. The chosen 6D buoy is the lumped buoy. The initial position and altitude of the 6D buoy is set as  $(x, y, z) = (0, 8, L - H + \frac{h}{2})$  in the global coordinate system, based on Figure 3.5 below.

Where:

H = Height of vessel deck above sea level [m]

L = Length of lifting line [m]

h = Height of the lifted object. [m]

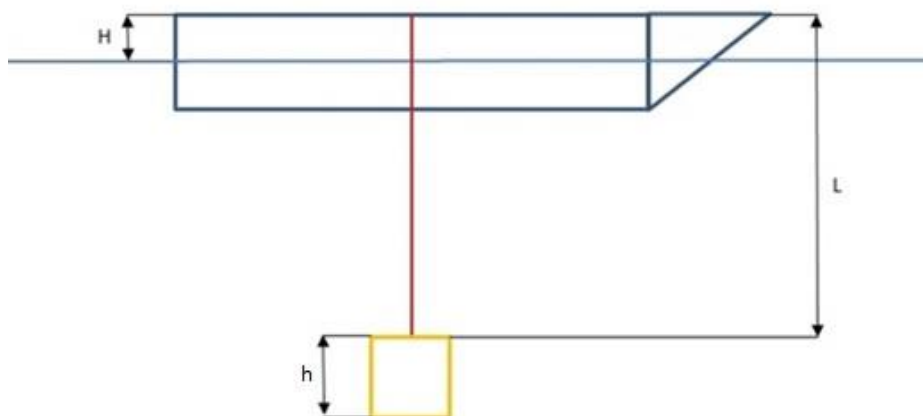


Figure 3.5: Determining Initial Position of the 6D buoy, ORCAFLEX

The shape of the 6D buoy can be modelled under the “Drawing” section. Drawing of the 6D buoy is based on connection between nodes, and position of nodes are set as (x, y, z) values according to the local coordinate system of the 6D buoy. The subsea tree and the manifold are modelled in ORCAFLEX according to Figure 3.6 and Figure 3.7 below. The local coordinate system of the 6D buoy is located in the volumetric center of the two figures below.

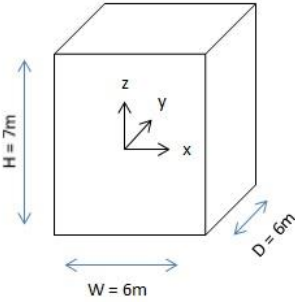


Figure 3.6: ORCAFLEX Model, Subsea Tree

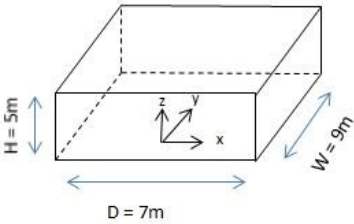


Figure 3.7: ORCAFLEX Model, Manifold

Under the “inertia section” the mass in air of the lifted objects, the mass moments of inertia and the center of mass can be altered for the 6D buoy. The center of mass is set as (x, y, z) = (0, 0, 0) for both the subsea tree and the manifold.

Under the “properties – geometry” section, the volume, height and center of volume for the 6D buoy can be altered. The volume input represents the volume of displaced water, and is used by ORCAFLEX to calculate the submerged weight of the 6D buoy. The center of volume is set to (x, y, z) = (0,0,0) for both structures.

Under the “properties – translational motion” the drag area and drag coefficient of the 6D buoy is set, along with the hydrodynamic added mass, the added mass coefficient and the inertia coefficient. Rotational motion of the 6D buoy is neglected in the analysis.

### 3.3.2.4 Environmental loading conditions

To model the environmental loading conditions, representing the sea-state in the Gulf of Mexico, the waves are modelled based on a Pierson – Moskowitz wave spectrum. According to the “Handbook of Offshore Engineering” by Subrata Chakrabarti REF [17], The Pierson-Moskowitz wave spectrum is applicable for operational purposes in the Gulf of Mexico. ORCAFLEX does not have a wave model based on the Pierson-Moskowitz wave spectrum, but according to DNV-RP-H103 section 2.2.6, a JONSWAP spectrum reduces to the Pierson-Moskowitz spectrum for peak parameter  $\gamma = 1$ . Hence the ORCAFLEX wave model is based on a JONSWAP wave spectrum with  $\gamma = 1$ . Different sea-states are modelled by changing the significant wave height and the wave zero up-crossing periods. The applied wave direction is set to  $180^\circ$ . The wave direction relative to the vessel heading ( $\Theta$ ) is presented in Figure 3.8 below.

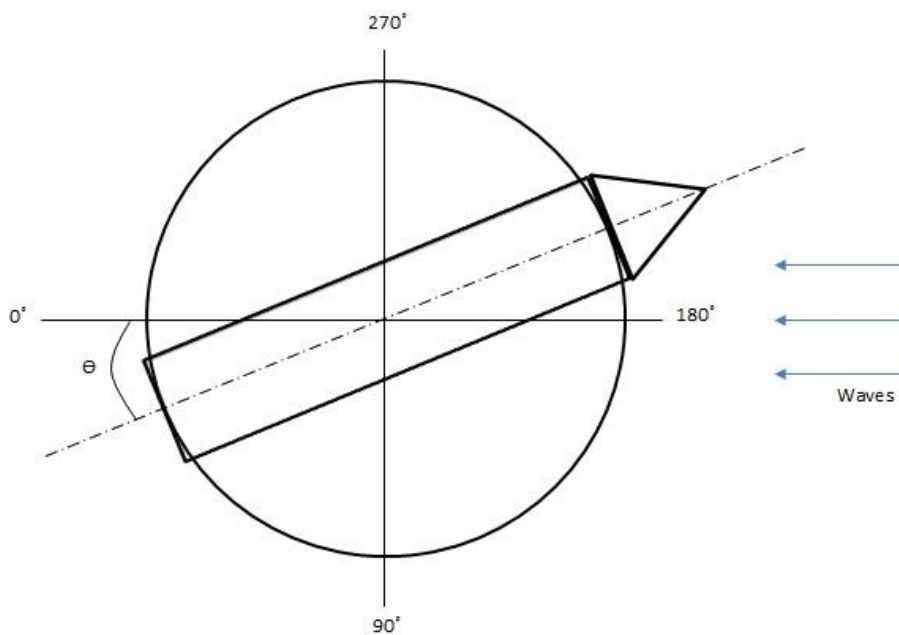


Figure 3.8: Wave Direction vs. Vessel Heading

The seabed origin is set to  $z = -3000\text{m}$ , and the sea surface is set to  $z = 0$ . No other environmental parameters are changed, and the effect of wind and current loads are not accounted for.

### 3.3.3 ORCAFLEX input parameters

To perform the ORCAFLEX analysis of the lowering to seabed operation, a set of input parameters are required.

#### 3.3.3.1 Lifting line properties

The lifting line properties required as input for the ORCAFLEX analysis is:

- Axial stiffness of the lifting line
- Weight in air per unit length
- Outer diameter of the lifting line

For the steel wire, the axial stiffness and weight in air per unit length is found in REF [16]. ORCAFLEX uses the outer diameter of the lifting line to determine the submerged weight of the lifting line. The

outer diameter of the lifting line is therefore calculated based on the metallic area, given for the steel wire in REF [16].

For the fiber rope, the weight in air per unit length is found in REF [14]. The axial stiffness of the rope is calculated based on the load/elongation curve presented in REF [14], and can be found as:

$$\frac{EA}{L} = \frac{F}{\Delta L} \text{ [N/m]}$$

$$EA = \frac{F}{\Delta L} L \text{ [N]}$$

Where:

EA = Axial stiffness of the fiber rope [N]

F = Applied load [N]

$\Delta L$  = Elongation of rope under applied load [m]

L = Initial length of rope [m]

The outer diameter of the fiber rope is calculated based on the buoyancy force, causing the submerged weight of the fiber rope given in REF [13], and found as:

$$F_B = \rho_{sw} * \nabla \text{ [kg]}$$

$$F_B = m - m_{sub} \text{ [kg]}$$

$$\nabla = \frac{\pi}{4} D_c^2 \text{ [m}^3\text{]}$$

Where:

$F_B$  = Buoyancy force [N]

$\rho_{sw}$  = Density of seawater [kg/m<sup>3</sup>]

$\nabla$  = Displaced volume of water [m<sup>3</sup>]

m = Weigh per unit length of fiber rope in air [kg]

$m_{sub}$  = Submerged weight per unit length of fiber rope [kg]

$D_c$  = Outer diameter of fiber rope [m]

### 3.3.3.2 Subsea structure properties

The properties required as input for the ORCAFLEX analysis for the two subsea structures is:

- Displaced volume of water
- Mass moment of inertia for rotation around each axis
- Drag area for all flow directions
- Drag coefficients for all flow directions
- Hydrodynamic added mass coefficients and corresponding hydrodynamic added mass for all flow directions
- Hydrodynamic inertia coefficient for all flow directions

ORCAFLEX uses the displaced volume of water to determine the submerged weight of the lifted object. The displaced volume of water for the two different subsea structures is estimated as in section 3.2.1.

The mass moment of inertia represents the structures resistance against rotation around each axis and is calculated, e.g. for rotation around the x-axis, as:

$$I_x = \frac{1}{12} M (y^2 + z^2) \text{ [kg.m}^2\text{]}$$

Where:

$I_x$  = Mass moment of inertia [kg.m<sup>2</sup>]

M = Mass of object in air [kg]

y, z = Length of the object in y – and z –direction [m]

The drag area and drag coefficient for each direction is required, for ORCAFLEX to be able to determine the drag forces acting on the structure during installation. The drag area represents the area of the structure normal to the flow direction. Drag coefficients for objects subjected to an oscillatory flow, can be difficult to determine without experimental testing or computerized fluid dynamic analysis. The drag coefficient for flow in each direction is therefore set to:

$$C_{Dx} = C_{Dy} = C_{Dz} = 2.5 \text{ [-]}$$

In accordance with DNV-RP-H103, Section 4.6.2.4, “*Drag coefficients on typical subsea structures in oscillatory flow*”.

The hydrodynamic added mass and added mass coefficient is required for ORCAFLEX to determine the dynamic behavior of the structure during installation. The hydrodynamic added mass can be seen as the mass of water affected by the motion of the lifted object. An illustration of hydrodynamic added mass is presented in Figure 3.9 below.

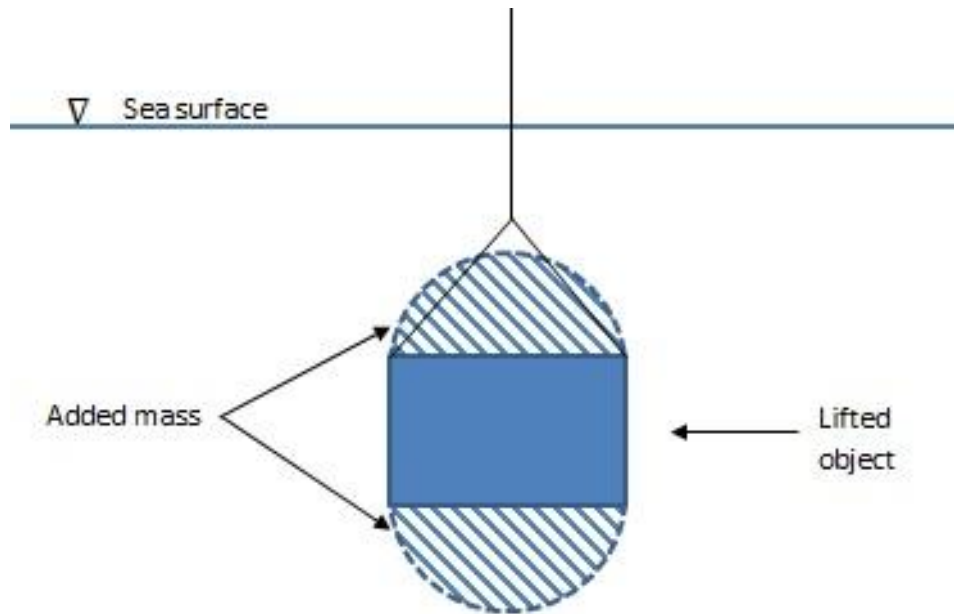


Figure 3.9: Hydrodynamic Added Mass

Calculation of hydrodynamic added mass coefficients and corresponding hydrodynamic added mass is based on DNV-RP-H103, APPENDIX A, Table A-2. The effect of vertical sides and structure perforation are based on DNV-RP-H103, section 4.6.

The added mass coefficients are found from DNV-RP-H103, APPENDIX A, Table A-2.

- The subsea tree is seen as a flat rectangular plate normal to flow direction, for flow in all directions.
- The manifold is seen as a flat rectangular plate normal to flow direction, for flow in all directions.

Added mass coefficients are found by using linear interpolation between the tabulated values.

The hydrodynamic added mass is calculated as:

$$A_{330} = \rho_{SW} * C_A * V_R [\text{kg}]$$

Where:

$A_{330}$  = Hydrodynamic added mass [kg]

$C_A$  = Hydrodynamic added mass coefficient [-]

$\rho_{SW}$  = Density of seawater [kg/m<sup>3</sup>]

$V_R$  = Reference volume [m<sup>3</sup>]

The reference volume for rectangular plates can be found as:

$$V_R = \frac{\pi}{4} a^2 b$$

Where:

a = Short side of the object area normal to flow direction

b = Long side of the object area normal to flow direction

To account for the vertical sides of the flat rectangular plates, the following simplified approximation of the hydrodynamic added mass for non-perforated structures can be applied:

$$A_{33s} = \left[ 1 + \sqrt{\frac{1-\lambda^2}{2(1+\lambda^2)}} \right] * A_{330} \text{ [kg]}$$

$$\lambda = \frac{\sqrt{A_p}}{h + \sqrt{A_p}} \text{ [-]}$$

Where:

$A_{33s}$  = Hydrodynamic added mass, effect of perforation not accounted for [kg]

$A_p$  = Projected area of submerged object normal to flow direction [m<sup>2</sup>]

h = Height of the object [m]

Subsea structures are not designed as solid objects, and the effect of perforation have to be taken into account. The perforation of a lifted object will reduce the added mass and affect the dynamic behavior of the object during installation. The subsea tree is assumed to be 10% perforated and the manifold is assumed to be 30% perforated. The added mass reduction factors are found in DNV-RP-H103, section 4.6, Figure 4-7. And the added mass can be calculated as:

$$A_{33} = A_{33s} * \text{Added mass reduction factor [kg]}$$

The hydrodynamic inertia coefficient can be found as:

$$C_M = 1 + C_A \text{ [-]}$$

Where:

$C_M$  = Hydrodynamic inertia coefficient [-]

Input parameters for the two lifting lines and the two subsea structures are calculated based on equations above, and presented in Table 3.10 and Table 3.11 below.

**Table 3.10: Input Parameters, Lifting Line, ORCAFLEX Analysis**

Parameter	Steel Wire	Fiber Rope
Cable stiffness [EA]	511 * 10 <sup>6</sup> N	148.3 * 10 <sup>6</sup> N
Weight in air per unit length (m)	45.24 kg/m	6.931 kg/m
Line outer diameter (D <sub>C</sub> )	0.0816m	0,087m

Table 3.11: Input Parameters, Subsea Structure, ORCAFLEX Analysis

Parameter	Subsea Tree	Manifold
Volume of displaced water	8.86m <sup>3</sup>	14.56m <sup>3</sup>
Height of object	7m	5m
Mass of object in air (M)	70Te	115Te
Mass moment of inertia x-direction (I <sub>x</sub> )	495.8Te.m <sup>2</sup>	1015.8Te.m <sup>2</sup>
Mass moment of inertia y-direction (I <sub>y</sub> )	495.8Te.m <sup>2</sup>	709.2Te.m <sup>2</sup>
Mass moment of inertia z-direction (I <sub>z</sub> )	420Te.m <sup>2</sup>	1245.8Te.m <sup>2</sup>
Projected area normal to flow x-direction (A <sub>x</sub> )	42m <sup>2</sup>	45m <sup>2</sup>
Projected area normal to flow y-direction (A <sub>y</sub> )	42m <sup>2</sup>	35m <sup>2</sup>
Projected area normal to flow z-direction (A <sub>z</sub> )	36m <sup>2</sup>	63m <sup>2</sup>
Drag coefficient x-y-z-direction (C <sub>Dx</sub> , C <sub>Dy</sub> , C <sub>Dz</sub> )	2.5	2.5
Hydrodynamic added mass coefficient x-direction (C <sub>Ax</sub> )	0.621	0.731
Hydrodynamic added mass coefficient y-direction (C <sub>Ay</sub> )	0.621	0.671
Hydrodynamic added Mass Coefficient z-direction (C <sub>Az</sub> )	0.627	0.649
Hydrodynamic added mass x-direction (A <sub>33x</sub> )	187.8Te	102.9Te
Hydrodynamic added mass y-direction (A <sub>33y</sub> )	187.8Te	75.8Te
Hydrodynamic added mass z-direction (A <sub>33z</sub> )	153.3Te	170Te
Hydrodynamic inertia coefficient x-direction (C <sub>Mx</sub> )	1.621	1.731
Hydrodynamic inertia coefficient y-direction (C <sub>My</sub> )	1.621	1.671
Hydrodynamic inertia coefficient z-direction (C <sub>Mz</sub> )	1.627	1.641

### 3.3.4 Critical Lengths of Lifting Line

To assess the effect of resonant motion during the lowering to seabed operation, the natural period of the lifting system need to be found as a function of line length, for the different installation scenarios. The natural period of the lifting system can then be compared to the crane tip motion transfer function, and line lengths resulting in resonant motion can be identified.

#### 3.3.4.1 Natural period of the lifting system

According to REF [20] equation (31), the natural period of the lifting system can be found as:

$$T_0 = 2\pi \sqrt{\frac{M + \frac{mL}{3}}{K_E}} \text{ [s]}$$



Where:

$$K_E = \frac{EA}{L} \text{ [N/m]}$$

$M'$  = Weight of lifted object in air + hydrodynamic added mass z-direction [kg]

$m$  = Weight of lifting line in air per unit length [kg/m]

$L$  = Length of lifting line[m]

$K_E$  = Stiffness of lifting system [N/m]

$EA$  = Axial stiffness of the lifting line [N]

Input parameters used for natural period calculations are presented in section 3.3.3, Table 3.10 and 3.11. The natural period of the lifting system is calculated based on the equation above, and presented as a function of line length in Figure 3.10 and Figure 3.11 below.

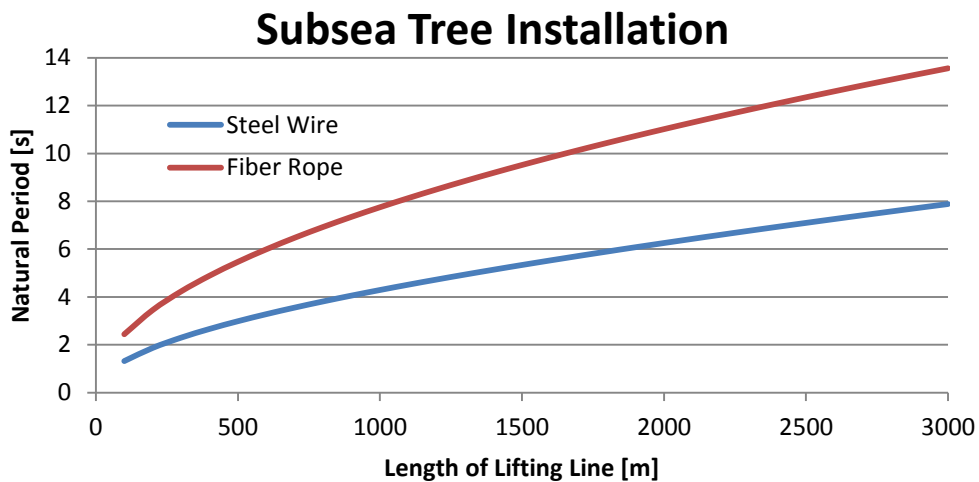


Figure 3.10: Natural Period of Lifting System, Subsea Tree Installation

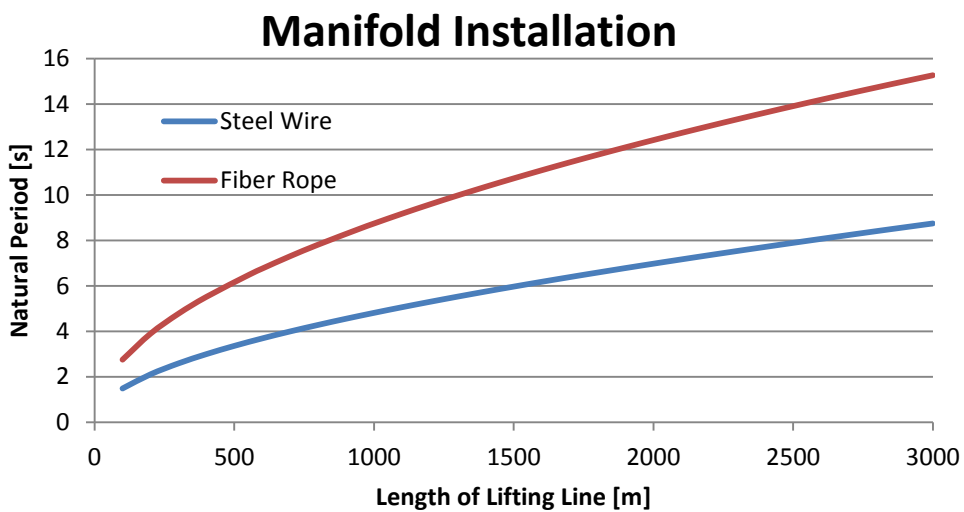


Figure 3.11: Natural Period of Lifting System, Manifold Installation

### 3.3.4.2 Crane tip motion transfer function

The transfer function for vertical crane tip motion, describes the reaction at the crane tip in different sea-states. I.e. The RAO curve for the crane tip. The vertical crane tip motion transfer function is dependent on location of the deployment system on the vessel. For this analysis, the model is created to simulate a lowering operation over side of the vessel. The vertical crane tip motion will hence be highly dependent of the vessel heave and roll motion. Because the “Line” in the ORCAFLEX model is connected at the amid ship point for pitch motion, the effect of vessel pitch motion is neglected. Using the superposition principle, the transfer function for vertical crane tip motion is found as:

$$\text{Vertical crane tip motion} = \text{RAO}_{\text{Heave}} + y * \sin(\text{RAO}_{\text{Roll}}) \text{ [m/m]}$$

Where:

$\text{RAO}_{\text{Heave}}$  = Vessel vertical displacement amplitude in heave [m/m]

$y$  = Distance from the amid ship point for roll motion to location of crane tip [m]

$\text{RAO}_{\text{Roll}}$  = Vessel roll angle amplitude [deg/m]

Vessel RAOs for heave and roll are collected from ORCAFLEX, for a vessel heading of 22.5°. Vessel RAO data, for a vessel heading of 22.5°, is presented in APPENDIX A.1. The crane tip motion transfer function is found based on the equation above and presented in Figure 3.12 below.

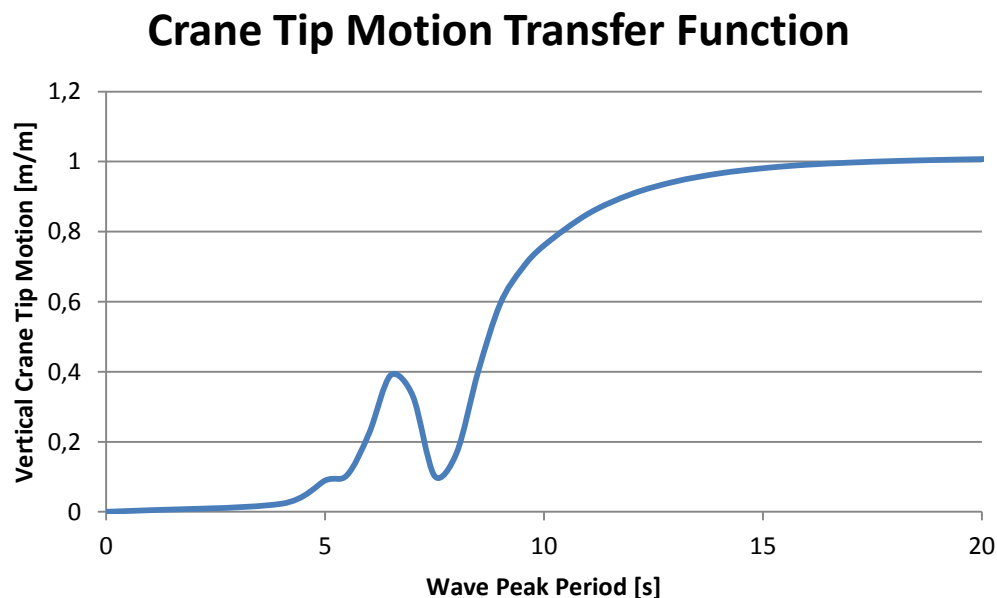


Figure 3.12: Vertical Crane Tip Motion Transfer Function

From Figure 3.12 above, it is seen that the vertical crane tip motion transfer function has a peak for wave peak periods equal to 6.5s. This is the vessels natural period in roll, and large crane tip motion can be expected.

### 3.3.4.3 Summary - critical lengths of lifting line

The length of the lifting line, resulting in a natural period of the lifting system equal to the peak in the vertical crane tip motion transfer function, will be the most critical scenario for resonant motion. Large rapid motion of the crane tip and the lifted object will result in large dynamic forces. The lifting system can be in resonance with the crane tip motion for other periods as well. However due to limited crane tip motion or long oscillating periods, the dynamic effects will be less critical.

The critical lengths of lifting line are presented in Table 3.12 below for the different installation scenarios.

Table 3.12: Length of Lifting Line Causing Resonant Motion

Lifting Line	Subsea Structure	Length of Lifting Line[m]
Steel Wire	Subsea Tree	2145
	Manifold	1760
Fiber Rope	Subsea Tree	705
	Manifold	555

### 3.3.5 Operational criteria

The results from the dynamic analysis will be compared to a set of operational criteria that need to be fulfilled, for the lowering operation to be performed in a safe manner.

According to DNV-RP-H103, section 4.4, both of the following operational criteria need to be fulfilled:

1. The static and dynamic loads on lifted structure, crane, cable and rigging shall not exceed capacity requirements.
2. Snap loads due to slack slings or slack cable shall be avoided.

For the purpose of this analysis it is assumed that the governing capacity requirement is the capacity of the lifting line. Also the effect of entrapped water is not accounted for.

Operational criterion 1 states that:

The static force in the lifting line + the dynamic force in the lifting line cannot exceed the safe working load of the line, and can be expressed as:

$$F_{\text{stat}} + F_{\text{dyn}} < SWL_{\text{Line}} \text{ [kg]}$$

$$F_{\text{stat}} = M_{\text{sub}} + L * m_{\text{sub}} \text{ [kg]}$$

Where:

$F_{\text{stat}}$  = The static force in the lifting line [kg]

$F_{\text{dyn}}$  = Dynamic force in lifting line [kg]

$SWL_{\text{Line}}$  = Safe working load of the lifting line [kg]

$M_{\text{sub}}$  = Submerged weight of the lifted object [kg]

$m_{\text{sub}}$  = Submerged weight of lifting line [kg/m]

L = Length of lifting line [m]

Hence the maximum allowable dynamic force in the lifting line, according to operational criterion 1, can be found as:

$$F_{\text{dyn,max}} = SW_{\text{Line}} - F_{\text{Stat}} \text{ [kg]}$$

According to DNV-RP-H103, section 4.4.3, slack sling conditions may occur if the dynamic force exceeds the static weight of the lifted object. Applying a 10% margin to the start of slack sling, operational criterion 2 can be expressed as:

$$F_{\text{dyn}} < 0.9 * M_{\text{sub}} \text{ [kg]}$$

And the maximum allowable dynamic force in the lifting line, according to operational criterion 2, can be found as:

$$F_{\text{dyn,max}} = 0.9 * M_{\text{sub}} \text{ [kg]}$$

Operational criterion 1 is dependent on the static force in the lifting line. The maximum allowable dynamic force in the lifting line will hence be dependent on the length of the lifting line. The maximum allowable dynamic force in the lifting line, according to operational criterion 1, is found based on the equation above, for all installation scenarios, and results are presented in Table 3.13 and Table 3.14 below.

**Table 3.13: Maximum Allowable Dynamic Force in Lifting Line, Operational Criterion 1, Subsea Tree Installation**

Subsea Tree Installation	Maximum Allowable Dynamic Force [Te]	
	Steel Wire	Fiber Rope
Length of Lifting Line [m]		
500	163.8	63.6
1000	143.9	63.2
1500	124	62.8
2000	104	62.3
2500	84.1	61.9
2950	66.1	61.5

**Table 3.14: Maximum Allowable Dynamic Force in Lifting Line, Operational Criterion 1, Manifold Installation**

Manifold Installation	Maximum Allowable Dynamic Force [Te]	
	Steel Wire	Fiber Rope
Length of Lifting Line [m]		
500	124.7	24.6
1000	104.7	24
1500	84.8	23.6
2000	64.8	23.2
2500	44.9	22.7
2950	27	22.3

Operational criterion 2 is only dependent on the submerged weight of the lifted object, and the maximum allowable dynamic force in the lifting line will not vary for different lifting lines. The maximum allowable dynamic force will also be constant for all line lengths. The maximum allowable dynamic force, according to operational criterion 2, is found based on the equation above, for installation of the two subsea structures, and results are presented in Table 3.15 below.

**Table 3.15: Maximum Allowable Dynamic Force in Lifting Line, Operational Criterion 2**

Subsea Structure	Maximum Allowable Dynamic Force [Te]
Subsea Tree	54.8
Manifold	90.1

It is seen from Table 3.13, Table 3.14 and Table 3.15 above, that for installation of the subsea tree operational criteria 2 will be governing for both lines and all line lengths. For installation of the manifold with fiber rope, operational criteria 1 will be governing for all line lengths. For installation of the manifold with steel wire operational criteria 2 will be governing for line lengths < 1370m, and operational criteria 1 will be governing for line lengths >1370m.

### 3.3.6 Results - dynamic analysis ORCAFLEX

The dynamic analysis is carried out for different lengths of lifting line and different sea-states. For all installation scenarios, the analysis is performed in line length steps of 500m. In addition, the line lengths resulting in resonant motion, presented in section 3.3.4, Table 3.12, are assessed.

The sea-states covered in the analysis are presented in Table 3.16 below.

**Table 3.16: Seatates Covered in the Dynamic Analysis**

Significant Wave Height (H <sub>s</sub> ) [m]	Zero Crossing Period (T <sub>Z</sub> ) [s]	
	From	To
1	3	13
1.5	3	13
2	4	13
2.5	4	13
3	5	13
3.5	5	13
4	6	13

This is in accordance with DNV-RP-H103 section 3.4.2.22, which states that “The performed analysis should cover the following zero-up-crossing wave period range for a given significant wave height H<sub>s</sub>”.

$$8.9 * \sqrt{\frac{H_s}{g}} \leq T_Z \leq 13 [s]$$

Where:

H<sub>s</sub> = Significant wave height [m]

g = Gravitational acceleration [m/s<sup>2</sup>]

T<sub>Z</sub> = wave zero up-crossing period [s]

For line lengths resulting in resonant motion a wave zero up-crossing period of 4.6s, which equals a wave peak period of 6.5s, is covered for all significant wave heights. From the wave model in ORCAFLEX it is found that:

$$T_p = 1.4075 * T_Z$$

Where:

$T_p$  = Wave peak period

The applied simulation time is set to 1800s, in accordance with DNV-RP-H103, section 3.4.3.5.

### 3.3.6.1 Lowering to seabed

The maximum dynamic force at end A (Line connection to vessel) in the lifting line, for the whole  $T_z$  range is presented in Figure 3.13 - Figure 3.16. The maximum dynamic force is plotted as a function of line length for all installation scenarios, and compared to the governing operational criterion. The dynamic force is found as:

$$\text{Max Dynamic Force} = \text{Max effective tension in lifting line} - \text{Static tension in lifting line [Te]}$$

Tabulated values are presented in APPENDIX A.3: Comparison study – maximum dynamic force in lifting line.

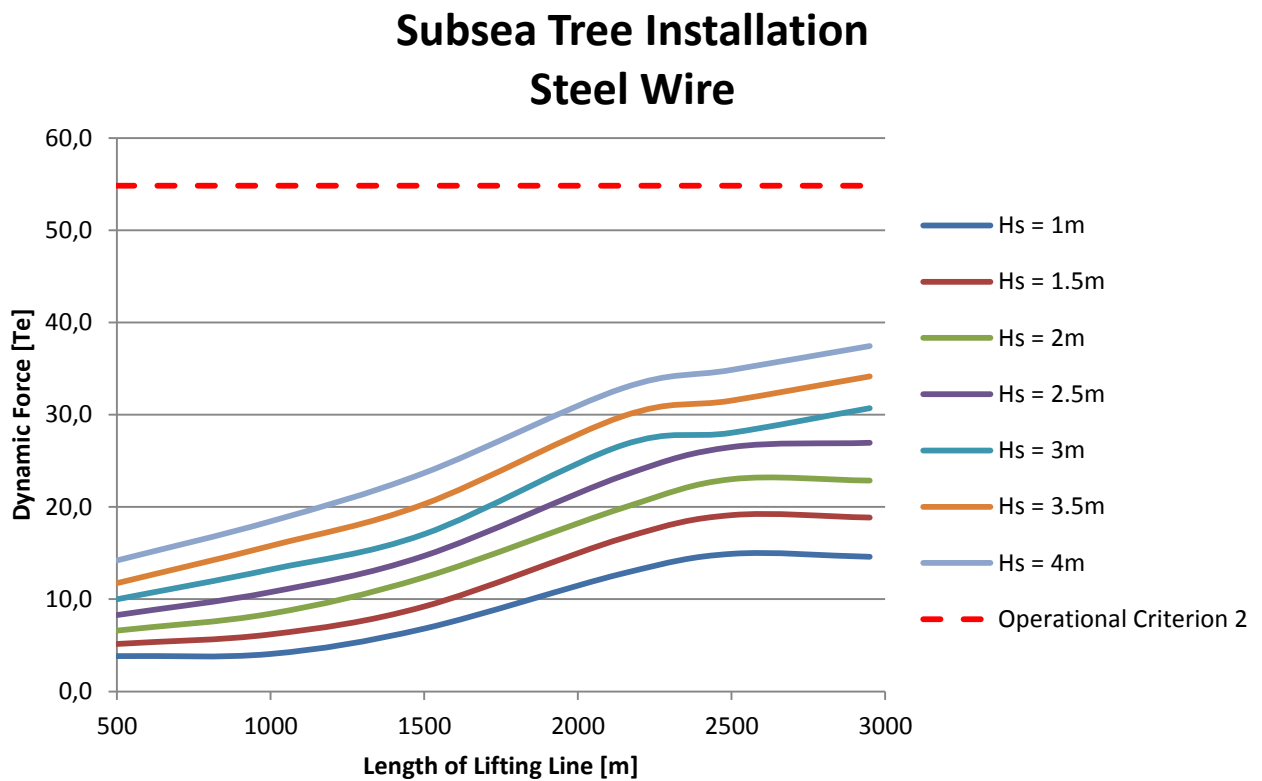


Figure 3.13: Dynamic Force, Subsea Tree Installation, Steel Wire

## Subsea Tree Installation Fiber Rope

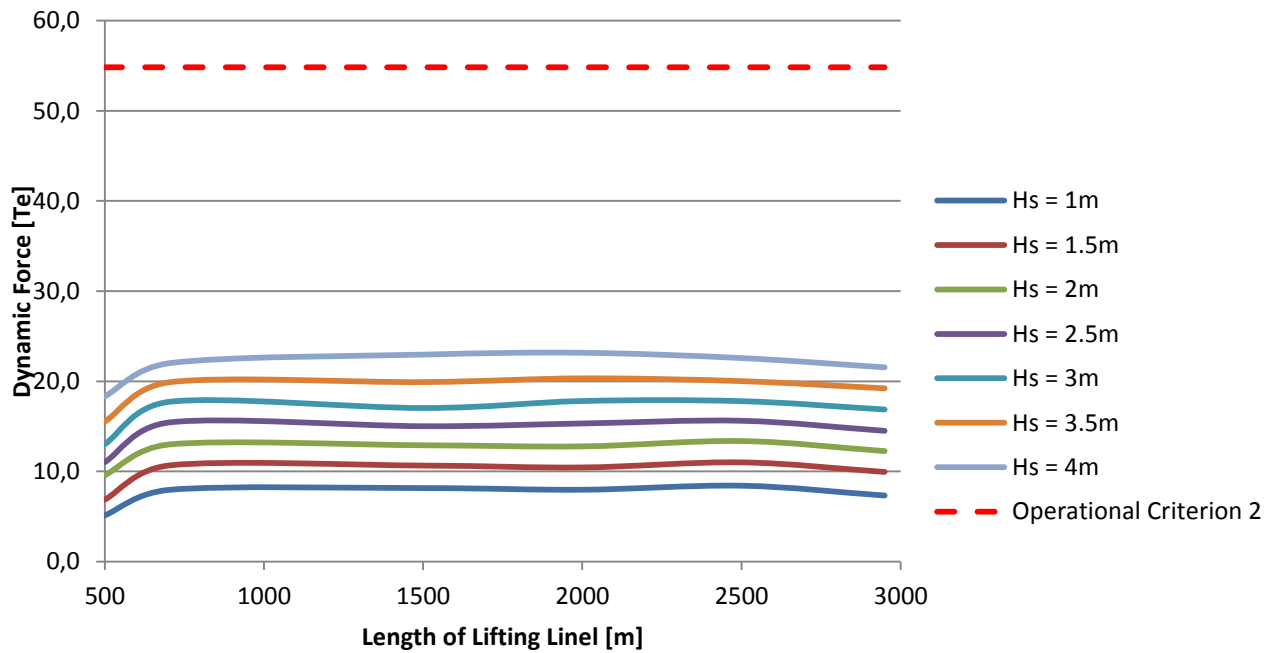


Figure 3.14: Dynamic Force, Subsea Tree Installation, Fiber Rope

## Manifold Installation Steel Wire

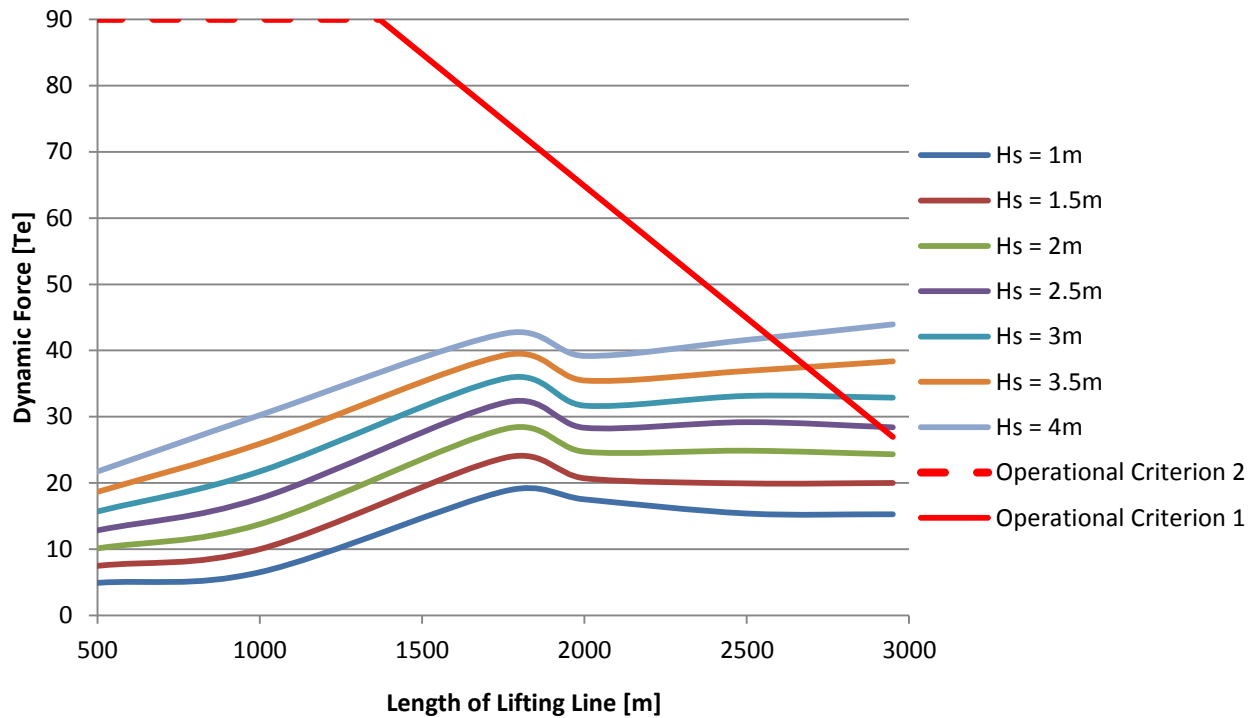


Figure 3.15: Dynamic Force, Manifold Installation, Steel Wire

## Manifold Installation Fiber Rope

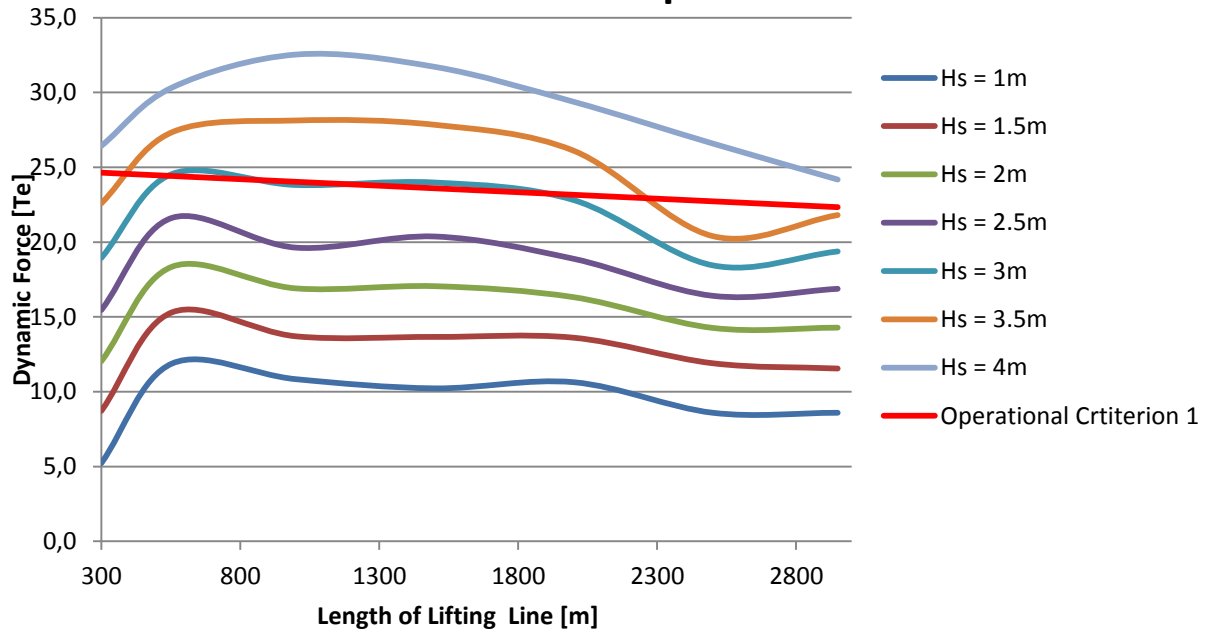


Figure 3.16: Dynamic Force, Manifold Installation, Fiber Rope

### 3.3.6.2 Landing on seabed

To assess the difference in landing on seabed operations, when utilizing the two different lifting lines, motion of the lifted object close to the seabed will be compared. The analysis is performed for a line length equal to 2950m, for all installation scenarios. The results are presented in Figure 3.17 - Figure 3.20 below. Motion of the lifted object is found as:

$$\text{Motion of lifted object} = \text{Max position during simulation} - \text{Static position [m]}$$

Motion of the lifted object is presented as a function of significant wave height and wave zero up-crossing period. Tabulated values are presented in APPENDIX A.4: Comparison study – motion of lifted object.



## Subsea Tree Installation Steel Wire

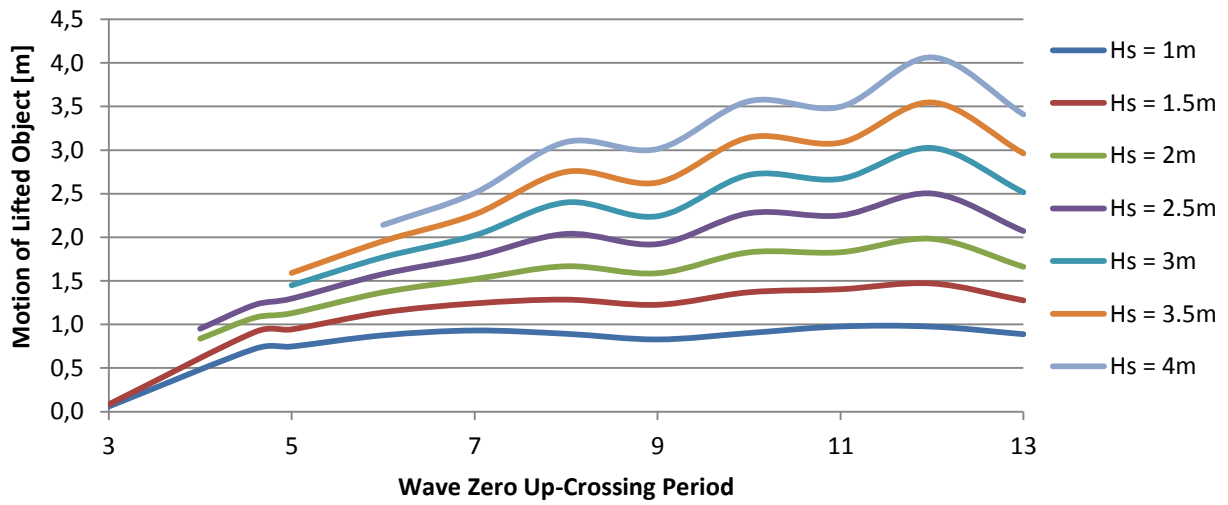


Figure 3.17: Motion of Lifted Object, Subsea Tree, Steel Wire

## Subsea Tree Installation Fiber Rope

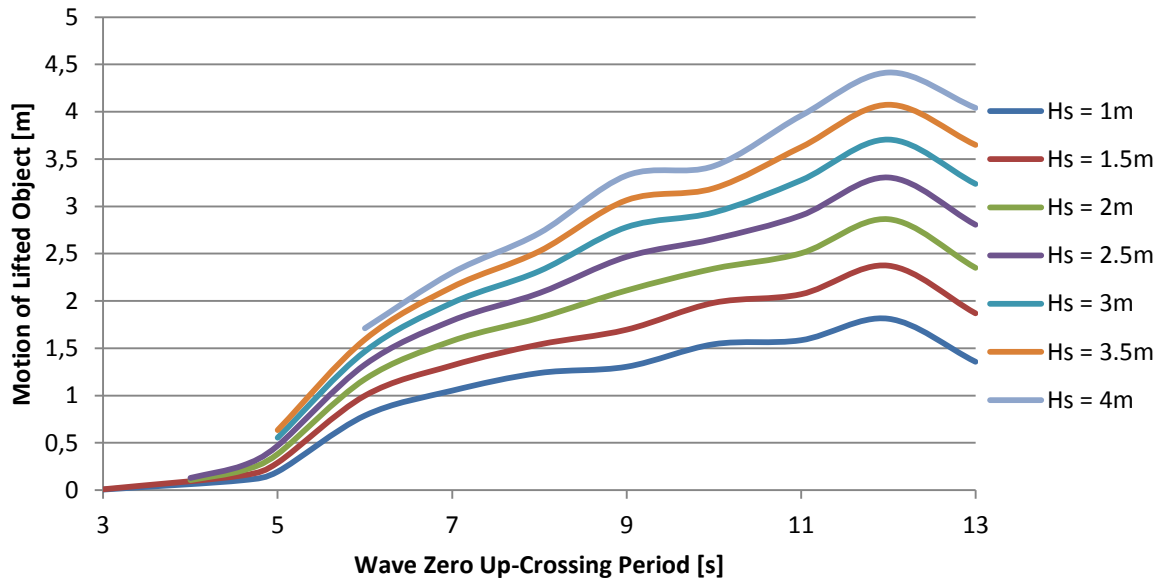


Figure 3.18: Motion of Lifted Object, Subsea Tree, Fiber Rope

## Manifold Installation Steel Wire

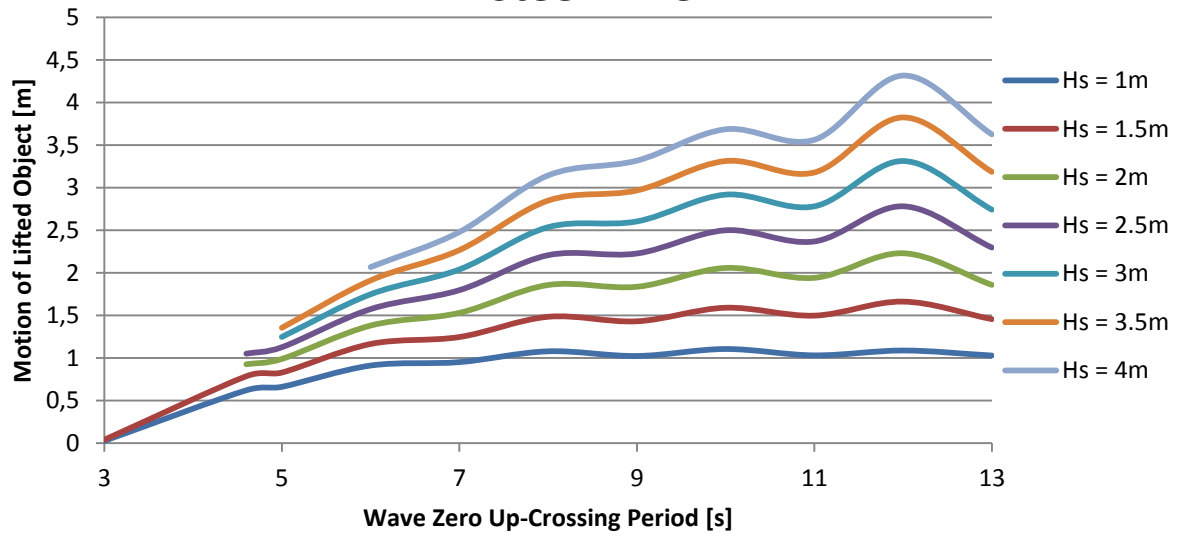


Figure 3.19: Motion of Lifted Object, Manifold, Steel Wire

## Manifold Installation Fiber Rope

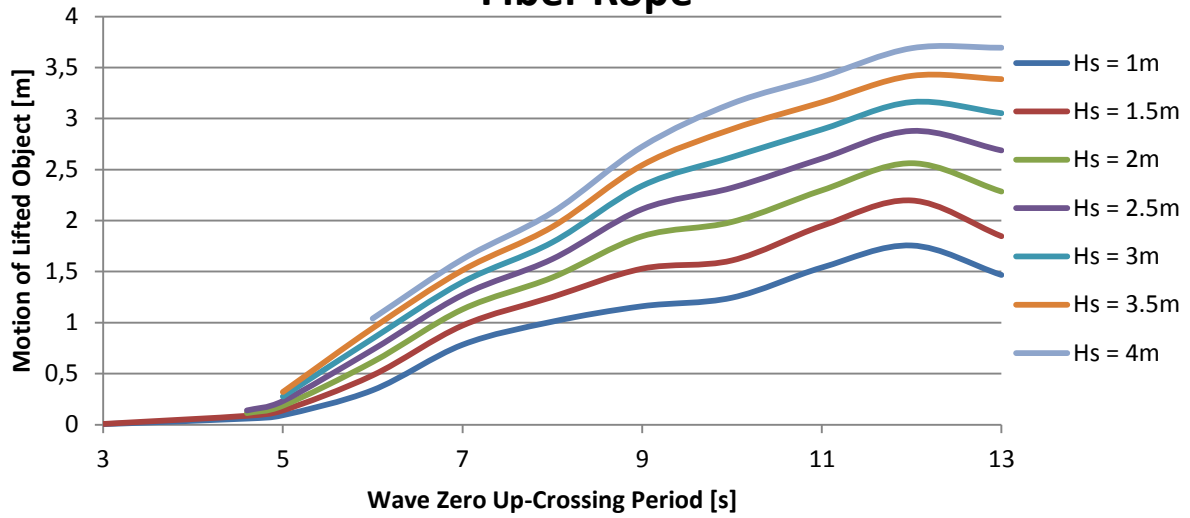


Figure 3.20: Motion of Lifted Object, Manifold, Fiber Rope

### 3.3.7 Summary - dynamic analysis

From Figure 3.13 - Figure 3.16 above it is seen that for the subsea tree installation, no weather limiting criteria is obtained for the lowering to seabed operation. For the manifold analysis, it is seen that the weather limiting criteria for the lowering to seabed operation is stricter for the conventional steel wire system than for the fiber rope deployment system. The operation can only be performed for significant wave heights  $\leq 2\text{m}$  for the steel wire system, while the fiber rope deployment system is limited to sea-states with significant wave height  $\leq 2.5\text{m}$ .

From Figure 3.15 and Figure 3.16 above it is however seen that due to the large payload capacity of the steel wire at surface, lowering to seabed of the manifold has no weather limiting criteria down to a water depth of 2500m.

It is also seen from Figure 3.13 - Figure 3.16 above that the dynamic forces in the lifting line is significantly higher when using steel wire compared to fiber rope. This means that the selection of applicable wire sizes is crucial to obtain a significant payload capacity at large water depths.

From Figure 3.17 - Figure 3.20 above it is seen that there is no distinctive difference related to motion of the lifted object close to seabed, when utilizing the two different lifting lines. For installation of the subsea tree, motion of the lifted object is somewhat higher when using fiber rope than when using steel wire. For the manifold installation however, motion of the lifted object is lower when using fiber rope than when using steel wire. Problems related to landing on seabed operations is therefore seen as equal for the two lifting lines, and differences will be dependent on the weight and shape of the lifted object.

## 3.4 Laboratory exercise - verification of the ORCAFLEX model

The axial stiffness of the lifting line is crucial for the dynamic behavior of the lifting system. To verify the ORCAFLEX model and input parameters, a laboratory exercise is performed where elongation of a fiber rope subjected to various loads is measured. The measured elongation is compared to the rope elongation in an ORCAFLEX model, and to theoretically calculated rope elongation. The fiber rope to be tested is a 6mm, Plasma® 12 strand fiber rope, delivered by Cortland Selantic AS - Bergen.

### 3.4.1 Experimental setup

The fiber rope will be connected to a rigid point at one end, and to a car at the other end. The car is used for loading the fiber rope. An overhead crane was considered to be utilized for loading the fiber rope, to obtain more stable loading situations. This would however limit the rope length to 3m. Due to the limited capacity of the weight transducer, a rope length of 3m would result in non-measurable results, and a car was used to optimize the possible rope length.

Close to the rigid point, a weight transducer is connected between two rope segments, allowing measurement of the applied load. The weight transducer is connected to a SPIDER8, which receives signals from the weight transducer and presents the signal reading on a computer with a real-time graph. Rope tension can hence be monitored in real-time.

The rope is marked with black adhesive tape, at a position between the weight transducer and the car, to allow for surveillance of rope elongation. Graph paper is placed behind the marked rope to indicate the rope elongation. A camera is used to record movement of the marked rope during loading situations. The experimental setup is presented in Figure 3.21 and Figure 3.22 below.

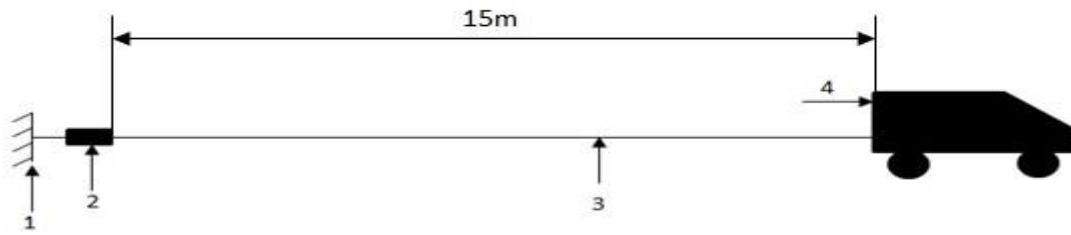


Figure 3.21: Experimental Setup, Side View

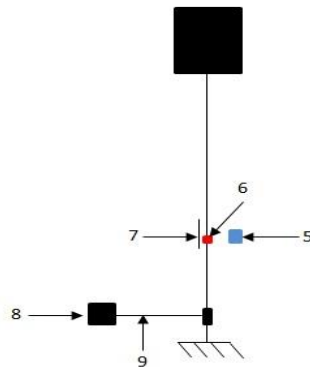


Figure 3.22: Experimental Setup, Top View

Where:

1. Rigid point
2. Weight transducer
3. Fiber Rope
4. Car
5. Camera
6. Marked Rope
7. Graph Paper
8. SPIDER8 and computer
9. Computer Cable

The car applies a load to the rope and the weight transducer measure the applied load. The camera records movement of the marked rope segment and the graph paper indicates rope elongation. The determination of rope length is presented in Figure 3.23 below.

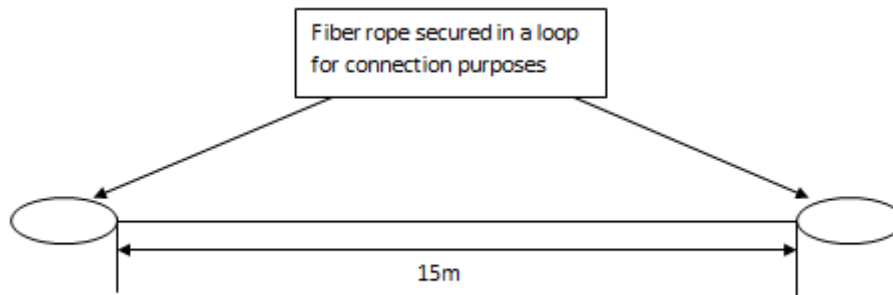


Figure 3.23: Determination of Rope Length

### 3.4.2 Equipment

The equipment used in the experiment is listed below:

1. HBM U2A 200kg weight transducer
2. SPIDER8
3. CATMAN EASY 2.0.2.0
4. Plasma® 12 strand fiber rope, 6mm
5. Car
6. Camera with video function
7. 4 x 5mm wire lock
8. Biltema analog fish weight, range 0 – 25kg
9. Graph Paper
10. Adhesive tape

CATMAN EASY 2.0.2.0 is the computer program used to record the signals from the weight transducer. A screenshot of the real-time graph from CATMAN EASY during measurements is presented in Figure 3.24 below. The vertical axis represents the applied load [kg], while the horizontal axis represents time [s].

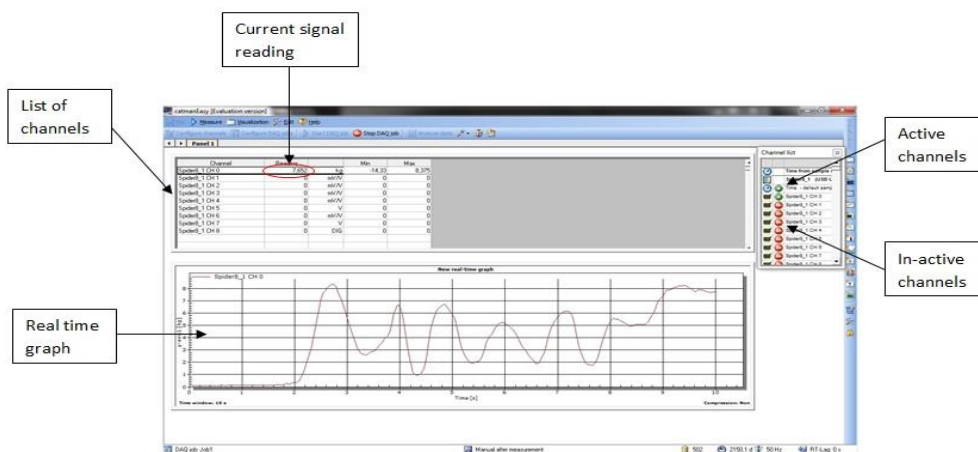


Figure 3.24: Real-Time Graph, CATMAN EASY

The 5mm wire locks are used to secure the fiber rope in a loop for connection purposes, and the analog fish weight is used to calibrate the weight transducer. Figure 3.25 and Figure 3.26 below presents the analog fish weight and the rope secured in a loop respectively.



Figure 3.25: Analog Fish Weight



Figure 3.26: Fiber Rope Secured in a Loop

“The Spider8 is a multi-channel PC measurement electronics for parallel, dynamic measurement data acquisition using a computer” REF [18]. The certificate of conformance for the fiber rope is presented in APPENDIX A.2: Fiber rope certificate of conformance

### 3.4.3 Experimental procedure

The experiment is performed in the following steps:

#### 1. *Connecting the rope and calibrating the weight transducer:*

A rope segment is connected to the rigid connection point at one end, and to the weight transducer at the other end. The weight transducer is connected to SPIDER8, and SPIDER8 is connected to the computer. CATMAN EASY is turned on, all channels not used during the experiment are de-activated, and the signal reading from the weight transducer is checked. Calibration of the weight transducer is performed by the following two steps:

- The weight transducer is set in a position where no load is applied, and the signal reading is set equal to 0kg.
- A load of 5kg is applied to the weight transducer by the fish weight, and the signal reading is set equal to 5kg.

The next rope segment is then connected to the weight transducer at one end and to the car at the other end. This rope segment is marked with black adhesive tape for surveillance of rope elongation. Connection of the weight transducer is presented in Figure 3.27 below.



Figure 3.27: Weight Transducer Connection

## 2. Pre – loading the fiber rope

According to REF [19], the nominal diameter of the fiber rope, reflects the rope size after 10 load cycles at 50% of minimum tensile strength. The minimum tensile strength of the rope is 3600kg and pre-loading should be performed at 1800kg. Due to the limited capacity of the weight transducer, the fiber rope is subjected to 15 load cycles at loads in the range 100 – 180kg to avoid excessive elongation during testing. Pre-loading of the fiber rope is presented in Figure 3.28 below.



Figure 3.28: Pre - Loading the Fiber Rope

When the 15 load cycles have been performed, the rope is pre-loaded to approximately 20kg to avoid large elevation of the rope during testing.

The camera and graph paper is then set up for surveillance of rope elongation. The camera view is presented in Figure 3.29 below. The distance between two black/red lines is equal to 1cm.

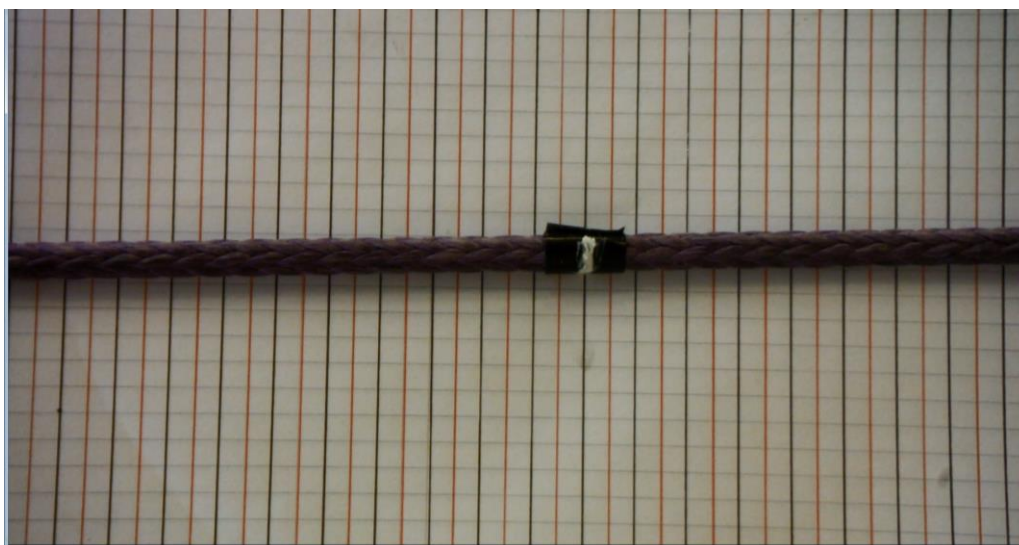


Figure 3.29: Camera view

### 3. Execution

The camera is started, CATMAN EASY is activated, and load is applied until the target load is reached. The rope is de-tensioned and video + load measurements are saved.

### 4. Data processing and gathering of results

Measurements of the applied load can be retrieved as tabulated values. The highest measured load, for the given load case, is selected for comparison with the largest rope elongation. Elongation of the rope is collected from the video as presented in Figure 3.30 and Figure 3.31 below.

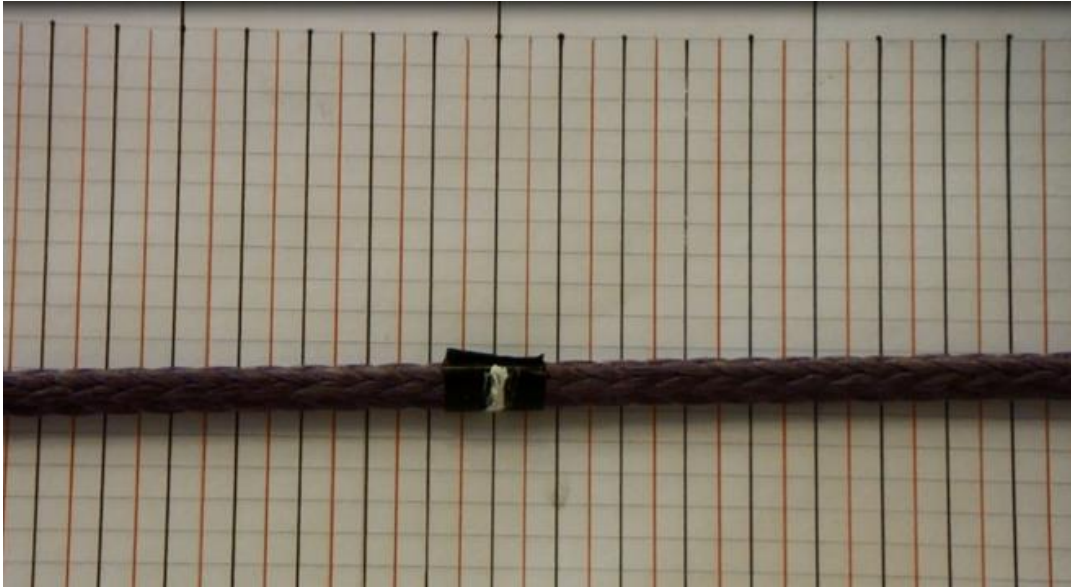


Figure 3.30: Fiber Rope Initial Position

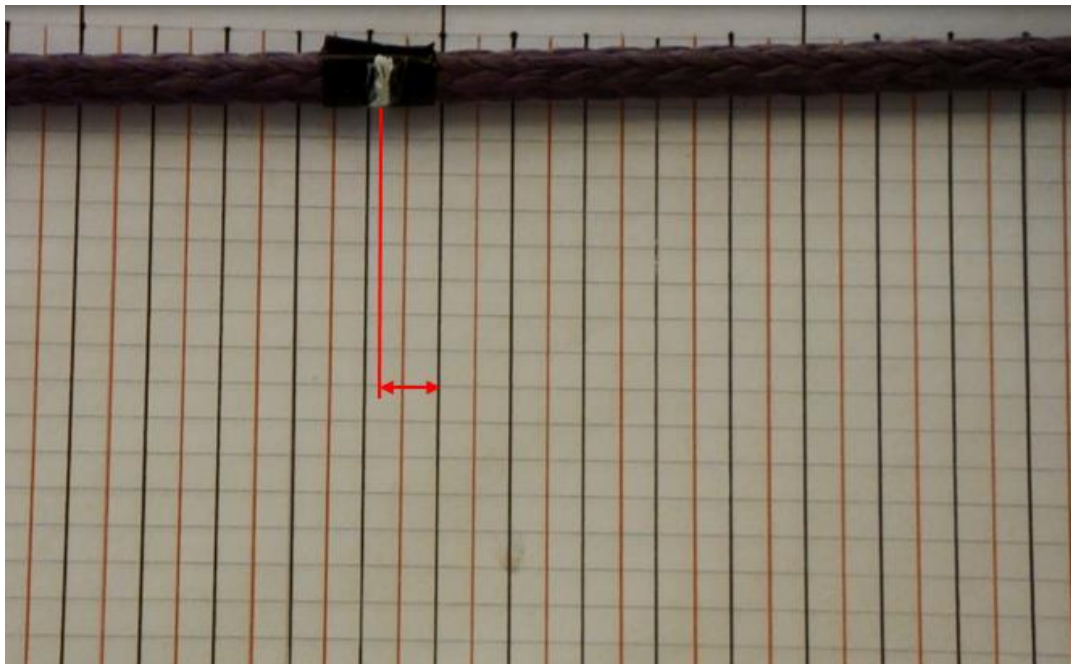


Figure 3.31: Fiber Rope Maximum Position and Rope Elongation



### 3.4.4 Sources of error

The following is considered to be possible sources of error in the laboratory exercise:

- Calibration of the weight transducer is performed by applying a given load, measured by a fish weight. The applied load is hence only an approximate value, dependent on the accuracy of the fish weight and readings
- Accurate measurement of rope elongation is limited to 0.5cm
- Possible slipping of rope in wire locks
- Camera angle relative to rope angle
- Angle of graph paper relative to rope angle
- Motion of adhesive tape relative to rope elongation
- Inaccurate measurement of rope length

The possible sources of error listed above can result in inaccurate measured values of rope elongation.

### 3.4.5 Results – laboratory exercise

Results from the laboratory exercise are presented in Table 3.17 below.

Table 3.17: Results Laboratory Exercise

Target Load [kg]	Max Load Measured [kg]	Pre – Load [kg]	Max Applied Load Measured [kg]	Max Elongation Measured [cm]
50	80.9	28.8	52.1	0.5
70	108.8	33.5	75.3	0.7
90	111.5	20.5	91	0.9
130	146.5	11.2	135.3	1.7
170	179.1	11.5	167.6	2.0

The measured elongation will be compared to the rope elongation in an ORCAFLEX model and theoretically calculated rope elongation. This is done to assess accuracy of line modelling and input parameters in ORCAFLEX.

The fiber rope is modelled by using the “Winch” function in ORCAFLEX. The “Winch” function works as a massless connection, with a given stiffness, between two objects. The line tension will hence only depend on the submerged weight of the lifted object. The axial stiffness of the winch is needed as input. The axial stiffness of the fiber rope is calculated based on the load/elongation curve found in REF [19], and can be found as:

$$\frac{EA}{L} = \frac{F}{\Delta L} \text{ [N/m]}$$

$$EA = \frac{F}{\Delta L} L \text{ [N]}$$

Where:

EA = Axial stiffness of the fiber rope [N]

F = Applied load [N]

$\Delta L$  = Elongation of rope under applied load [m]

L = Initial rope length [m]

The diameter of the winch in ORCAFLEX is set to the nominal diameter of the fiber rope.

The lifted object is modelled with the “6D buoy” function in ORCAFLEX. The displaced volume of water is set to 1m<sup>3</sup>, and the object will be subjected to a buoyancy force of 1025kg. The weight in air of the object is set to:

$$M = (\rho_{sw} * \nabla) + \text{Max applied load measured [kg]}$$

Resulting in a submerged weight of the lifted object of:

$$M_{sub} = ((\rho_{sw} * \nabla) + \text{Max applied load measured}) - (\rho_{sw} * \nabla) \text{ [kg]}$$

$$M_{sub} = \text{Max applied load measured [kg]}$$

Where:

M = Weight of lifted object in air [kg]

M<sub>sub</sub> = Submerged weight of lifted object [kg]

ρ<sub>sw</sub> = Density of seawater [kg/m<sup>3</sup>]

∇ = Displaced volume of water [m<sup>3</sup>]

No other parameters of the “6D Buoy” are changed.

A static simulation is performed in ORCAFLEX for each load case. The elongation of the line in the ORCAFLEX model is found as:

$$\Delta L = L_s - L \text{ [m]}$$

Where:

L<sub>s</sub> = Stretched length of rope [m]

L = Initial rope length [m]

ΔL = Rope elongation [m]

The rope elongation is calculated theoretically as:

$$\Delta L = \frac{F * L}{EA} \text{ [m]}$$

Length of the rope segment, connected to the rigid point and the weight transducer, is not accounted for in the ORCAFLEX analysis or the theoretical calculations. The applied rope length is 15m.

Results from the ORCAFLEX simulation and theoretic calculations are presented and compared to the measured values in Table 3.18 below

**Table 3.18: Max Elongation Measured vs. ORCAFLEX/Calculated Rope Elongation**

Load [kg]	Max Elongation Measured [cm]	ORCAFLEX Line Elongation [cm]	Theoretic Line Elongation [cm]
52.1	0.5	0.68	0.68
75.3	0.7	0.98	0.98
91	0.9	1.18	1.18
135.3	1.7	1.76	1.76
167.6	2.0	2.18	2.18

It is seen from Table 3.18 above that the measured rope elongation differs slightly from the ORCAFLEX/calculated line elongation. To assess the effect of the deviations on rope stiffness, average rope stiffness is calculated based on the measured values. The result is presented in Table 3.19 below and compared to the theoretical rope stiffness obtained from the load/elongation curve found in REF [19].

**Table 3.19: Rope Stiffness, Measured vs. Theoretical**

	Rope Stiffness [N]
Theoretic	$113 * 10^4$
Avg. from measured values	$116.8 * 10^4$

### 3.4.6 Discussion & conclusion – laboratory exercise

From Table 3.18 above, it is seen that the measured elongation of the fiber rope is slightly lower than the line elongation obtained from ORCAFLEX/calculations. The length of the rope segment, connected to the rigid point and the weight transducer, was not accounted for in the ORCAFLEX analysis/calculations. The measured values were hence expected to be slightly higher.

It is also seen from Table 3.18 above, that the ORCAFLEX line elongation is equal to the theoretically calculated line elongation. Line modelling in ORCAFLEX is hence considered to be accurate, and the input parameter for line stiffness is considered to be the source of deviation.

It is however seen from Table 3.19 above, that the deviation between the measured values and the results obtained from ORCAFLEX/calculations has a relatively small impact on the rope stiffness.

Deviations in rope elongation are considered to be a result of sources of error related to the laboratory exercise, inaccurate readings from the load/elongation curve provided by the rope manufacturer, and deviation in the rope manufacturing process. The ORCAFLEX model is hence considered to be realistic for modelling of rope stiffness.

## 4 Feasibility study - deepwater installation with smaller vessels

The weight of fiber ropes, with sufficient payload capacity to perform deepwater lifting operations, is significantly lower than the weight of a similar steel wire. Due to the weight difference, the deck-load and the deployment system power requirement will be lower than for a steel wire system. The fiber rope deployment system is therefore seen as applicable for deepwater installation with smaller vessels. This could possibly reduce the vessel availability problems seen in the industry today.

The fiber rope deployment system has active heave compensation and constant tension systems, making it applicable for overboarding and splash zone lifting. A feasibility study of utilizing a fiber rope deployment system on a smaller vessel, rigged with an A-frame, to perform splash zone lifting and lowering to seabed operations is performed. Usage of an A-frame vessel will avoid the requirement of large deck cranes.

### 4.1 A-frame vessel

The A-frame vessel to be utilized in this feasibility study is a multi-purpose offshore vessel from Vuyk Engineering Rotterdam B.V. The vessel is equipped with a 50Te SWL deck crane, a 150Te SWL A-frame, and a 130Te tow winch. [21]

The vessel is designed for various types of offshore work, and is applicable for [21]:

- Pipeline trenching
- Cable laying and burying
- Cable and pipeline inspection and maintenance
- Diving support
- ROV operations
- Towing
- Anchor handling

The vessel hull form aft is designed to allow for large load handling. The vessel is fitted with bilge keels to reduce vessel motion and equipped with an anti-roll system. The vessel is also fitted with a class 2 dynamic positioning system for station keeping during operations. The dynamic positioning system is limited to operations in sea-states comprised of  $H_s \leq 3m$ . [21]

The feasibility study aims to replace the 130Te tow winch with a 125Te SWL fiber rope deployment system, which will be used as the lift system for the A-frame. The system utilizes an 88mm BOB fiber rope delivered by the company Cortland, REF [14].

### 4.2 Dynamic analysis

The main challenge for performing deepwater lifting operations with an A-frame vessel is related to vessel motion and location of the A-frame. Typical offshore installation vessels aim to locate the deck crane as close to the amid ship point for pitch motion as possible. This is done to avoid the effect of vessel pitch motion experienced by the crane tip. The A-frame is located aft on the vessel, and vessel pitch motion will introduce large crane tip motion. A smaller vessel will also be more sensitive to environmental loading conditions.

A dynamic lifting analysis is performed in ORCAFLEX to assess the operable sea-states, when using an A-frame vessel for deepwater lifting operations. The analysis covers splash zone lifting and critical

water depths leading to resonant motion. The analysis is performed for two different subsea structures. The two chosen structures are a subsea tree with dimensions 6x6x7m weighing 70Te, and a manifold with dimensions 9x5x7m weighing 115Te.

The results from the dynamic analysis will be compared to an annual scatter diagram for the deepwater regions Gulf of Mexico and offshore Angola, to assess the operability of the A-frame vessel in different geographical areas.

#### 4.2.1 ORCAFLEX model

The RAO data for the A-frame vessel discussed in section 4.1 is unknown, and an altered model of the standard vessel model in ORCAFLEX is used for the analysis. The ORCAFLEX model is otherwise modelled as in the comparison study, section 3.3.2. The line connection to vessel, line length, and initial position and altitude of the lifted object is however determined differently during splash zone lifting. A complete overview of the ORCAFLEX model is presented in APPENDIX A.5: ORCAFLEX model A-frame vessel.

##### 4.2.1.1 A - frame vessel

To model the A-frame vessel discussed in section 4.1 the standard vessel model in ORCAFLEX is altered.

ORCAFLEX allow for vessel scaling of the original model, and scaling is done using Freude scaling. Each item of data is scaled by a factor dependent on the unit of that item. If R = ratio of vessel length to vessel type length, the scaling factor applied is [22]:

- All lengths are scaled by R
- All masses and added masses are scaled by R<sup>3</sup>
- All times are scaled by R<sup>0.5</sup>

Data items represented by other units are scaled by writing the units in term of the fundamental units of mass, length and time. Dimensionless data items, such as RAO data for surge, sway and heave are not scaled, but the periods related to the RAO data is scaled. RAO data for roll, pitch and yaw are scaled. Phase angles remain constant during vessel scaling. [22]

For the ORCAFLEX vessel model to be representable as the A-frame vessel, the vessel type width is altered to give a width of the scaled vessel equal to 18.5m. The vessel type length is equal to 103m. The vessel length of the scaled model is 79.95m, resulting in a scaling factor:

$$R = \frac{\text{Vessel length}}{\text{Vessel type length}} [-]$$

The vessel type width is hence set to:

$$\text{Vessel type width} = \frac{\text{Vessel width}}{R} [\text{m}]$$

The vessel heading is set to 0° to assess the “worst case scenario” related to vessel pitch motion, REF Figure 3.8. The lifting line in the ORCAFLEX model can be connected to the vessel at any arbitrary position, and the A-frame does not have to be modelled.

#### 4.2.1.2 Environmental Loading Conditions

In order to model the environmental loading conditions, representing the sea state in the Gulf of Mexico and offshore Angola, the waves are modelled based on a Pierson – Moskowitz wave spectrum. According to the “Handbook of Offshore Engineering” by Subrata Chakrabarti REF [17], The Pierson-Moskowitz wave spectrum is applicable for operational purposes in the Gulf of Mexico and offshore Angola. According to DNV-RP-H103, section 2.2.5 The Pierson – Moskowitz wave spectrum is applicable for modelling wind waves for non-fetch limited seas. The sea-state offshore Angola is however also subjected to swells and a double peaked wave spectrum should have been applied. The effect of swells is not accounted for in this analysis and all waves are considered to be wind waves. Environmental loading conditions are otherwise modelled as in the comparison study, section 3.3.2.

#### 4.2.2 ORCAFLEX input parameters

Input parameters required for the ORCAFLEX analysis, for the lifting line and the subsea structures, are equal to the input parameters used in the comparison study, section 3.3.3, Table 3.10 and Table 3.11. However, the splash zone lifting operation will be performed for different submergence levels of the lifted object, and the hydrodynamic added mass will vary with submergence level. Depth of submergence is considered to be the distance from still water line to the bottom of the subsea structure.

The hydrodynamic added mass at different submergence levels is presented in Table 4.1 and Table 4.2, for the subsea tree and the manifold respectively. Determination of hydrodynamic added mass during splash zone lifting is presented in APPENDIX A.6: Determination of added mass during splash zone lifting.

Table 4.1: Hydrodynamic Added Mass at Different Submergence Levels, Subsea Tree

Depth of submergence [m]	Hydrodynamic Added Mass X - direction [Te]	Hydrodynamic Added Mass Y-direction [Te]	Hydrodynamic Added Mass Z-direction [Te]
0	0	0	48.8
-1	7.1	7.1	62.3
-3.5	56.5	56.5	71.5
-8	187.8	187.8	108.6
-10	187.8	187.8	153.3

Table 4.2: Hydrodynamic Added Mass at Different Submergence Levels, Manifold

Depth of submergence [m]	Hydrodynamic Added Mass X - direction [Te]	Hydrodynamic Added Mass Y-direction [Te]	Hydrodynamic Added Mass Z-direction [Te]
0	0	0	48.8
-1	7.1	7.1	62.3
-3.5	56.5	56.5	71.5
-8	187.8	187.8	108.6
-10	187.8	187.8	153.3

For the splash zone lifting operation some additional input parameters are also required. The hydrodynamic slam coefficient for both entry and exit is set to:

$$C_S = C_E = 5$$

In accordance with DNV-RP-H103, section 3.4.2.20.

To account for the effect of perforation, the slam area is estimated as:

$$A_s = A_p * (1 - p) \text{ [m}^2\text{]}$$

Where:

$A_s$  = Slam area [m<sup>2</sup>]

$A_p$  = Projected area normal to flow in z-direction [m<sup>2</sup>]

$p$  = Perforation ratio [-]

Input values of slam coefficients and slam area are presented in Table 4.3 below.

**Table 4.3: Slam Coefficient & Slam Area**

Subsea Structure	$C_s, C_E$ [-]	$A_s$ [m <sup>2</sup> ]
Subsea Tree	5	32.4
Manifold	5	44.1

#### 4.2.3 Crane tip motion transfer function

The vertical crane tip motion transfer function for the A – frame vessel is needed to identify the critical lengths of lifting line, causing resonant motion between the oscillating crane tip and the lifting system. When scaling a vessel in ORCAFLEX the tabulated RAO data is unchanged, but the vessel response to waves during simulation is different. The vertical crane tip motion transfer function is therefore found by usage of linear wave theory. The waves are modelled in ORCAFLEX as Airy waves instead of with a Pierson-Moskowitz wave spectra.

Airy wave theory represent a constant sinusoidal wave with a given wave height wave period, as presented in Figure 4.1 below. [1]

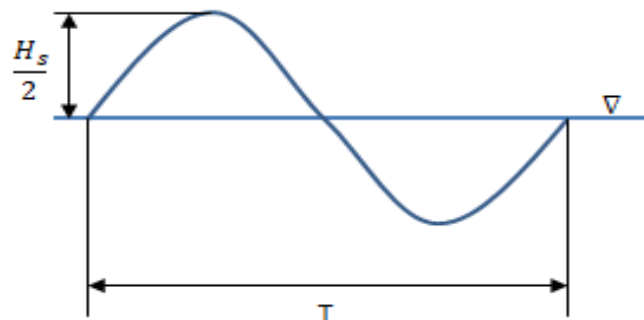


**Figure 4.1: Airy Wave**

The crane tip motion transfer function is found by running simulations in ORCAFLEX, for different wave peak periods, with a constant significant wave height of 2m. The crane tip motion transfer function is found as:

$$\frac{\text{Maximum position of crane tip during simulation} - \text{Static position of crane tip}}{\frac{H_S}{2}} \text{ [m/m]}$$

The crane tip motion transfer function for the A-frame vessel is presented in Figure 4.2 below for the subsea tree installation.

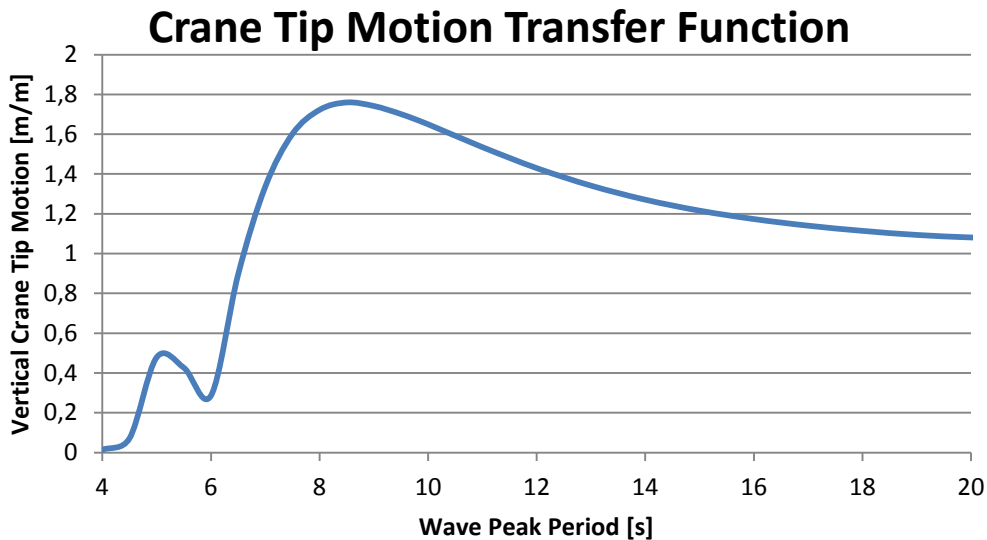


Figure 4.2: Crane Tip Motion Transfer Function, Subsea Tree

Due to the different crane boom extension for the two installation scenarios, the crane tip motion transfer function during the manifold installation will differ from the subsea tree installation. The crane tip motion transfer function will however peak for the same wave peak period, due to the vessel natural period in pitch. From Figure 4.2 above it is seen that the largest peak in the vertical crane tip motion transfer function, occur for wave peak periods equal to 8.5s. This is the vessel natural pitch period and large crane tip motion can be expected. The first peak appears at wave peak periods equal to 5s, and is caused by the vessel natural period in heave.

The critical lengths of lifting line, resulting in a natural period of the lifting system equal to the largest peak in the vertical crane tip motion transfer function, is presented in Table 4.4 below. The natural period of the lifting system is presented in section 3.3.4, Figure 3.10 and Figure 3.11.

Table 4.4: Critical Lengths of Lifting Line, A-Frame Vessel Installation

Subsea Structure	Length of Lifting Line[m]
Subsea Tree	1200
Manifold	945



### 4.3 Operational criteria

For the splash zone lifting operation, the operation has a transition from lift in air to subsea lifting. Both the maximum allowable dynamic force in lifting line and the slack sling criteria will vary with depths of submergence, due to the buoyancy force acting on the lifted object. The two operational criteria are calculated as in section 3.3.5, for both subsea structures, and results are presented in Table 4.5 - Table 4.8 below.

Table 4.5: Subsea Tree, Operational Criterion 1, Splash Zone Lifting

Depth of Submergence [m]	Operational Criterion 1 Maximum Allowable Dynamic Force [Te]
1	55
0	55
-1	56.3
-3.5	59.5
-8	64
-10	64

Table 4.6: Subsea Tree, Operational Criterion 2, Splash Zone Lifting

Depth of Submergence [m]	Operational Criterion 2 Maximum Allowable Dynamic Force [Te]
1	63
0	62.9
-1	61.8
-3.5	58.8
-8	54.8
-10	54.8

Table 4.7: Manifold, Operational Criterion 1, Splash Zone Lifting

Depth of Submergence [m]	Operational Criterion 1 Maximum Allowable Dynamic Force [Te]
1	10
0	10
-1	12.6
-2.5	17.6
-6	24.9
-8.5	24.9

**Table 4.8: Manifold, Operational Criterion 2, Splash Zone Lifting**

Depth of Submergence [m]	Operational Criterion 2 Maximum Allowable Dynamic Force [Te]
1	103.5
0	103.3
-1	100.6
-2.5	96.6
-6	90
-8.5	90

From Table 4.5 - Table 4.8 above it is seen that for the subsea tree installation, operational criterion 1 is governing for submergence depths down to -1, while operational criterion 2 is governing for submergence depths greater than -1. For the manifold installation, operational criterion 1 is governing for all depths of submergence.

For resonant motion, the operational criteria are as stated in section 3.3.5 for installation with fiber rope. For the subsea tree installation operational criteria 2 will be governing, while operational criterion 1 will be governing for the manifold installation. The operational criterion for both installation scenarios is presented in Table 4.9, at line lengths presented in section 4.2.3, Table 4.4.

**Table 4.9: Operational Criteria, Resonant Motion**

Subsea Structure	Maximum Allowable Dynamic Force [Te]
Subsea Tree	54.8
Manifold	23.9

## 4.4 Results - dynamic analysis

The dynamic analysis is performed for the same range of zero up-crossing periods as stated in section 3.3.6. Due to the limitation of the dynamic positioning system of the A-frame vessel, the analysis only cover significant wave heights  $\leq 3\text{m}$ . Sea-states with a significant wave height exceeding 3m are considered to be non-operable sea-states. The applied simulation time is set to 1800s, in accordance with DNV-RP-H103, section 3.4.3.5.

### 4.4.1 Splash zone lifting

During the splash zone lifting analysis, a depth of submergence = 1, resulted in severe pendulous motion of the lifted object, when applying a simulation time of 1800s. This resulted in unrealistic large dynamic forces, and all simulations for submergence level 1 is limited to a simulation time of 400s. The largest dynamic forces during splash zone lifting are experienced at submergence levels 0 to -3.5/-2.5, and the limited simulation time is not considered to be critical for the analysis. The rapidly increasing effective tension in the lifting line, during severe pendulous motion, is presented in Figure 4.3 below. The horizontal axis represents time [s] and the vertical axis represents effective tension [kN] in the lifting line. The figure is collected from an ORCAFLEX simulation with  $H_s = 1\text{m}$  and  $T_z = 3\text{s}$ .

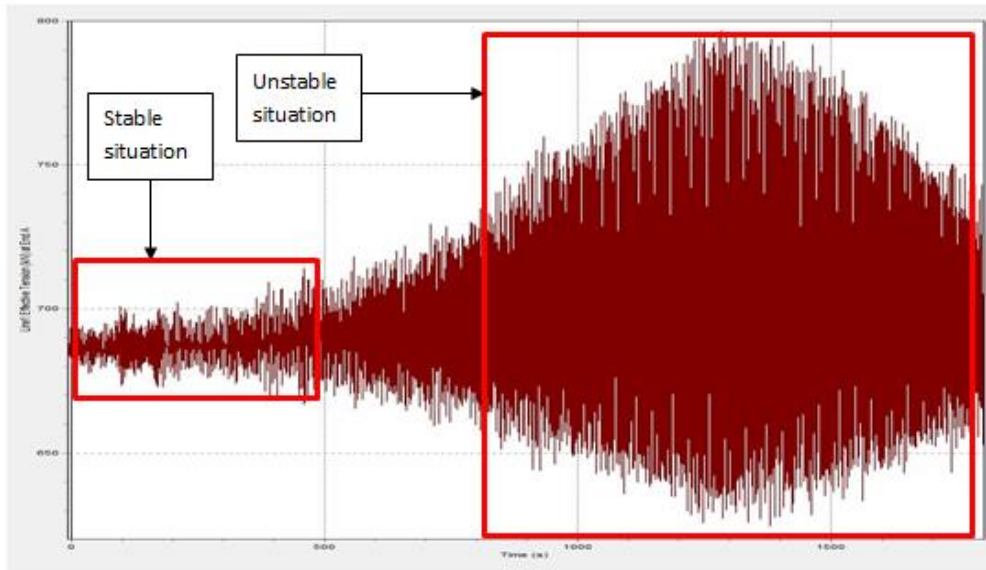


Figure 4.3: Effective Tension in Lifting Line during Severe Pendulous Motion of the Lifted Object

A separate identical simulation was performed, utilizing steel wire as lifting line, to determine that the pendulous motion was not a result of the reduced stiffness of fiber rope. The severe pendulous motion is hence considered to occur because the effect of guide wires and lifting slings are not included in the analysis.

The maximum dynamic force at end A (Line connection to vessel) in the lifting line, is presented in Table 4.10 and Table 4.11 below for the two installation scenarios. The dynamic force is found as in section 3.3.6. The maximum dynamic force is presented as tabulated values for all significant wave heights, and wave zero up-crossing periods. Tabulated results for all wave heights, wave zero up-crossing periods and levels of submergence is presented in APPENDIX A.7: Splash zone lifting – maximum dynamic force in lifting line.

= Maximum dynamic force for all depths of submergence, not exceeding the operational criteria

= Maximum dynamic force, exceeding the operational criteria

N/A = Sea-states outside the considered  $T_z$  – range

Table 4.10: Subsea Tree Installation, Dynamic Force in Lifting Line [Te], Splash Zone

$H_s$ [m]						$T_z$ [s]					
	3	4	5	6	7	8	9	10	11	12	13
1	31.8	15.9	23.4	14.9	14.9	14.0	9.9	6.9	6.4	5.9	4.6
1.5	71.7	52.1	38.5	30.6	31.1	28.9	15.1	11.6	11.1	9.1	6.8
2	N/A	83.7	62.0	52.1	53.2	48.5	24.4	18.9	18.5	12.3	8.9
2.5	N/A	157.0	184.6	123.5	80.9	70.1	35.8	28.0	27.8	16.4	11.4
3	N/A	N/A	230.1	254.8	123.5	96.2	49.7	37.7	39.0	22.3	15.8

**Table 4.11: Manifold Installation, Dynamic Force in Lifting Line [Te], Splash zone**

H <sub>s</sub> [m]						T <sub>z</sub> [s]						
	3	4	5	6	7	8	9	10	11	12	13	
1	43.5	30.7	29.8	24.0	23.9	22.1	10.2	9.3	8.8	7.6	6.4	
1.5	94.4	67.4	63.3	52.1	51.5	45.6	25.1	18.2	15.2	12.1	9.6	
2	N/A	158.8	108.7	89.0	89.3	76.0	41.7	30.3	28.7	19.5	13.0	
2.5	N/A	229.1	164.8	126.0	116.8	93.8	52.2	37.3	33.4	21.1	14.0	

The splash zone analysis is only performed for significant wave heights  $\leq 2.5\text{m}$  for the manifold installation.  $H_s = 2.5\text{m}$  result in limiting sea-states for all zero up - crossing periods.

#### 4.4.2 Resonant motion

The maximum dynamic force at end A (Line connection to vessel) in the lifting line is presented in Table 4.12 and Table 4.13 below for the two operational scenarios. Results are presented for critical lengths of lifting line identified in section 4.2.3. The dynamic force is found as in section 3.3.6.

**Table 4.12: Subsea Tree Installation, Dynamic Force in Lifting Line [Te], Resonance**

H <sub>s</sub> [m]						T <sub>z</sub> [s]						
	3	4	5	6	7	8	9	10	11	12	13	
1	3.9	18.0	25.7	27.0	24.3	23.9	20.3	17.1	17.7	15.7	12.6	
1.5	5.8	22.6	33.3	34.8	33.2	32.3	26.6	24.2	24.5	21.1	17.4	
2	N/A	26.7	40.3	42.0	41.7	40.3	32.7	31.5	31.5	26.3	21.9	
2.5	N/A	30.5	46.7	49.2	49.9	48.1	38.5	38.7	38.4	31.3	26.3	
3	N/A	N/A	52.9	56.3	57.8	56.0	44.1	45.8	45.3	37.3	30.6	

**Table 4.13: Manifold Installation, Dynamic Force in Lifting Line [Te], Resonance**

H <sub>s</sub> [m]						T <sub>z</sub> [s]						
	3	4	5	6	7	8	9	10	11	12	13	
1	4.4	19.9	31.4	32.7	32.0	29.7	25.6	23.7	24.1	21.1	17.6	
1.5	6.5	25.6	40.6	42.7	43.3	40.7	33.8	33.5	33.4	28.2	23.8	
2	N/A	30.9	48.9	52.2	53.9	51.4	41.4	42.8	42.6	35.0	29.7	

The dynamic analysis for resonant motion is only performed for  $H_s \leq 2\text{m}$  for the manifold analysis.  $H_s = 2\text{m}$  result in limiting sea-states for all zero up-crossing periods.

## 4.5 Operable sea-states

From Table 4.10 and Table 4.12 above, it is seen that the effect of resonant motion does not introduce additional weather restrictions for installation of the subsea tree. The total operable sea-states will hence be as presented in Table 4.10 above. From Table 4.11 and Table 4.13 above, it is seen that resonant motion introduces additional weather restrictions for installation of the manifold. The total operable sea-states for the manifold installation are presented in Table 4.14 below.

Table 4.14: Manifold, Operable Sea-states

H <sub>s</sub> [m]						T <sub>z</sub> [s]					
	3	4	5	6	7	8	9	10	11	12	13
1											
1.5											
2	N/A										
2.5	N/A										

## 4.6 Vessel operability

The results from the dynamic analysis are compared to an annual scatter diagram for sea-states in the deepwater regions Gulf of Mexico, REF [23], and offshore Angola, REF [24], to assess the operability of the A-frame vessel at different geographical areas. Due to the excessive amount of non-operable sea-states for the manifold installation, only the subsea tree installation will be considered.

The scatter diagrams represent the number of observations of sea-states, specified by a significant wave height and wave peak period. The relationship between wave peak period and wave zero up-crossing period is found from the ORCAFLEX model to be:

$$T_p = 1.4075 * T_z [s]$$

Where:

T<sub>p</sub> = Wave peak period [s]

T<sub>z</sub> = Wave zero up-crossing period [s]


Wave zero up-crossing periods considered in the analysis, resulting in a peak period in the range 4.0-4.99s is applied as T<sub>p</sub> = 4s in the scatter diagram for Gulf of Mexico. Peak periods in the range 5.0 – 5.99s is applied as T<sub>p</sub> = 5s, etc.

In addition H<sub>s</sub> = 1m and H<sub>s</sub> = 1.5m is applied as H<sub>s</sub> = 1m in the scatter diagram for the Gulf of Mexico. H<sub>s</sub> = 2m and H<sub>s</sub> = 2.5m is applied as H<sub>s</sub> = 2m, etc.

In the scatter diagram for sea-states offshore Angola, peak periods in the range 4.0-5.99s is applied as T<sub>p</sub> = 4s, etc. H<sub>s</sub> = 1m is applied as H<sub>s</sub> = 1 - 1.49m, etc.

Results from the dynamic analysis are compared to annual scatter diagrams for sea-states in the Gulf of Mexico and Offshore Angola and presented in Table 4.15 and Table 4.16 below.

 = Operable sea-state

 = Non-operable sea-state


 = Sea-state not covered by the analysis/ sea-state with no waves

Table 4.15: Subsea Tree Installation, Operable Sea-states Gulf of Mexico

H <sub>s</sub> [m]	T <sub>p</sub> [s]															
	2	3	4	5	6	7	8	9	10	11	12	13	14	15	16	17
<1	73	1647	4072	2293	2127	1512	1352	1214	546	164	171	196	66	90	236	25
1		9	2251	14562	15511	6584	5631	1353	431	178	164	343	195	458	198	320
2				163	5829	12110	3806	343	155	82	25	57	123	252	17	65
3					16	897	9017	1022	113	32	17	16	49	57		
4							171	921	449							
5								16	415	25						
6									16	16						
7										9						
8										9	16					
9											25					

Table 4.16: Subsea Tree Installation, Operable Sea-states Offshore Angola

H <sub>s</sub> [m]	T <sub>p</sub> [s]										
	2	4	6	8	10	12	14	16	18	20	22
0-0.49			7	21	28	42	42				
0.5-0.99	7	694	2764	1264	3590	3833	2569	812	236	90	7
1-1.49		417	4361	7277	7978	7902	6381	1993	576	132	42
1.5-1.99			42	1986	4013	3305	2444	1048	375	83	7
2-2.49				49	653	923	729	236	69	7	
2.5-2.99					28	97	160	69	21		
3-3.49							14	7			

#### 4.7 Summary - feasibility study

From Table 4.15 and Table 4.16 above the A-frame vessel is seen as applicable for performing deepwater installation of the subsea tree, both in the Gulf of Mexico and offshore Angola. The A-frame vessel is able to perform the installation in a wide range of sea-states in the Gulf of Mexico, and in most of the sea-states offshore Angola. However, the effect of swells offshore Angola is not accounted for and the range of operable sea-states could be somewhat reduced.

From Table 4.14 above it is seen that the A-frame vessel is not applicable for performing deepwater installation of the manifold. The dynamic forces experienced both during splash zone lifting and at resonant conditions, exceed the system capacity for most sea-states.

### 5 Discussion

The payload capacity of the fiber rope deployment system, at great water depths, is found to be slightly reduced compared to its payload capacity at surface. This is a result of the low submerged weight of the fiber rope. The fiber rope deployment system is hence found to be applicable for solving the problems related to self-weight of steel wire. It is also found that a rapid increase in wire size is necessary for obtaining the same SWL at 3000m water depth with a steel wire system. This leads to challenges related to logistics, allowable deck load on the installation vessel and required winch power for the deployment system. A larger wire size also require a larger drum winch to fulfill the D:d ratio required for bending steel wire.

The horizontal offset of the lifted object due to current, is found to be significantly higher when using fiber rope as lifting line compared to usage of steel wire. This is a result of the low submerged weight of the fiber rope, causing a lower counteracting force, for the drag force acting on the lifted object and lifting line. The difference is however reduced when performing installation of heavier subsea structures. The submerged weight of the subsea structure becomes more dominant as a counteracting force, and submerged weight of the lifting line is less crucial. A larger horizontal offset of the lifted object, when utilizing fiber rope as lifting line, can cause challenges related to positioning of the lifted object on the seafloor. This could lead to an increase in the operational weather window needed for the installation.

The fiber rope deployment system is found to have a better weather limiting criteria, for lowering to seabed operations, than a conventional steel wire system. The dynamic forces experienced in the lifting line during lowering to seabed operations, is also found to be significantly lower when using fiber rope compared to steel wire. Selection of wire size applicable for deepwater installation is hence crucial to obtain a sufficient payload capacity at large water depths. It is however seen that due to the large payload capacity of the steel wire at surface, the lowering to seabed operation of the manifold has no weather limiting criteria down to a water depth of 2500m.

Landing on seabed operations is found to be similar for usage of the two lifting lines. Difference in motion of the lifted object, close to the seafloor, varies for installation of different structures and no distinctive difference is identified from the analysis performed.

Results from the laboratory exercise imply that the tested fiber rope has a somewhat larger stiffness than provided by the rope manufacturer. Deviation between the measured line elongation and the theoretically calculated/ORCAFLEX line elongation does however have a relatively small impact on

the rope stiffness. Deviations are considered to be a result of sources of error related to the experiment, inaccurate readings from the load/elongation curve provided by the rope manufacturer, and deviation in the rope manufacturing process. Modelling of line stiffness in ORCAFLEX is hence considered to be representable for real life situations.

From the dynamic analysis performed in the feasibility study, it is seen that the largest dynamic forces occur for short wave zero up-crossing periods during splash zone lifting. Waves with short wave zero up-crossing periods have a higher water particle velocity than longer waves. Large water particle velocity combined with short crane tip oscillation period, results in large dynamic forces in the lifting line. At resonant condition, large dynamic forces occur at longer wave zero up-crossing periods. The effect of resonant motion is hence found to further limit the range of operable sea-states for installation of the manifold.

From the feasibility study, it is found that the A-frame vessel is able to perform deepwater installation of the subsea tree. The subsea tree installation can be performed in a wide range of sea-states in the Gulf of Mexico, and in most sea-states offshore Angola. The effect of swells offshore Angola is not accounted for, and the range of operable sea-states may be somewhat reduced. For deepwater installation of the manifold, the dynamic forces experienced both during splash zone lifting and at resonant conditions, exceed the system capacity for most sea-states. The A-frame vessel is hence considered to be unable of performing deepwater installation of the manifold.



## 6 Conclusion

The fiber rope deployment system is considered to be a viable substitute for the conventional steel wire system for deepwater installation of subsea structures. The system successfully solves the problems related to self-weight of the steel wire, and has a better weather limiting criteria for lowering to seabed operations.

Positioning of the lifted object on the seabed is found to be more challenging when utilizing fiber rope as lifting line. This could increase the operational weather window needed for the installation. ROV monitoring and guidance of the lifted object during deployment, is considered to be a possible solution to the challenges related to positioning. Increased deployment speed of the fiber rope system, compared to a steel wire system, will compensate for the increased time needed for positioning.

The A-frame vessel, rigged with a fiber rope deployment system, is considered to be applicable for deepwater installation of the subsea tree described in this thesis. The installation can be performed for a wide range of sea-states in the deepwater regions Gulf of Mexico and offshore Angola. Utilizing smaller vessels, rigged with an A-frame and a fiber rope deployment system, for deepwater installation subsea structures weighing  $\leq 70\text{Te}$  is considered to be a possibility. This could reduce the vessel availability problems faced in the offshore industry. The vessel could be applicable for installation of a variety of subsea structures, such as:

- Riser base
- PLET
- SDA
- Pumping Modules

The vessel would however need to be equipped with a skidding system for module handling on deck, due to the limited in-board crane boom radii of the A-frame and limited capacity of the deck crane.

## 7 Further work

Due to the limitations of this thesis, the possibility of performing deepwater installation with smaller vessels should be further assessed. A dynamic lifting analysis, based on RAO data for a real A-frame vessel should be performed, and the effect of active heave compensation should be included. The analysis should also be performed with more accurate values for drag factor in oscillating flow and slam coefficient, for the subsea structure to be installed. A separate analysis, accounting for the effect of swells offshore Angola, should also be conducted to obtain a more realistic view of the vessel operability. A less conservative approach to the weight and size of the subsea tree should also be considered.

The size and weight of the 125Te SWL fiber rope deployment system, is in this thesis assumed to be applicable for mobilization on an A-frame vessel. The actual size and weight of the system should hence be assessed.

## References

- [1]: Gudmestad Ove Tobias, lectures Marine Technology and Marine Operations, spring and autumn 2013
- [2]: Sarkar Arunjyoti, Gudmestad Ove T, 2010, Splash Zone Lifting Analysis of Subsea Structures, Sanghai, China, 29<sup>th</sup> International Conference on Ocean, Offshore and Arctic Engineering
- [3]: Rowe Stephen J, Mackenzie Brian, Snell Richard, 2001, Deepwater Installation of Subsea Hardware, Huston, Texas, Proceedings of the 10<sup>th</sup> Offshore Symposium
- [4]: Wang Alan, Yang Yun, Zhu Shaohua, Li Huailiang, Xu Jingkuo, He Min, 2012, Latest Progress in Deepwater Installation Technologies, Rhodes, Greece, Proceedings of the Twenty-second (2012) International Offshore and Polar Engineering Conference
- [5]: Wang Alan M, Zhu Shaoua, Zhu Xiaohuan, Xu Jingkuo, He Min, Zhang Changzhi, 2013, Pendulous Installation Method and its Installation Analysis for a Deepwater Manifold in South China Sea, Anchorage, Alaska, USA, Proceedings of the Twenty-third (2013) International Offshore and Polar Engineering
- [6]: Mork Henrik, Lunde Johannes, 2007, A Cost-Effective and Safe Method for Transportation and Installation of Subsea Structures – The Pencil Buoy Method, Aberdeen, Scotland, U.K, SPE Offshore Europe
- [7]: Gramnæs Jan H, Hilmersen Lars, Tveitnes Ivar, 2004, Subsurface Towing using Pencil Buoy Method as alternative to Offshore Lifting, slide 13 - 33 , Aker Marine Contractors AS
- [8]: Joensen Arnbjorn, Paul David, 2011, A Low Tech, Low Risk System for the Installation of Large Structures in Deep Water, Aberdeen, U.K, SPE Offshore Europe Oil and Gas Conference and Exhibition
- [9]: Accessed 08.04.2014, <http://www.sdsltd-uk.com/Downloads/SDS-PR-002-V1%20Mini%20Brochure.pdf>
- [10]: Accessed 08.04.2012, <http://www.sdsltd-uk.com/sdsmain-outlinemethod.html>
- [11]: Torben Sverre, Ingeberg Per, Bunes Øyvind, 2008, Fiber Rope Deployment System and Rope Management Process, Vancouver, BC, Canada, Proceedings of the Eighteenth (2008) International Offshore and Polar Engineering Conference
- [12]: Torben Sverre Rye, Ingeberg Per, 2010, Field Pilot of Deep Water Installation in Two-Fall Using Fibre Rope, Rio de Janeiro, Rio Oil & Gas Expo and Conference 2010 Proceedings
- [13]: Johansson Daniel, 2010, Practical use of a Fiber Rope Lifting System on the Petrobras SESV, “Skandi Santos”, slide 12 - 32, Stavanger, Subsea Lifting Conference
- [14]: Accessed 08.04.2014, [http://www.cortlandcompany.com/sites/default/files/downloads/media/technical-literature-braid-optimized-bending-bob-tech-sheet\\_1.pdf](http://www.cortlandcompany.com/sites/default/files/downloads/media/technical-literature-braid-optimized-bending-bob-tech-sheet_1.pdf)

- [15]: Bøe Tormod, 2007, DNV Marine Operations`Rules for Subsea Lifting, New Simplified Method for Prediction of Hydrodynamic Forces, slide 12
- [16]: Accessed 08.04.2014, <http://www.kiswire.com/korean/pop/N2HYROPE.pdf>
- [17]: Chakrabarti Subrata k, 2005, Handbook of Offshore Engineering, Volume 1, Table 3.14, Elsevier, Illinois, USA
- [18]: Accessed 08.06.2014,  
<http://www.hbm.com/fileadmin/mediapool/hbmdoc/technical/s2002.pdf>
- [19]: Accessed 02.06.2014,  
<http://www.cortlandcompany.com/sites/default/files/downloads/media/technical-literature-plasma-12-strand-tech-sheet.pdf>
- [20]: Bøe T., Nestegård A., 2010, Dynamic Forces during Deepwater Lifting Operations, Beijing, China, Proceedings of the Twentieth International Offshore and Polar Engineering Conference
- [21]: Accessed 02.06.2014,  
[http://www.vuykrotterdam.com/uploads/FinalPDF/Multi\\_Purpose\\_Offshore\\_Vessel.PDF](http://www.vuykrotterdam.com/uploads/FinalPDF/Multi_Purpose_Offshore_Vessel.PDF)
- [22]: ORCAFLEX help menu, system modelling: data and results, vessels, vessel data
- [23]: Albert B. Aalbers, 2006, Fuel Consumption and Emission Predictions: Application to a DP-FPSO Concept, Table 4, Dynamic Positioning Conference, Maritime Research Institute Netherlands
- [24]: Ingvild Lodden, 2013, Considerations When Lifting a Large Module in Different Geographical Areas, APPENDIX D, Table 27, Master`s Thesis
- [25]: Accessed 02.06.2014, <http://mathworld.wolfram.com/CircularSegment.html>

## APPENDIX

## A.1: ORCAFLEX RAO data

RAO data for the standard vessel model in ORCAFLEX is presented in figure A.1.1 below, for a vessel heading of 22.5°.

0°	22,5°	45°	67,5°	90°	112,5°	135°	157,5°	180°				
Periods: <input type="text" value="22"/>												
Period (s)	Surge		Sway		Heave		Roll		Pitch		Yaw	
	Ampl. (m/m)	Phase (deg)	Ampl. (m/m)	Phase (deg)	Ampl. (m/m)	Phase (deg)	Ampl. (deg/m)	Phase (deg)	Ampl. (deg/m)	Phase (deg)	Ampl. (deg/m)	Phase (deg)
0,00	0,000	0,0	0,000	360,0	0,000	360,0	0,000	0,0	0,000	0,0	0,000	360,0
4,00	0,0081	68,3	0,00082	206,8	0,014	282,6	0,065	106,7	0,056	-97,1	0,035	247,0
5,00	0,012	-88,5	0,016	264,8	0,065	133,4	0,175	-63,7	0,265	-220,4	0,032	214,2
5,50	0,017	66,2	0,018	126,2	0,091	190,1	0,099	63,4	0,678	-177,4	0,122	182,6
6,00	0,033	99,9	0,044	89,6	0,166	237,5	0,410	80,6	0,887	-165,6	0,087	134,3
6,50	0,029	104,8	0,044	65,1	0,306	239,5	0,607	79,1	0,660	-135,3	0,140	40,8
7,00	0,024	-55,5	0,030	12,7	0,244	211,8	0,625	73,2	1,079	-93,8	0,270	18,2
7,50	0,108	-70,6	0,046	-49,3	0,042	169,3	0,433	68,2	1,558	-89,5	0,372	11,3
8,00	0,203	-75,4	0,078	-69,1	0,149	22,9	0,129	135,0	1,804	-89,7	0,441	8,2
8,50	0,295	-78,6	0,113	-74,2	0,299	15,6	0,747	176,2	1,892	-90,6	0,479	6,7
9,00	0,378	-80,8	0,150	-77,2	0,422	12,4	1,233	145,5	1,880	-91,2	0,498	6,1
9,50	0,449	-82,3	0,182	-80,6	0,525	10,3	1,222	124,5	1,814	-91,6	0,504	5,6
10,00	0,510	-83,4	0,208	-82,7	0,608	8,8	1,093	114,0	1,725	-91,7	0,500	4,9
11,00	0,607	-84,8	0,248	-84,8	0,730	6,5	0,864	104,9	1,526	-91,6	0,470	4,0
12,00	0,678	-85,7	0,277	-85,9	0,809	4,9	0,704	101,1	1,338	-91,3	0,429	3,3
13,00	0,730	-86,3	0,299	-86,6	0,861	3,9	0,588	99,1	1,172	-91,0	0,387	2,7
14,00	0,768	-86,9	0,315	-87,1	0,897	3,2	0,498	97,8	1,030	-90,8	0,347	2,3
15,00	0,797	-87,3	0,328	-87,5	0,921	2,7	0,428	96,8	0,910	-90,7	0,312	2,0
16,00	0,819	-87,6	0,337	-87,8	0,939	2,3	0,372	96,2	0,808	-90,5	0,280	1,8
17,00	0,836	-87,9	0,344	-88,1	0,952	2,0	0,326	95,6	0,721	-90,4	0,252	1,6
18,00	0,849	-88,1	0,350	-88,3	0,961	1,7	0,289	95,2	0,646	-90,4	0,228	1,4
19,00	0,860	-88,3	0,355	-88,5	0,969	1,5	0,257	94,8	0,582	-90,3	0,207	1,3
20,00	0,869	-88,5	0,358	-88,6	0,975	1,4	0,231	94,5	0,527	-90,3	0,188	1,1
21,00	0,877	-88,6	0,362	-88,8	0,979	1,3	0,208	94,2	0,480	-90,3	0,172	1,0
22,00	0,883	-88,7	0,365	-88,9	0,982	1,1	0,189	94,0	0,438	-90,2	0,158	0,95
Infinity	0,924	90,0	0,383	90,0	1,000	0,0	0,000	0,0	0,000	0,0	0,000	0,0

Figure A.1. 1: RAO Data, ORCAFLEX Vessel

## A.2: Fiber rope certificate of conformance



1012 Second Street  
Anacortes, WA 98221 USA  
Telephone: 360/293-8488  
Fax: 360/293-8480  
Web: www.psrope.com  
Email: sales@psrope.com

### CERTIFICATE OF CONFORMANCE

September 11, 2008

Customer: Myhre Maritime

Customer Purchase Order Number: 35141

Puget Sound Rope Invoice Number: 29189

Type and Size of Rope: 1/4" dia. (3/4" circ.) Plasma 12-Strand *6 mm*

PSR Specification Number: T304

US Military Specification: N/A

ABS Type Certification: Not approved

DNV Type Approval Certificate: Not approved

Minimum Tensile Strength-lbs.: 8,000 lbs.

Notes:

**We hereby certify that the described product meets published specifications and is in conformance with the requirements of your purchase order. We further certify this product was manufactured, tested and inspected in accordance with a registered ISO 9001 Quality Management System.**

  
\_\_\_\_\_  
Sherrie Rust



Figure A.2. 1: Fiber Rope Certificate of Conformance

### A.3: Comparison study – maximum dynamic force in lifting line

The maximum dynamic force in the lifting line is presented as tabulated values, in Table A.3.1 – A.3.4 below, for the different installation scenarios.

Table A.3. 1: Subsea Tree Installation, Steel Wire, Maximum Dynamic Force in Lifting Line [Te]

Subsea Tree Installation - Steel Wire							
L	H <sub>s</sub>						
	1	1.5	2	2.5	3	3.5	4
500	3.8	5.1	6.6	8.3	10.0	11.7	14.2
1000	4.1	6.2	8.4	10.8	13.2	15.8	18.4
1500	6.8	9.2	12.4	14.7	17.1	20.3	23.7
2145	12.8	16.6	19.9	23.4	26.7	29.8	32.9
2500	14.9	19.1	23.0	26.5	28.0	31.5	34.9
2950	14.6	18.9	22.9	27.0	30.7	34.2	37.4

Table A.3. 2: Subsea Tree Installation, Fiber Rope, Maximum Dynamic Force in Lifting Line [Te]

Subsea Tree Installation – Fiber Rope							
L	H <sub>s</sub>						
	1	1.5	2	2.5	3	3.5	4
500	5.1	6.9	9.6	11.0	13.0	15.5	18.3
705	8.0	10.7	13.0	15.4	17.7	19.9	22.0
1500	8.2	10.6	12.9	15.0	17.0	19.9	23.0
2000	8.0	10.4	12.8	15.3	17.8	20.3	23.2
2500	8.4	11.0	13.4	15.6	17.8	20.0	22.6
2950	7.3	9.9	12.3	14.5	16.9	19.2	21.5

Table A.3. 3: Manifold Installation, Steel Wire, Maximum Dynamic Force in Lifting Line [Te]

Manifold Installation – Steel Wire							
L	H <sub>s</sub>						
	1	1.5	2	2.5	3	3.5	4
500	4.9	7.5	10.1	12.8	15.7	18.7	21.7
1000	6.5	10.0	13.8	17.7	21.7	25.9	30.2
1760	18.8	23.9	28.2	32.2	35.8	39.3	42.6
2000	17.5	20.7	24.7	28.3	31.7	35.5	39.2
2500	15.4	19.9	24.9	29.2	33.1	36.9	41.6
2950	15.3	20.0	24.3	28.4	32.9	38.4	44.0

Table A.3. 4: Manifold Installation, Fiber Rope, Maximum Dynamic Force in Lifting Line [Te]

Manifold Installation – Fiber Rope							
L	H <sub>s</sub>						
	1	1.5	2	2.5	3	3.5	4
300	5.2	8.7	12.0	15.5	18.9	22.6	26.4
555	11.9	15.3	18.4	21.6	24.6	27.3	30.3
1000	10.8	13.7	16.9	19.6	23.8	28.1	32.5
1500	10.2	13.7	17.1	20.4	24.0	27.8	31.7
2000	10.6	13.6	16.3	18.9	22.8	26.1	29.4
2500	8.6	11.9	14.3	16.4	18.4	20.4	26.6
2950	8.6	11.5	14.3	16.9	19.4	21.8	24.2



#### A.4: Comparison study – motion of lifted object

The maximum displacement of the lifted object, at line length 2950m, is presented in Table A.4.1 – A.4.4 below, for the different installation scenarios.

Table A.4. 1: Subsea Tree Installation, Steel Wire, Maximum Displacement of Lifted Object [m]

Subsea Tree Installation – Steel Wire											
H <sub>s</sub>						T <sub>z</sub> [s]					
	3	4.6	5	6	7	8	9	10	11	12	13
1	0.06	0.72	0.75	0.88	0.93	0.89	0.83	0.90	0.98	0.98	0.89
1,5	0.08	0.91	0.94	1.14	1.24	1.28	1.23	1.37	1.40	1.47	1.28
2,00		1.08	1.13	1.37	1.52	1.67	1.59	1.83	1.83	1.98	1.66
2,5		1.23	1.30	1.58	1.78	2.04	1.92	2.28	2.25	2.50	2.07
3			1.45	1.77	2.02	2.40	2.24	2.71	2.67	3.02	2.52
3,5			1.59	1.96	2.26	2.75	2.63	3.14	3.09	3.55	2.96
4,00				2.14	2.51	3.09	3.01	3.56	3.50	4.06	3.41

Table A.4. 2: Subsea Tree Installation, Fiber Rope, Maximum Displacement of Lifted Object [m]

Subsea Tree Installation – Fiber Rope											
H <sub>s</sub>						T <sub>z</sub> [s]					
	3	4.6	5	6	7	8	9	10	11	12	13
1	0.01	0.11	0.20	0.79	1.05	1.24	1.30	1.54	1.59	1.81	1.36
1.5	0.01	0.16	0.29	1.00	1.32	1.54	1.70	1.98	2.07	2.37	1.87
2		0.21	0.38	1.17	1.58	1.82	2.11	2.34	2.50	2.86	2.35
2.5		0.26	0.47	1.33	1.79	2.08	2.47	2.65	2.90	3.31	2.81
3			0.55	1.47	1.98	2.32	2.78	2.94	3.28	3.71	3.24
3.5			0.64	1.59	2.15	2.53	3.07	3.19	3.63	4.07	3.65
4				1.71	2.30	2.72	3.33	3.43	3.96	4.41	4.04

Table A.4. 3: Manifold Installation, Steel Wire, Maximum Displacement of Lifted Object [m]

Manifold Installation – Steel Wire											
H <sub>s</sub>						T <sub>z</sub> [s]					
	3	4.6	5	6	7	8	9	10	11	12	13
1	0.03	0.62	0.66	0.91	0.95	1.08	1.02	1.11	1.03	1.09	1.03
1.5	0.04	0.79	0.83	1.17	1.25	1.48	1.43	1.59	1.50	1.66	1.46
2		0.93	0.99	1.38	1.53	1.86	1.84	2.06	1.94	2.23	1.86
2.5		1.05	1.13	1.57	1.80	2.21	2.23	2.50	2.37	2.78	2.30
3			1.25	1.75	2.04	2.54	2.60	2.92	2.78	3.31	2.74
3.5			1.35	1.91	2.27	2.85	2.97	3.31	3.18	3.82	3.19
4				2.07	2.48	3.14	3.32	3.68	3.56	4.32	3.62

Table A.4. 4: Manifold Installation, Fiber Rope, Maximum Displacement of Lifted Object [m]

Manifold Installation – Fiber Rope											
H <sub>s</sub>						T <sub>z</sub> [s]					
	3	4,6	5	6	7	8	9	10	11	12	13
1	0.00	0.06	0.09	0.34	0.78	1.01	1.16	1.24	1.54	1.76	1.47
1,5	0.01	0.09	0.14	0.48	0.97	1.25	1.53	1.61	1.95	2.20	1.85
2		0.11	0.19	0.62	1.13	1.44	1.85	1.99	2.30	2.56	2.28
2,5		0.14	0.23	0.73	1.27	1.62	2.11	2.32	2.61	2.88	2.69
3			0.28	0.84	1.40	1.79	2.34	2.62	2.89	3.16	3.05
3,5			0.32	0.95	1.51	1.94	2.54	2.90	3.16	3.42	3.39
4				1.04	1.62	2.08	2.73	3.15	3.41	3.69	3.69

## A.5: ORCAFLEX model A-frame vessel

### Vessel Model:

The scaled A-frame vessel model is presented in Figure A.5.1 below.

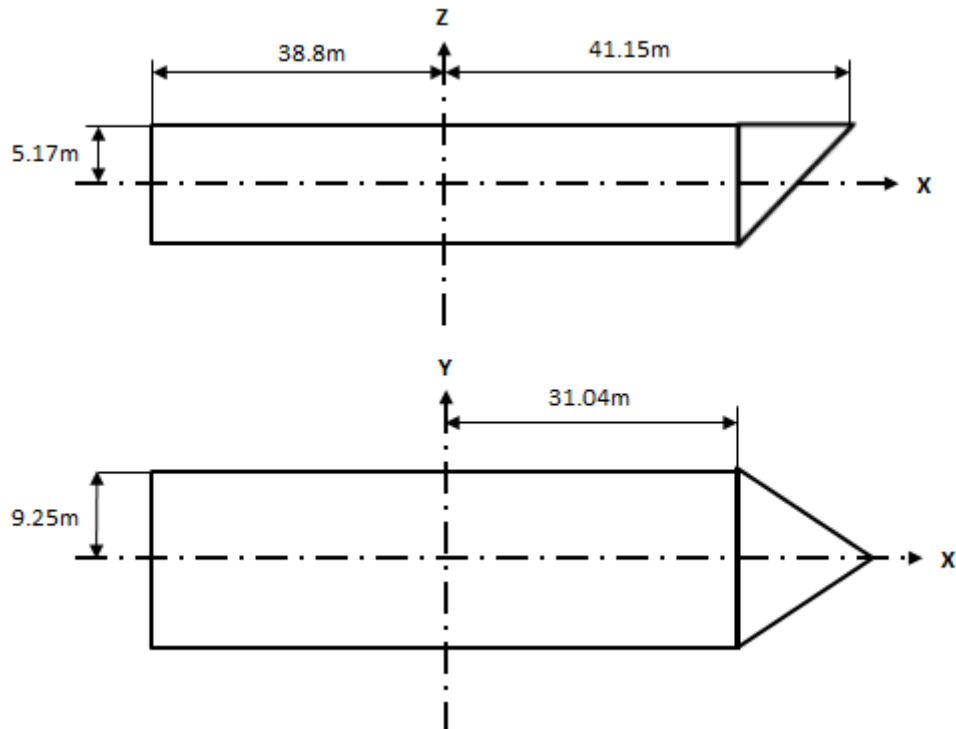


Figure A.5. 1: A-frame Vessel Model, ORCAFLEX

### Lifting Line:

Modelling of the lifting line is performed as in the comparison study, section 3.3.2. The connection of the lifting line to the vessel is set as  $(x, y, z) = (L_1 + 2 * \frac{w}{2}, 0, h + H)$  based on figure xx below. A clearance from vessel aft to the lifted object, equal to half the width of the lifted object, is applied for each operational scenario. Length of the A-frame is assumed to be 10m.

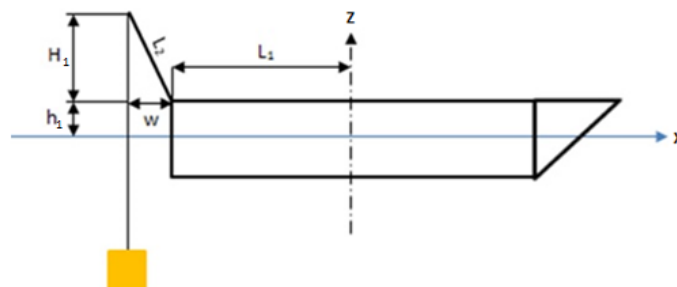


Figure A.5. 2: Determination of Line Connection to A-frame Vessel, ORCAFLEX

Where:

$$H = \sqrt{L_2^2 - w^2}$$

$H_1$  = Height of “Crane tip” above vessel deck

$h_1$  = Height of vessel deck above still water line

$w$  = width of lifted object

$L_1$  = Distance from amid ship point to A-frame

$L_2$  = Length of A – frame

The splash zone lifting operation will be performed for different submergence levels of the lifted object relative to the still water line. The line length, during splash zone lifting is determined as shown in Figure A.5.3 below.

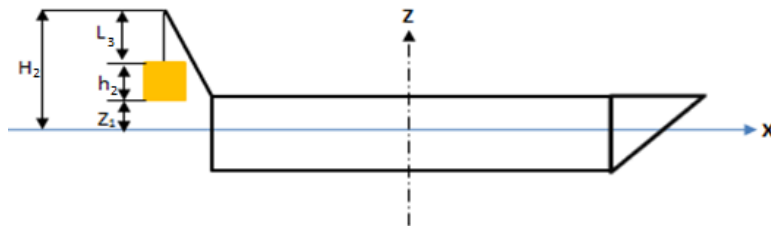


Figure A.5. 3: Determination of Line Length & Initial Position of Lifted Object, Splash Zone Lifting, ORCAFLEX

Where:

$L_3$  = Length of lifting line

$H_2$  = Distance from still water line to “crane tip”

$Z_1$  = submergence level, positive above still water line and negative below still water line

$h_2$  = height of lifted object

And the line length is found as:

$$L_3 = H_2 - z_1 - h_2 \text{ [m]}$$

**Subsea Structures:**

The two subsea structures are modelled as in the comparison study, section 3.3.3. For the splash zone lifting operation the initial position and altitude of the lifted object is determined differently. Based on Figure A.5.2 and A.5.3 above, the initial position and altitude of the lifted object is set to  $(x, y, z) = (L_1 + w, 0, H_2 - z_1 - \frac{h_2}{2})$  for splash zone lifting.

## A.6: Determination of added mass during splash zone lifting

The hydrodynamic added mass will vary with different levels of submergence, as presented in Figure A.6.1 below.

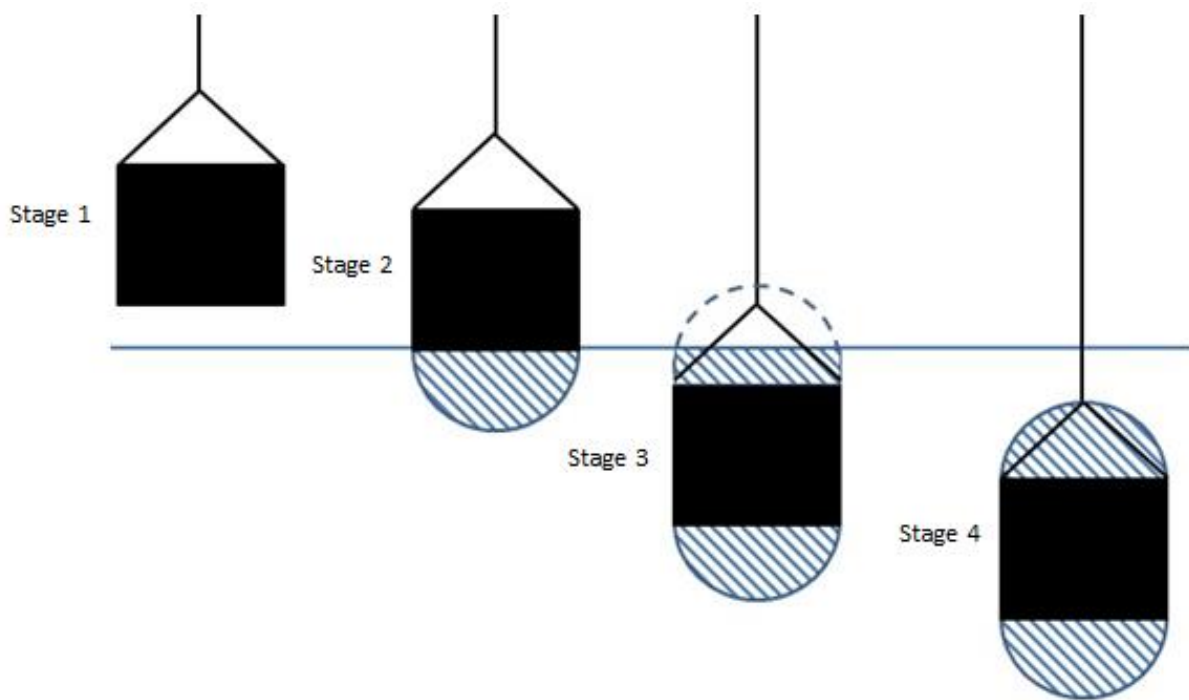


Figure A.6. 1: Development of Hydrodynamic Added Mass at Different Levels of Submergence, Splash Zone Lifting

Stage 1: Object in air

Stage 2: Object touching the still water line

Stage 3: Object slightly submerged

Stage 4: Object fully submerged

Calculation of added mass coefficients and corresponding hydrodynamic added mass is based on DNV-RP-H103, APPENDIX A, Table A-2. The effect of vertical sides and structure perforation are based on DNV-RP-H103, section 4.6. The subsea tree is assumed to be 10% perforated, while the manifold is assumed to be 30% perforated.

In order to estimate the hydrodynamic added mass in z-direction for the different stages the following approximations are made:

- The hydrodynamic added mass for stage 1 and 2 is set equal to:  
Half the hydrodynamic added mass of a fully submerged object, effect of object height is not accounted for. The hydrodynamic added mass for stage 1 and 2 is found as:

$$A_{330} = \rho_{sw} * C_A * \frac{\pi}{4} a^2 b * \text{Added mass reduction factor [kg]}$$

Hydrodynamic added mass for stage 1 is applied, to account for added mass when the object gets hit by the oscillating sea surface.

- The hydrodynamic added mass for stage 3 is set equal to:  
Half the hydrodynamic added mass of a fully submerged object + volume of water on top of the lifted object, up to the still water line REF [1]. Effect of object height is accounted for. The volume of water on top of the lifted object is found as:

$$V = V_{\text{Tot}} - V_{\text{Air}} \text{ [m}^3\text{]}$$

$$V_{\text{Tot}} = \frac{\pi}{4} a^2 b \text{ [m}^3\text{]}$$

$$V_{\text{Air}} = \left[ \left(\frac{a}{2}\right)^2 * \cos^{-1} \left(\frac{\frac{a}{2}-h}{\frac{a}{2}}\right) - \left(\frac{a}{2} - h\right) \sqrt{ah - h^2}\right] * b \text{ [m}^3\text{]}, \text{ REF [25]}$$

The formula is based on Figure A.6.2 below.

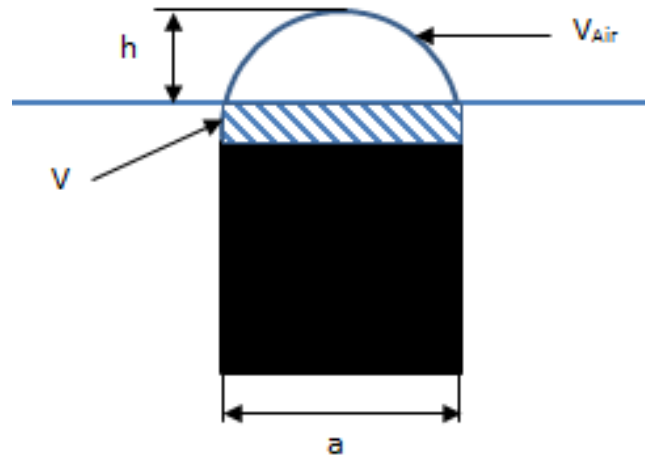


**Figure A.6. 2: Hydrodynamic Added Mass, Lifted Object Slightly Submerged**

Where:

$V$  = Volume of water on top of the lifted object

$V_{\text{Tot}}$  = Volume of half circle

$V_{\text{Air}}$  = Volume of half circle above still water line

$a$  = width of the lifted object

$b$  = depth of the lifted object

$h$  = height from still water line to the top of the half circle.

The hydrodynamic added mass for stage 3 can now be found as:

$$A_{33} = \left[ 1 + \sqrt{\frac{1-\lambda^2}{2(1+\lambda^2)}} \right] * \left( V * \rho_{sw} + \frac{A_{33o}}{2} \right) * \text{Added mass reduction factor [kg]}$$

$$\lambda = \frac{\sqrt{A_p}}{h_1 + \sqrt{A_p}} [-]$$

$$A_{33o} = \rho_{sw} * C_A * \frac{\pi}{4} a^2 b \text{ [kg]}$$

Where:

$\rho_{sw}$  = Density of seawater

$h_1$  = Submerged height of lifted object

$A_p$  = Projected area of lifted object normal to flow direction

$A_{33o}$  = Added mass of fully submerged object, effect of object height not accounted for

$C_A$  = Hydrodynamic added mass coefficient

- The hydrodynamic added mass for stage 4 is found as:

$$A_{33} = \left[ 1 + \sqrt{\frac{1-\lambda^2}{2(1+\lambda^2)}} \right] * A_{33o} * \text{Added mass reduction factor [kg]}$$

Added mass in x and y – direction during splash zone lifting is found based on the submerged projected area normal to flow direction, and found as added mass in z-direction stage 4.



## A.7: Splash zone lifting – maximum dynamic force in lifting line

The maximum dynamic force in the lifting line during splash zone lifting is presented for all submergence depths, wave heights and wave zero up-crossing periods in table A.7.1 – A.7.5 below for the subsea tree analysis, and table A.7.6 – A.7.9 for the manifold analysis.

Table A.7. 1: Subsea Tree Installation, Maximum Dynamic Force in Lifting Line [Te], Hs = 1m

H <sub>s</sub> = 1m						T <sub>z</sub> [s]					
Z [m]	3	4	5	6	7	8	9	10	11	12	13
1	2.3	7.9	23.4	13.1	5.1	4.3	3.0	2.7	3.0	1.9	2.0
0	23.6	15.9	15.3	11.4	11.9	9.8	6.4	4.3	3.9	2.9	1.7
-1	31.8	14.1	17.2	13.7	13.6	13.6	7.4	5.4	5.1	3.6	2.5
-3,5	14.0	11.0	16.7	14.6	14.9	14.0	7.0	6.0	5.6	3.7	2.9
-8	13.3	13.3	13.7	12.3	10.2	9.7	8.9	6.1	5.7	5.4	3.8
-10	10.1	13.3	16.1	14.9	11.6	10.8	9.9	6.9	6.4	5.9	4.6

Table A.7. 2: Subsea Tree Installation, Maximum Dynamic Force in Lifting Line [Te], Hs = 1.5m

H <sub>s</sub> = 1.5m						T <sub>z</sub> [s]					
Z [m]	3	4	5	6	7	8	9	10	11	12	13
1	20.8	27.1	38.5	21.0	11.4	8.7	4.9	4.2	4.9	3.1	3.0
0	51.1	39.0	32.3	26.6	27.2	23.2	14.3	9.3	8.4	5.8	3.4
-1	71.7	52.1	37.0	29.4	29.7	28.9	14.9	10.7	10.1	6.7	4.8
-3,5	27.3	26.0	35.1	30.6	31.1	28.5	14.4	11.6	11.1	7.0	5.1
-8	20.0	21.3	22.8	19.8	15.9	14.8	13.8	9.3	8.9	8.2	5.6
-10	15.6	19.2	24.8	22.6	17.3	16.1	15.1	10.6	9.9	9.1	6.8

Table A.7. 3: Subsea Tree Installation, Maximum Dynamic Force in Lifting Line [Te], Hs = 2m

H <sub>s</sub> = 2m						T <sub>z</sub> [s]					
Z [m]	4	5	6	7	8	9	10	11	12	13	
1	45.7	43.3	33.6	19.2	21.5	7.1	5.7	7.8	4.5	3.9	
0	83.7	62.0	50.3	47.1	42.2	24.4	16.4	14.7	9.4	5.9	
-1	82.9	60.5	50.8	51.3	48.5	24.1	17.5	17.3	10.7	7.7	
-3,5	60.8	60.6	52.1	53.2	47.1	24.2	18.9	18.5	11.2	7.9	
-8	29.1	31.2	27.7	22.2	20.8	19.8	13.1	12.3	11.0	7.5	
-10	28.5	33.0	30.3	24.1	21.7	20.3	14.4	13.5	12.3	8.9	

Table A.7. 4: Subsea Tree Installation, Maximum Dynamic Force in Lifting Line [Te], Hs = 2.5m

H <sub>s</sub> = 2.5m					T <sub>z</sub> [s]					
Z [m]	4	5	6	7	8	9	10	11	12	13
1	77.6	80.4	62.7	28.8	42.2	10.3	7.6	13.4	6.0	4.9
0	122.9	98.4	83.4	67.0	63.7	35.6	24.8	22.7	13.6	9.4
-1	157.0	116.7	89.8	79.7	70.1	33.4	25.7	26.4	15.3	11.4
-3,5	125.3	184.6	123.5	80.9	69.2	35.8	28.0	27.8	16.4	11.3
-8	45.0	53.2	53.0	47.4	47.5	26.6	17.6	16.7	14.0	9.6
-10	41.0	41.9	39.3	31.8	29.7	25.8	18.4	17.2	15.6	11.1

Table A.7. 5: Subsea Tree Installation, Maximum Dynamic Force in Lifting Line [Te], Hs = 3m

H <sub>s</sub> = 3m					T <sub>z</sub> [s]					
Z [m]	5	6	7	8	9	10	11	12	13	
1	119.1	106.0	48.1	67.4	14.7	11.4	19.7	6.5	6.0	
0	149.1	137.0	103.0	90.3	46.6	33.8	32.2	18.3	13.7	
-1	183.3	155.4	123.5	95.1	46.0	36.1	37.5	21.3	15.8	
-3,5	230.1	254.8	113.2	96.2	49.7	39.7	39.0	22.3	15.3	
-8	130.7	85.4	83.8	76.4	34.5	23.6	20.7	17.6	12.0	
-10	55.1	51.5	41.0	38.2	31.8	22.7	21.1	19.0	13.4	

Table A.7. 6: Manifold Installation, Maximum Dynamic Force in Lifting Line [Te], Hs = 1m

H <sub>s</sub> = 1m						T <sub>z</sub> [s]					
Z [m]	3	4	5	6	7	8	9	10	11	12	13
1	3.1	16.2	23.0	14.2	10.8	6.8	5.3	4.3	5.1	3.1	3.3
0	39.1	30.7	21.3	19.1	20.1	14.7	10.2	8.3	5.9	4.7	2.8
-1	43.5	29.5	26.4	20.0	20.6	20.2	10.9	8.3	7.7	5.6	3.7
-2,5	23.7	18.8	29.8	24.0	23.9	22.1	12.8	9.0	8.8	6.3	4.2
-6	25.1	18.9	21.4	17.1	15.4	15.3	13.2	8.5	8.3	6.7	5.7
-8,5	16.0	17.6	23.6	21.4	16.3	15.8	13.9	9.3	8.6	7.6	6.4

Table A.7. 7: Manifold Installation, Maximum Dynamic Force in Lifting Line [Te], Hs = 1.5m

<b>H<sub>s</sub> = 1.5m</b>						<b>T<sub>z</sub> [s]</b>					
Z [m]	3	4	5	6	7	8	9	10	11	12	13
1	27.8	35.2	37.5	26.8	21.9	16.9	8.9	6.4	7.7	4.7	4.9
0	75.2	67.4	48.8	39.1	42.4	32.4	20.8	13.6	12.9	9.2	5.2
-1	94.4	54.4	54.7	42.9	45.5	42.4	22.4	16.4	15.2	10.7	7.1
-2,5	51.0	45.1	63.3	52.1	51.5	45.6	25.1	18.2	16.9	12.1	8.0
-6	43.2	29.5	35.4	29.0	25.7	25.2	20.8	14.1	13.2	11.2	8.7
-8,5	25.6	26.5	35.4	32.5	25.8	25.9	20.8	14.3	13.3	11.7	9.6

Table A.7. 8: Manifold Installation, Maximum Dynamic Force in Lifting Line [Te], Hs = 2m

<b>H<sub>s</sub> = 2m</b>						<b>T<sub>z</sub> [s]</b>					
Z [m]	4	5	6	7	8	9	10	11	12	13	
1	76.1	63.2	60.5	30.8	38.7	13.0	8.6	13.3	6.4	6.5	
0	127.0	85.2	70.9	73.9	57.1	34.7	23.7	21.8	14.8	9.1	
-1	158.8	90.1	78.2	79.7	71.1	37.4	27.2	25.6	17.1	11.5	
-2,5	88.8	108.7	89.0	89.3	76.0	41.7	30.3	28.7	19.5	13.0	
-6	40.2	50.2	44.1	42.6	40.6	30.1	20.7	18.6	16.7	11.8	
-8,5	35,6	48.7	44.8	38.1	38.0	28.0	20.2	18.5	16.0	12.8	

Table A.7. 9: Manifold Installation, Maximum Dynamic Force in Lifting Line [Te], Hs = 2.5m

<b>H<sub>s</sub> = 2.5m</b>						<b>T<sub>z</sub> [s]</b>					
Z [m]	4	5	6	7	8	9	10	11	12	13	
1	137.3	121.8	98.2	53.9	65.2	16.6	13.6	23.4	8.2	8.2	
0	229.1	164.8	126.0	116.8	93.8	52.2	37.3	33.4	21.1	14.0	